Nonequilibrium fluctuations in small systems: From physics to biology

F Ritort

Department de Fisica Fonamental, Faculty of Physics, Universitat de Barcelona,
Diagonal 647, 08028 Barcelona, Spain;
E-Mail: ritort@ffn.ub.es

May 2006

Abstract

In this paper I am presenting an overview on several topics related to nonequilibrium fluctuations in small systems. I start with a general discussion about fluctuation theorems and applications to physical examples extracted from physics and biology: a bead in an optical trap and single molecule force experiments. Next I present a general discussion on path thermodynamics and consider distributions of work/heat fluctuations as large deviation functions. Then I address the topic of glassy dynamics from the perspective of nonequilibrium fluctuations due to small cooperatively rearranging regions. Finally, I conclude with a brief digression on future perspectives.

Contents

1 What are small systems?

Thermodynamics, a scientific discipline inherited from the 18th century, is facing new challenges in the description of nonequilibrium small (sometimes also called mesoscopic) systems. Thermodynamics is a discipline built in order to explain and interpret energetic processes occurring in macroscopic systems made out of a large number of molecules on the order of the Avogadro number. Although thermodynamics makes general statements beyond reversible processes its full applicability is found in equilibrium systems where it can make quantitative predictions just based on a few laws. The subsequent development of statistical mechanics has provided a solid probabilistic basis to thermodynamics and increased its predictive power at the same time. The development of statistical mechanics goes together with the establishment of the molecular hypothesis. Matter is made out of interacting molecules in motion. Heat, energy and work are measurable quantities that depend on the motion of molecules. The laws of thermodynamics operate at all scales.

Let us now consider the case of heat conduction along polymer fibers. Thermodynamics applies at the microscopic or molecular scale, where heat conduction takes place along molecules linked along a single polymer fiber, up to the macroscopic scale where heat is transmitted through all the fibers that make a piece of rubber. The main difference between the

two cases is the amount of heat transmitted along the system per unit of time. In the first case the amount of heat can be a few $k_B T$ per millisecond whereas in the second can be on the order of $N_f k_B T$ where N_f is the number of polymer fibers in the piece of rubber. The relative amplitude of the heat fluctuations are on the order of 1 in the molecular case and $1/\sqrt{N_f}$ in the macroscopic case. Because N_f is usually very large, the relative magnitude of heat fluctuations is negligible for the piece of rubber as compared to the single polymer fiber. We then say that the single polymer fiber is a small system whereas the piece of rubber is a macroscopic system made out of a very large collection of small systems that are assembled together.

Small systems are those in which the energy exchanged with the environment is a few times $k_B T$ and energy fluctuations are observable. A few can be 10 or 1000 depending on the system. A small system must not necessarily be of molecular size or contain a few number of molecules. For example, a single polymer chain may behave as a small system although it contains millions of covalently linked monomer units. At the same time, a molecular system may not be small if the transferred energy is measured over long times compared to the characteristic heat diffusion time. In that case the average energy exchanged with the environment during a time interval t can be as large as desired by choosing t large enough. Conversely, a macroscopic system operating at short time scales could deliver a tiny amount of energy to the environment, small enough for fluctuations to be observable and the system being effectively small.

Because macroscopic systems are collections of many molecules we expect that the same laws that have been found to be applicable in macroscopic systems are also valid in small systems containing a few number of molecules [1, 2]. Yet, the phenomena that we will observe in the two regimes will be different. Fluctuations in large systems, are mostly determined by the conditions of the environment. Large deviations from the average behavior are hardly observable and the structural properties of the system cannot be inferred from the spectrum of fluctuations. In contrast, small systems will display large deviations from their average behavior. These turn out to be less sensitive to the conditions of the surrounding environment (temperature, pressure, chemical potential) and carry information about the structure of the system and its nonequilibrium behavior. We may then say that information about the *structure* is carried in the tails of the statistical distributions describing molecular properties.

The world surrounding us is mostly out of equilibrium, equilibrium being just an idealization that requires of specific conditions to be met in the laboratory. Even today we do not have a general theory about nonequilibrium macroscopic systems as we have for equilibrium ones. Onsager theory is probably the most successful attempt albeit its domain of validity is restricted to the linear response regime. In small systems the situation seems to be the opposite. Over the past years, a set of theoretical results, that go under the name of fluctuation theorems, have been unveiled . These theorems make specific predictions about ennergy processes in small systems that can be scrutinized in the laboratory.

The interest of the scientific community on small systems has been boosted by the recent advent of micromanipulation techniques and nanotechnologies. These provide adequate scientific instruments that can measure tiny energies in physical systems under nonequilibrium conditions. Most of the excitement comes also from the more or less recent observation that biological matter has successfully exploited the smallness of biomolecular structures (such as complexes made out of nucleic acids and proteins) and the fact that they are embedded in nonequilibrium environment to become wonderfully complex and efficient at the same time [3, 4].

The goal of this review is to discuss these ideas from a physicsist perspective by emphasizing the underlying common aspects in a broad category of systems, from glasses to biomolecules. We aim to put together some concepts in statistical mechanics that may become the building blocks underlying a future theory of small systems. This is not a review in the traditional sense but rather a survey of a few selected topics in nonequilibrium statistical mechanics concerning systems that range from physics to biology. The selection is biased by my own particular taste and expertise. For this reason I have not tried to cover most of the relevant references for each selected topic but rather emphasize a few of them that make explicit connection with my discourse. Interested readers are advised to look at other reviews that have been recently been written on related subjects [5, 6, 7]

The outline of the review is as follows. Section 2 introduces two examples, one from physics and the other from biology, that are paradigms of nonequilibrium behavior. Section 3 is devoted to cover most important aspects of fluctuation theorems whereas Section 4 presents applications of fluctuation theorems to physics and biology. Section 5 presents the discipline of path thermodynamics and briefly discusses large deviation functions. Section 6 discusses the topic of glassy dynamics from the perspective of nonequilibrium fluctuations in small cooperatively rearranging regions. We conclude with a brief discussion on future perspectives.

2 Small systems in physics and biology

2.1 Colloidal systems

Condensed matter physics is full of examples where nonequilibrium fluctuations of mesoscopic regions governs the nonequilibrium behavior that is observed at the macroscopic level. A class of systems that have attracted a lot of attention for many decades and that still remain poorly understood are glassy systems, such as supercooled liquids and soft materials [8]. Glassy systems can be prepared in a nonequilibrium state, e.g. by fast quenching the sample from high to low temperatures, and subsequently following the time evolution of the system as a function of time (also called age of the system). Glassy systems display extremely slow relaxation and aging behavior, i.e. an age dependent response to the action of an external perturbation. Aging systems respond slower as they *get older* keeping memory of their age for timescales that range from picoseconds to years. The slow dynamics observed in glassy systems is dominated by intermittent, large and rare fluctuations where mesoscopic regions release some stress energy to the environment. Current experimental evidence suggests that these events correspond to structural rearrangements of clusters of molecules inside the glass that release some energy through an activated and cooperative process. These cooperatively rearranging regions are responsible of the heterogeneous dynamics observed in glassy systems and lead to a great disparity of relaxation times. The fact that slow dynamics of glassy systems virtually takes forever, indicates that the average amount of energy released in any rearrangement event must be small enough to account for an overall net energy release of the whole sample that is not larger than the stress energy contained in the system in the initial nonequilibrium state.

In some systems, such as colloids, the free-volume (i.e. the volume of the system that is available for motion to the colloidal particles) is the relevant variable, and the volume fraction of colloidal particles ϕ is the parameter governing the relaxation rate. Relaxation in colloidal systems is determined by the release of tensional stress energy and free volume in spatial re-

gions that contain a few particles. Colloidal systems offer great advantages to do experiments for several reasons: 1) In colloids the control parameter is the volume fraction, ϕ, a quantity easy to control in experiments; 2) Under appropriate solvent conditions colloidal particles behave as hard spheres, a system that is pretty well known and has been theoretically and numerically studied for many years; 3) The size of colloidal particles is typically of a few microns making possible to follow the motion of a small number particles using video microscopy and spectroscopic techniques. This allows to detect cooperatively rearranging clusters of particles and characterize their heterogeneous dynamics. Experiments have been done with PMMA poly(methyl methacrylate) particles of $\simeq 1\mu m$ radius suspended in organic solvents [9, 10]. Confocal microscopy then allows to acquire images of spatial regions of extension on the order of tens of microns that contain a few thousand of particles, small enough to detect the collective motion of clusters. In experiments carried by Weeks and collaborators [11] a highly stressed nonequilibrium state is produced by mechanically stirring a colloidal system at volume fractions $\phi \sim \phi_g$ where ϕ_g is the value of the volume fraction at the glass transition where colloidal motion arrests. The subsequent motion is then observed. A few experimental results are shown in Figure 1. The mean square displacement of the particles inside the confocal region show aging behavior. Importantly also, the region observed is small enough to observe temporal heterogeneity, i.e. the aging behavior is not smooth with the age of the system as usually observed in light scattering experiments. Finally, the mean square displacement for a single trajectory shows abrupt events characteristic of collective motions involving a few tens of particles. By analyzing the average number of particles belonging to a single cluster Weeks et al. [11] find that no more than 40 particles participate in the rearrangment of a single cluster suggesting that cooperatively rearranging regions are not larger than a few particle radii in extension. Large deviations, intermittent events and heterogeneous kinetics are the main features observed in these experiments.

2.2   Molecular machines

Biochemistry and molecular biology are scientific disciplines aiming to describe the structure, organization and function of living matter [12, 13]. Both disciplines seek an understanding of life processes in molecular terms. Their main object of study are biological molecules and the function they play in the biological process where they intervene. Biomolecules are small systems from several points of view. First, from their size, where they span just a few nanometers of extension. Second, from the energies they require to function properly, which is determined by the amount of energy that can be extracted by hydrolyzing one molecule of ATP (approximately 12 k_BT at room temperature or $300K$). Third, from the typically short amount of time that it takes to complete an intermediate step in a biological reaction. Inside the cell many reactions that would take an enormous long time under non-biological conditions are speeded up by several orders of magnitude in the presence of specific enzymes.

Molecular machines (also called molecular motors) are amazing complexes made out of several parts or domains that coordinate their behavior to perform specific biological functions by operating out of equilibrium. Molecular machines hydrolyze energy carrier molecules such as ATP to transform the chemical energy contained in the high energy bonds into mechanical motion [14, 15, 16, 17]. An example of a molecular machine that has been studied by molecular biologists and biophysicists is the RNA polymerase [18, 19]. This is an enzyme that synthesizes the pre-messenger RNA molecule by translocating along the DNA and reading, step by step,
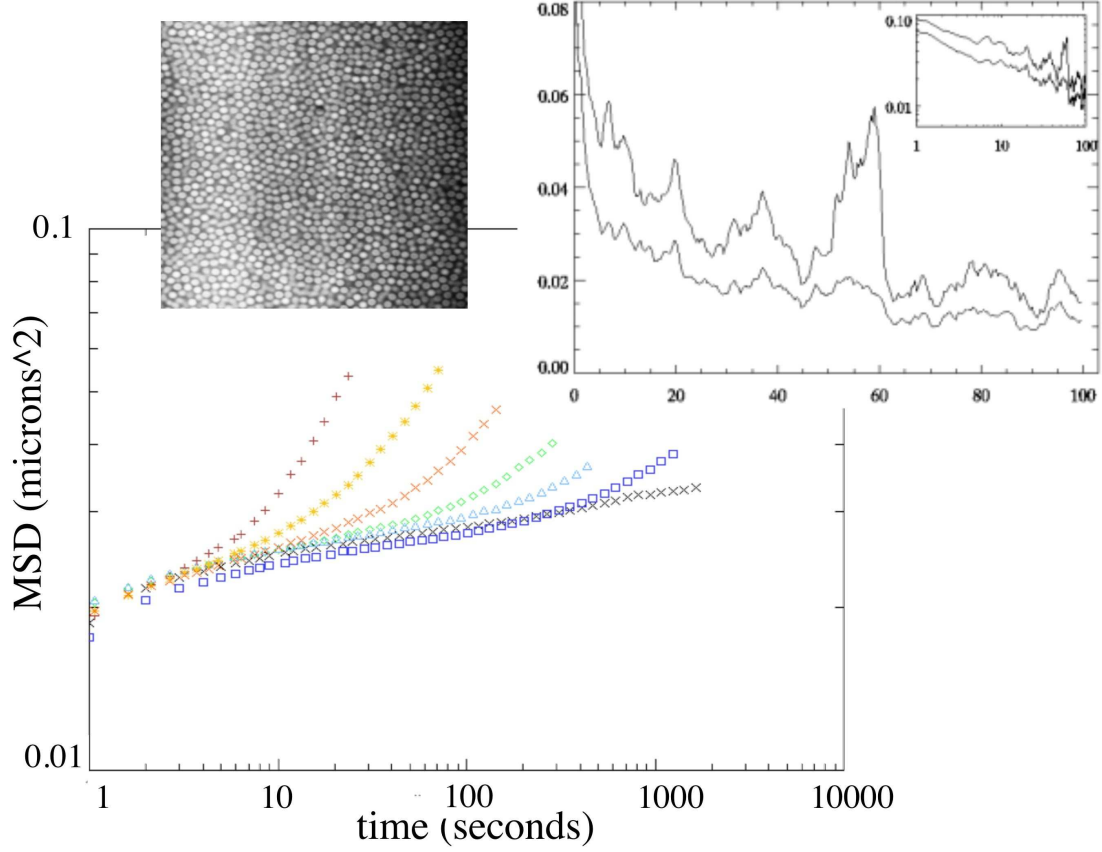
Figure 1: *(Left inset) A snapshot picture of a colloidal system obtained with confocal microscopy. (Left) Aging behavior observed in the mean square displacement (MSD), $\langle \Delta x^2 \rangle$, as a function of time for different ages. The colloidal system reorganizes slower as it becomes older. (Right) $\gamma = \sqrt{\langle \Delta x^4 \rangle / 3}$ (upper curve) and $\langle \Delta x^2 \rangle$ (lower curve) as a function of the age measured over a fixed time window $\Delta t = 10$min. For a diffusive dynamics both curves should coincide, however these measurements show deviations from diffusive dynamics as well as intermittent behavior (Inset: the same as in main panel but plotted in logarithmic timescale). Figures (A,B) taken from http://www.physics.emory.edu/weeks and Figure (C) taken from [11].*

the sequence of bases along the DNA backbone. The read out of the RNA polymerase is exported from the nucleus to the cytoplasm of the cell to later be translated in the ribosome, a huge molecular machine that synthesizes the protein coded into the messenger RNA [20]. Using single molecule experiments it is possible to grab one DNA molecule by both ends using optical tweezers and follow the translocation motion of the RNA polymerase [21, 22]. Current optical tweezer techniques have even resolved the motion of the enzyme at the level of a single base pair [23, 24]. The experiment requires flowing inside the fluidics chamber the enzymes and proteins that are necessary to initiate the transcription reaction. The subsequent motion and transcription by the RNA polymerase is called elongation and can be studied under applied force conditions that assist or oppose the motion of the enzyme [25]. In Figure 2 we show the results obtained in the Bustamante group for the RNA polymerase of *Escherichia Coli*, a bacteria found in the intestinal tracts of animals. In Figure 2A the polymerase apparently moves at a constant average speed but is characterized by pauses (black arrows) where motion temporarily arrests. In Figure 2B we show the transcription rate (or speed of the enzyme) as a function of time. Note the large intermittent fluctuations in the transcription rate, a typical feature of small systems embedded in a noisy thermal environment. In contrast to the slow dynamics observed in colloidal systems (Sec. 2.1) the kinetic motion of the polymerase is not progressively slower but steady and fast. We then say that the polymerase is in a nonequilibrium steady state. As in the previous case, large deviations, intermittent events and complex kinetics are the main features we observe in these experiments.

3   Fluctuation theorems (FTs)

Fluctuation theorems (FTs) make statements about energy exchanges that take place between a system and its surroundings under general nonequilibrium conditions. Since their discovery in the mid 90's [26, 27, 28] there has been an increasing interest to elucidate their importance and implications. FTs provide a fresh new look to our understanding of old questions such as the origin of irreversibility and the second law in statistical mechanics [29, 30]. In addition, FTs provide statements about energy fluctuations in small systems which, under generic conditions, should be experimentally observable. FTs have been discussed in the context of deterministic, stochastic and thermostatted systems. Although the results obtained differ depending on the particular model of the dynamics that is used, in the nutshell they look pretty equivalent.

FTs are related to the so called nonequilibrium work relations introduced by Jarzynski [31]. This fundamental relation can be seen as consequence of the FTs [32, 33]. It represents a new result beyond classical thermodynamics that shows the possibility to recover free energy differences using irreversible processes. Several reviews have been written on the subject [34, 35, 36, 37, 3] with specific emphasis on theory and/or experiments. In the next sections we review some of the main results. Throughout the text we will take $k_B = 1$.

3.1   Nonequilibrium states

An important concept in thermodynamics is the state variable. State variables are those that, once determined, uniquely specify the thermodynamic state of the system. Examples are the temperature, the pressure, the volume and the mass of the different components in a given system. To specify the state variables of a system it is common to put the system in contact with a bath. The bath is any set of sources (of energy, volume, mass, etc.) large enough to
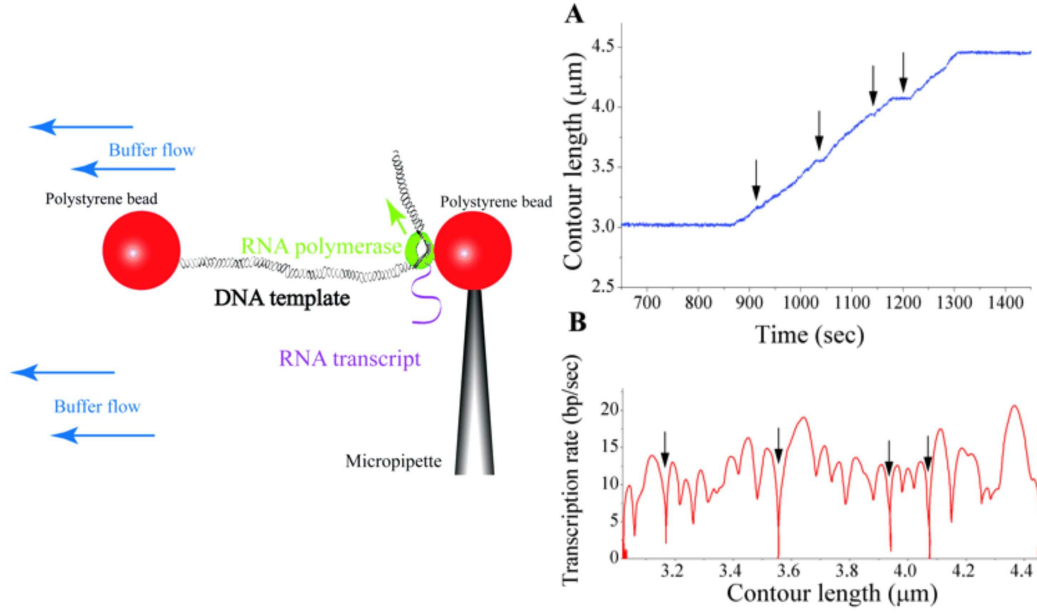
Figure 2: *(Left) Experimental setup in force-flow measurements. Optical tweezers are used to trap beads but forces are applied on the RNApol-DNA molecular complex using the Stokes drag force acting on the left bead immersed in the flow. In this setup force assists RNA transcription as the DNA tether between beads increases in length as a function of time. (A) The contour length of the DNA tether as a function of time (blue curve) and (B) the transcription rate (red curve) as a function of the contour length. Pauses (temporary arrests of transcription) are shown as vertical arrows. Figure taken from [25].*

remain unaffected by the interaction with the system under study. The bath ensures that a system can reach a given temperature, pressure, volume and mass concentrations of the different components when put in thermal contact with the bath (i.e. with all the relevant sources). Equilibrium states are then generated by putting the system in contact with a bath and waiting until the system properties relax to the equilibrium values. Under such conditions the system properties do not change with time and the average net heat/work/mass exchanged between the system and the bath is zero.

Nonequilibrium states can be produced under a great variety of conditions, either by continuously changing the parameters of the bath or by preparing the system in an initial nonequilibrium state that slowly relaxes toward equilibrium. In general a nonequilibrium state is produced whenever the system properties change with time and/or the net heat/work/mass exchanged by the system and the bath is non zero. We can distinguish at least three different types of nonequilibrium states:

- **Nonequilibrium transient state (NETS).** The system is initially prepared in an equilibrium state and later driven out of equilibrium by switching on an external perturbation. The system quickly returns to a new equilibrium state once the external perturbation stops changing.

- **Nonequilibrium steady-state (NESS).** The system is driven by external forces (either time dependent or non-conservative) in a stationary nonequilibrium state where its properties do not change with time. The steady state is an irreversible nonequilibrium process, that cannot be described by the Boltzmann-Gibbs distribution, where the average heat that is dissipated by the system (equal to the entropy production of the bath) is positive.

  There are still other categories of NESS. For example in nonequilibrium transient steady states the system starts in equilibrium but is driven out of equilibrium by an external perturbation to finally settle in a steady state.

- **Nonequilibrium aging state (NEAS).** The system is initially prepared in a nonequilibrium state and put in contact with the sources. The system is then let evolve alone but fails to reach thermal equilibrium in observable or laboratory time scales. In this case the system is in a non-stationary slowly relaxing nonequilibrium state called *aging state* and characterized by a very small entropy production of the sources. In the aging state two-times correlations decay slower as the system becomes older. Two-time correlation functions depend on both times and not just on their difference.

There are many examples of nonequilibrium states. A classic example of a NESS is an electrical circuit made out of a battery and a resistance. The current flows through the resistance and the chemical energy stored in the battery is dissipated to the environment in the form of heat; the average dissipated power, $\mathcal{P}_{\mathrm{dis}} = VI$, is identical to the power supplied by the battery. Another example is a sheared fluid between two plates or coverslips and one of them is moved relative to the other at a constant velocity v. To sustain such state a mechanical power that is equal to $\mathcal{P} \propto \eta v^2$ has to be exerted upon the moving plate where η is the viscosity of the fluid. The mechanical work produced is then dissipated in the form of heat through the viscous friction between contiguous fluid layers. Another examples of NESS are chemical reactions in metabolic pathways that are sustained by activated carrier

molecules such as ATP. In such case, hydrolysis of ATP is strongly coupled to specific oxidative reactions. For example, ionic channels use ATP hydrolysis to transport protons against the electromotive force.

A classic example of NETS is the case of a protein in its initial native state that is mechanically pulled (e.g. using AFM) by exerting force at the ends of the molecule. The protein is initially folded and in thermal equilibrium with the surrounding aqueous solvent. By mechanically stretching the protein is pulled away from equilibrium into a transient state until it finally settles into the unfolded and extended new equilibrium state. Another example of a NETS is a bead immersed in water and trapped in an optical well generated by a focused laser beam. When the trap is moved to a new position (e.g. by moving the lasr beams) the bead is driven into a NETS. After some time the bead reaches again equilibrium at the new position of the trap. In another experiment the trap is suddenly put in motion at a speed v so the bead is transiently driven away from its equilibrium average position until it settles into a NESS characterized by the speed of the trap. This results in the average position of the bead lagging behind the position of the center of the trap.

The classic example of a NEAS is a supercooled liquid cooled below its glass transition temperature. The liquid solidifies into an amorphous slowly relaxing state characterized by huge relaxational times and anomalous low frequency response. Other systems are colloids that can be prepared in a NEAS by the sudden reduction/increase of the volume fraction of the colloidal particles or by putting the system under a strain/stress.

The classes of nonequilibrium states previously described do not make distinctions whether the system is macroscopic or small. In small systems, however, it is common to speak about the control parameter to emphasize the importance of the constraints imposed by the bath that are externally controlled and do not fluctuate. The control parameter (λ) represents a value (in general, a set of values) that defines the state of the bath. Its value determines the equilibrium properties of the system, e.g. the equation of state. In macroscopic systems it is unnecessary to discern which value is externally controlled because fluctuations are small and all equilibrium ensembles give the same equivalent thermodynamic description, i.e. the same equation of state. Differences arise only when including fluctuations in the description. The nonequilibrium behavior of small systems is then strongly dependent on the protocol used to drive them out of equilibrium. The protocol is generally defined by the time evolution of the control parameter $\lambda(t)$. As a consequence, the characterization of the protocol $\lambda(t)$ is an essential step to unambiguously define the nonequilibrium state. Figure 3 shows a representation of a few examples of NESS and control parameters.

3.2   Fluctuation theorems (FTs) in stochastic dynamics

In this section we ae presenting a derivation of the FT based on stochastic dynamics. In contrast to deterministic systems, stochastic dynamics naturally incoporates crucial assumptions needed for the derivation such as the ergodicity hypothesis. The derivation we present here follows the approach introduced by Crooks-Kurchan-Lebowitz-Spohn [38, 39] and includes also some results recently obtained by Seifert using Langevin systems [40].
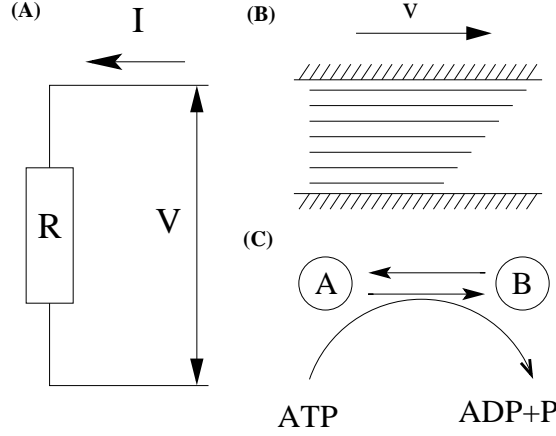
Figure 3: *Examples of NESS. (A) An electric current I flowing through a resistance R and maintained by a voltage source or control parameter V. (B) A fluid sheared between two plates that move at speed v (the control parameter) relative to each other. (C) A chemical reaction $A \to B$ coupled to ATP hydrolysis. The control parameter here are the concentrations of ATP and ADP.*

3.2.1 The master equation

Let us consider a stochastic system described by a generic variable $\mathcal{C}$. This variable may stand for the position of a bead in an optical trap, the velocity field of a fluid, the current passing through a resistance, the number of native contacts in a protein, etc. A trajectory or path Γ in configurational space is described by a discrete sequence of configurations in phase space,

$$\Gamma \equiv \{\mathcal{C}_0, \mathcal{C}_1, \mathcal{C}_2, ..., \mathcal{C}_M\} \tag{1}$$

where the system occupies configuration $\mathcal{C}_k$ at time $t_k = k\Delta t$ and Δt is the duration of the discretized elementary time-step. In what follows we consider paths that start at $\mathcal{C}_0$ at time $t = 0$ and end at the configuration $\mathcal{C}_M$ at time $t = M\Delta t$. The continuous time limit is recovered by taking $M \to \infty, \Delta t \to 0$ for a fixed value of t.

Let $\langle (...) \rangle$ denote the average over all paths that start at $t = 0$ at configurations $\mathcal{C}_0$ initially chosen from a distribution $P_0(\mathcal{C})$. We also define $P_k(\mathcal{C})$ as the probability, measured over all possible dynamical paths, that the system is in configuration $\mathcal{C}$ at time $t_k = k\Delta t$. Probabilities are normalized for any k,

$$\sum_{\mathcal{C}} P_k(\mathcal{C}) = 1 \qquad . \tag{2}$$

The system is assumed to be in contact with a thermal bath at temperature T. We also assume that the microscopic dynamics of the system is of the Markovian type: the probability for the system to be at a given configuration and at a given time only depends on its previous configuration. We then introduce the transition probability $\mathcal{W}_k(\mathcal{C} \to \mathcal{C}')$. This denotes the probability for the system to change from $\mathcal{C}$ to $\mathcal{C}'$ at time-step k. According to the Bayes formula,

$$P_{k+1}(\mathcal{C}) = \sum_{\mathcal{C}'} \mathcal{W}_k(\mathcal{C}' \to \mathcal{C}) P_k(\mathcal{C}') \tag{3}$$

where the $\mathcal{W}'s$ satisfy the normalization condition,

$$\sum_{\mathcal{C}'} \mathcal{W}_k(\mathcal{C} \to \mathcal{C}') = 1 \quad . \tag{4}$$

Using (2),(3) we can write the following Master equation for the probability $P_k(\mathcal{C})$,

$$\Delta P_k(\mathcal{C}) = P_{k+1}(\mathcal{C}) - P_k(\mathcal{C}) = \sum_{\mathcal{C}' \neq \mathcal{C}} \mathcal{W}_k(\mathcal{C}' \to \mathcal{C}) P_k(\mathcal{C}') - \sum_{\mathcal{C}' \neq \mathcal{C}} \mathcal{W}_k(\mathcal{C} \to \mathcal{C}') P_k(\mathcal{C}) \tag{5}$$

where the terms $\mathcal{C} = \mathcal{C}'$ have not been included as they cancel out in the first and second sums in the r.h.s. The first term in the r.h.s accounts for all transitions leading to the configuration $\mathcal{C}$ whereas the second term counts all processes leaving $\mathcal{C}$. It is convenient to introduce the rates $r_t(\mathcal{C} \to \mathcal{C}')$ in the continuous time limit $\Delta t \to 0$,

$$r_t(\mathcal{C} \to \mathcal{C}') = \lim_{\Delta t \to 0} \frac{\mathcal{W}_k(\mathcal{C} \to \mathcal{C}')}{\Delta t} \quad ; \quad \forall \mathcal{C} \neq \mathcal{C}' \tag{6}$$

Equation (5) becomes,

$$\frac{\partial P_t(\mathcal{C})}{\partial t} = \sum_{\mathcal{C}' \neq \mathcal{C}} r_t(\mathcal{C}' \to \mathcal{C}) P_t(\mathcal{C}') - \sum_{\mathcal{C}' \neq \mathcal{C}} r_r(\mathcal{C} \to \mathcal{C}') P_t(\mathcal{C}) \quad . \tag{7}$$

3.2.2 Microscopic reversibility

We now introduce the concept of the control parameter λ (see Sec. 3.1). In the present scheme the discrete-time sequence $\{\lambda_k; 0 \geq k \geq M\}$ defines the perturbation protocol. The transition probability $\mathcal{W}_k(\mathcal{C} \to \mathcal{C}')$ now depends explicitly on time through the value of an external time-dependent parameter λ_k. The parameter λ_k may indicate any sort of externally controlled variable that determines the state of the system, for instance the value of the external magnetic field applied on a magnetic system, the value of the mechanical force applied to the ends of a molecule, the position of a piston containing a gas or the concentrations of ATP and ADP in a molecular reaction coupled to hydrolisis (see Figure 3). The time variation of the control parameter, $\dot{\lambda} = (\lambda_{k+1} - \lambda_k)/\Delta t$, is used as tunable parameter which determines how much irreversible is the nonequilibrium process. In order to emphasize the importance of the control parameter, in what follows we will parametrize probabilities and transition probabilities by the value of the control parameter at time-step k, λ (rather than by the time t). Therefore we will write $P_\lambda(\mathcal{C}), \mathcal{W}_\lambda(\mathcal{C} \to \mathcal{C}')$ for the probabilities and transition probabilities respectively at a given time t.

The transition probabilities $\mathcal{W}_\lambda(\mathcal{C} \to \mathcal{C}')$ cannot be arbitrary but must guarantee that the equilibrium state $P_\lambda^{\text{eq}}(C)$ is a stationary solution of the master equation (5). The simplest way to impose such condition is to model the microscopic dynamics as ergodic and reversible for a fixed value of λ,

$$\frac{\mathcal{W}_\lambda(\mathcal{C} \to \mathcal{C}')}{\mathcal{W}_\lambda(\mathcal{C}' \to \mathcal{C})} = \frac{P_\lambda^{\text{eq}}(\mathcal{C}')}{P_\lambda^{\text{eq}}(\mathcal{C})} \quad . \tag{8}$$

The latter condition is commonly known as microscopic reversibility or local detailed balance. This property is equivalent to time reversal invariance in deterministic (e.g. thermostatted) dynamics. Although it can be relaxed by requiring just global (rather than detailed) balance

12

it is physically natural to think of equilibrium as a local property. Microscopic reversibility, a common assumption in nonequilibrium statistical mechanics, is the crucial ingredient in the present derivation.

Equation (8) has been criticized as a relation that is valid only very near to equilibrium because the rates appearing in (8) are related to the equilibrium distribution $P_\lambda^{\text{eq}}(C)$. However, we must observe that the equilibrium distribution evaluated at a given configuration depends only on the Hamiltonian of the system at that configuration. Therefore, (8) must be read as a relation that only depends on the energy of configurations. It is valid close but also far from equilibrium.

Let us now consider all possible dynamical paths Γ that are generated starting from an ensemble of initial configurations at time 0 (described by the initial distribution $P_{\lambda_0}(\mathcal{C})$) and which evolve according to (8) until time t ($t = M\Delta t$, M being the total number of discrete time-steps). Dynamical evolution takes place according to a given protocol, $\{\lambda_k, 0 \leq k \leq M\}$, the protocol defining the nonequilibrium experiment. Different dynamical paths will be generated because of the different initial conditions (weighted with the probability $P_{\lambda_0}(\mathcal{C})$) and because of the stochastic nature of the transitions between configurations at consecutive time-steps.

3.2.3 The nonequilibrium equality

Let us consider a generic observable $\mathcal{A}(\Gamma)$. The average value of A is given by,

$$\langle \mathcal{A} \rangle = \sum_\Gamma P(\Gamma) \mathcal{A}(\Gamma) \tag{9}$$

where Γ denotes the path and $P(\Gamma)$ indicates the probability of that path. Using the fact that the dynamics is Markovian together with the definition (1) we can write,

$$P(\Gamma) = P_{\lambda_0}(\mathcal{C}_0) \prod_{k=0}^{M-1} \mathcal{W}_{\lambda_k}(\mathcal{C}_k \to \mathcal{C}_{k+1}) \quad . \tag{10}$$

By inserting (10) into (9) we obtain,

$$\langle \mathcal{A} \rangle = \sum_\Gamma \mathcal{A}(\Gamma) P_{\lambda_0}(\mathcal{C}_0) \prod_{k=0}^{M-1} \mathcal{W}_{\lambda_k}(\mathcal{C}_k \to \mathcal{C}_{k+1}) \quad . \tag{11}$$

Using the detailed balance condition (8) this expression reduces to,

$$\langle \mathcal{A} \rangle = \sum_\Gamma P_{\lambda_0}(\mathcal{C}_0) \mathcal{A}(\Gamma) \prod_{k=0}^{M-1} \left[\mathcal{W}_{\lambda_k}(\mathcal{C}_{k+1} \to \mathcal{C}_k) \frac{P_{\lambda_k}^{\text{eq}}(\mathcal{C}_{k+1})}{P_{\lambda_k}^{\text{eq}}(\mathcal{C}_k)} \right] \tag{12}$$

$$= \sum_\Gamma \mathcal{A}(\Gamma) P_{\lambda_0}(\mathcal{C}_0) \exp\left[\sum_{k=0}^{M-1} \log\left(\frac{P_{\lambda_k}^{\text{eq}}(\mathcal{C}_{k+1})}{P_{\lambda_k}^{\text{eq}}(\mathcal{C}_k)} \right) \right] \prod_{k=0}^{M-1} \mathcal{W}_{\lambda_k}(\mathcal{C}_{k+1} \to \mathcal{C}_k) \quad . \tag{13}$$

This equation can not be worked out further. However, let us consider the following observable $\mathcal{S}(\Gamma)$, defined by,

$$\mathcal{A}(\Gamma) = \exp(-\mathcal{S}(\Gamma)) = \frac{b(\mathcal{C}_M)}{P_{\lambda_0}(\mathcal{C}_0)} \prod_{k=0}^{M-1} \left(\frac{P_{\lambda_k}^{\text{eq}}(\mathcal{C}_k)}{P_{\lambda_k}^{\text{eq}}(\mathcal{C}_{k+1})} \right) \tag{14}$$

13

where $b(\mathcal{C})$ is any positive definite and normalizable function,

$$\sum_{\mathcal{C}} b(\mathcal{C}) = 1 \tag{15}$$

and $P_{\lambda_0}(\mathcal{C}_0) > 0, \forall \mathcal{C}_0$. By inserting (14) into (13) we get,

$$\langle \exp(-\mathcal{S}) \rangle = \sum_{\Gamma} b(\mathcal{C}_M) \prod_{k=0}^{M-1} \mathcal{W}_{\lambda_k}(\mathcal{C}_{k+1} \to \mathcal{C}_k) = 1 \tag{16}$$

where we have applied a telescopic sum (we first summed over $\mathcal{C}_M$ and used (15) and subsequently summed over the rest of variables and used (4)). We call $\mathcal{S}(\Gamma)$ the **total dissipation** of the system. It is given by,

$$\mathcal{S}(\Gamma) = \sum_{k=0}^{M-1} \log\Big[\frac{P_{\lambda_k}^{\mathrm{eq}}(\mathcal{C}_{k+1})}{P_{\lambda_k}^{\mathrm{eq}}(\mathcal{C}_k)}\Big] + \log(P_{\lambda_0}(\mathcal{C}_0)) - \log(b(\mathcal{C}_M)) \quad . \tag{17}$$

The equality (16) immediately implies, by using Jensen's inequality, the following inequality,

$$\langle \mathcal{S} \rangle \geq 0 \tag{18}$$

which is reminiscent of second law of thermodynamics for nonequilibrium systems: the entropy of the universe (system plus the environment) always increases. Yet, we have to identify the different terms appearing in (17). It is important to stress that entropy production in nonequilibrium systems can be defined just in terms of the work/heat/mass transferred by the system to the external sources which represent the bath. The definition of the total dissipation (17) is arbitrary because it depends on an undetermined function $b(\mathcal{C})$ (15). Therefore, the total dissipation $\mathcal{S}$ may not necessarily have a general physical meaning and could be interpreted in different ways depending on the specific nonequilibrium context.

Equation (16) has appeared in the past in the literature [41] and is mathematically identical to the Jarzynski equality [31]. We analyze this connection below in Sec. 3.3.1.

3.2.4 The fluctuation theorem

A physical insight on the meaning of the total dissipation $\mathcal{S}$ can be obtained by deriving the fluctuation theorem. We start by defining the reverse path Γ^* of a given path Γ. Let us consider the path, $\Gamma \equiv \mathcal{C}_0 \to \mathcal{C}_1 \to ... \to \mathcal{C}_M$ corresponding to the forward (F) protocol which is described by the sequence of values of λ at different time-steps k, λ_k. Every transition occurring at time-step k, $\mathcal{C}_k \to \mathcal{C}_{k+1}$, is governed by the transition probability $\mathcal{W}_{\lambda_k}(\mathcal{C}_k \to \mathcal{C}_{k+1})$. The reverse path of Γ is defined as the time reverse sequence of configurations, $\Gamma^* \equiv \mathcal{C}_M \to \mathcal{C}_{M-1} \to ... \to \mathcal{C}_0$ corresponding to the reverse (R) protocol described by the time-reversed sequence of values of λ, $\lambda_k^R = \lambda_{M-k-1}$.

The probability of a given path and its reverse are given by,

$$\mathcal{P}_F(\Gamma) = \prod_{k=0}^{M-1} \mathcal{W}_{\lambda_k}(\mathcal{C}_k \to \mathcal{C}_{k+1}) \tag{19}$$

$$\mathcal{P}_R(\Gamma^*) = \prod_{k=0}^{M-1} \mathcal{W}_{\lambda_k^R}(\mathcal{C}_{M-k} \to \mathcal{C}_{M-k-1}) = \prod_{k=0}^{M-1} \mathcal{W}_{\lambda_k}(\mathcal{C}_{k+1} \to \mathcal{C}_k) \tag{20}$$

where in the last line we shifted variables $k \to M - 1 - k$. We use the notation $\mathcal{P}$ for the path probabilities rather than the usual letter P. This difference in notation is introduced to stress the fact that path probabilities (19,20) are non-normalized conditional probabilities, i.e. $\sum_\Gamma \mathcal{P}_{F(R)}(\Gamma) \neq 1$. By using (8) we get,

$$\frac{\mathcal{P}_F(\Gamma)}{\mathcal{P}_R(\Gamma^*)} = \prod_{k=0}^{M-1} \frac{P_{\lambda_k}^{\text{eq}}(\mathcal{C}_{k+1})}{P_{\lambda_k}^{\text{eq}}(\mathcal{C}_k)} = \exp(S_p(\Gamma)) \tag{21}$$

where we defined the **entropy production** of the system,

$$S_p(\Gamma) = \sum_{k=0}^{M-1} \log\Big(\frac{P_{\lambda_k}^{\text{eq}}(\mathcal{C}_{k+1})}{P_{\lambda_k}^{\text{eq}}(\mathcal{C}_k)}\Big) \qquad . \tag{22}$$

Note that $S_p(\Gamma)$ is just a part of the total dissipation introduced in (17),

$$\mathcal{S}(\Gamma) = S_p(\Gamma) + B(\Gamma) \tag{23}$$

where $B(\Gamma)$ is the so-called **boundary term**,

$$B(\Gamma) = \log(P_{\lambda_0}(\mathcal{C}_0)) - \log(b(\mathcal{C}_M)) \qquad . \tag{24}$$

We tend to identify $S_p(\Gamma)$ as the entropy production in a nonequilibrium system whereas $B(\Gamma)$ is a term that contributes just at the beginning and end of the nonequilibrium process. Note that the entropy production $S_p(\Gamma)$ is antisymmetric under time reversal, $S_p(\Gamma^*) = -S_p(\Gamma)$, expressing the fact that the entropy production is a quantity related to irreversible motion. According to (21) paths that produce a given amount of entropy are much more probable than those that consume the same amount of entropy. How much improbable is entropy consumption depends exponentially on the amount of entropy consumed. The larger the system is, the larger the probability to produce (rather than consume) a given amount of entropy S_p.

Equation (21) has already the form of a fluctuation theorem. However, in order to get a proper fluctuation theorem we need to specify relations between probabilities for physically measurable observables rather than paths. From (21) it is straightforward to derive a fluctuation theorem for the total dissipation $\mathcal{S}$. Let us take $b(\mathcal{C}) = P_{\lambda_M}(\mathcal{C})$. With this choice we get,

$$\mathcal{S}(\Gamma) = S_p(\Gamma) + B(\Gamma) = \sum_{k=0}^{M-1} \log\Big(\frac{P_{\lambda_k}^{\text{eq}}(\mathcal{C}_{k+1})}{P_{\lambda_k}^{\text{eq}}(\mathcal{C}_k)}\Big) + \log(P_{\lambda_0}(\mathcal{C}_0)) - \log(P_{\lambda_M}(\mathcal{C}_M)) \quad . \tag{25}$$

The physical motivation behind this choice is that $\mathcal{S}$ becomes now an antisymmetric observable under time reversal. Albeit $S_p(\Gamma)$ is always antisymmetric, the choice (25) is the only one that guarantees that the total dissipation $\mathcal{S}$ changes sign upon reversal of the path, $\mathcal{S}(\Gamma^*) = -\mathcal{S}(\Gamma)$. The symmetry property of observables under time reversal and the possibility to consider boundary terms where $\mathcal{S}$ is symmetric (rather than antisymmetric) under time reversal has been discussed in [42].

The probability to produce a total dissipation $\mathcal{S}$ along the forward protocol is given by,

$$P_F(\mathcal{S}) = \sum_\Gamma P_{\lambda_0}(\mathcal{C}_0)\mathcal{P}_F(\Gamma)\delta(\mathcal{S}(\Gamma) - \mathcal{S}) = \sum_\Gamma P_{\lambda_0}(\mathcal{C}_0)\mathcal{P}_R(\Gamma^*)\exp(S_p(\Gamma))\delta(\mathcal{S}(\Gamma) - \mathcal{S}) =$$

$$\sum_\Gamma P_{\lambda_M}(\mathcal{C}_M)\mathcal{P}_R(\Gamma^*)\exp(\mathcal{S}(\Gamma))\delta(\mathcal{S}(\Gamma) - \mathcal{S}) =$$

$$\exp(\mathcal{S})\sum_{\Gamma^*} P_{\lambda_M}(\mathcal{C}_M)\mathcal{P}_R(\Gamma^*)\delta(\mathcal{S}(\Gamma^*) + \mathcal{S}) = \exp(\mathcal{S})P_R(-\mathcal{S}) \quad . \quad (26)$$

In the first line of the derivation we used (21), in the second we used (25) and in the third we took into account the antisymmetric property of $\mathcal{S}(\Gamma)$ and the unicity of the assignment $\Gamma \to \Gamma^*$. This result is known under the generic name of **fluctuation theorem**,

$$\frac{P_F(\mathcal{S})}{P_R(-\mathcal{S})} = \exp(\mathcal{S}) \quad . \quad (27)$$

It is interesting to observe that this relation is not satisfied by the entropy production because the inclusion of boundary term (24) in the total dissipation is required to respect the fluctuation symmetry. In what follows we discuss some of its consequences in some specific situations.

- **Jarzynski equality.** The nonequilibrium equality (16) is just a consequence of (27) that is obtained by rewriting it as $P_R(-\mathcal{S}) = P_F(\mathcal{S})\exp(-\mathcal{S})$ and integrating both sides of the equation from $\mathcal{S} = -\infty$ to $\mathcal{S} = \infty$.

- **Linear response regime.** Equation (27) is trivially satisfied for $\mathcal{S} = 0$ if $P_F(0) = P_R(0)$. The process where $P_{F(R)}(\mathcal{S}) = \delta(\mathcal{S})$ is called quasistatic or reversible. When $\mathcal{S}$ is different from zero but small ($\mathcal{S} < 1$) we can expand (27) around $\mathcal{S} = 0$ to obtain,

$$\mathcal{S}P_F(\mathcal{S}) = \mathcal{S}\exp(\mathcal{S})P_R(-\mathcal{S})$$
$$\langle\mathcal{S}\rangle_F = \langle(-\mathcal{S} + \mathcal{S}^2)\rangle_R + \mathcal{O}(\mathcal{S}^3)$$
$$\langle(\mathcal{S}^2)\rangle_{F(R)} = 2\langle\mathcal{S}\rangle_{F(R)} \quad (28)$$

where we used $\langle\mathcal{S}\rangle_F = \langle\mathcal{S}\rangle_R$, valid up to second order in $\mathcal{S}$. Note the presence of the subindex $F(R)$ for the expectation values in the last line of (28) which emphasizes the equality of these averages along the forward and reverse process. The relation (28) is a version of the fluctuation-dissipation theorem (FDT) valid in the linear response region and equivalent to the Onsager reciprocity relations [43].

3.3 Applications of the FT to nonequilibrium states

The FT (27) finds application in several nonequilibrium contexts. Here we describe specific results for transient and steady states.

3.3.1 Nonequilibrium transient states (NETS)

We will assume a system initially in thermal equilibrium that is transiently brought to a nonequilibrium state. We are going to show that, under such conditions, the entropy production (22) is equal to the heat delivered by the system to the sources. We rewrite (22) by

introducing the potential energy function $G_\lambda(\mathcal{C})$,

$$P_\lambda^{\text{eq}}(\mathcal{C}) = \frac{\exp(-G_\lambda(\mathcal{C}))}{\mathcal{Z}_\lambda} = \exp(-G_\lambda(\mathcal{C}) + \mathcal{G}_\lambda) \tag{29}$$

where $\mathcal{Z}_\lambda = \sum_{\mathcal{C}} \exp(-G_\lambda(\mathcal{C})) = \exp(-\mathcal{G}_\lambda)$ is the partition function and $\mathcal{G}_\lambda$ is the thermodynamic potential. The existence of the potential $G_\lambda(\mathcal{C})$ and the thermodynamic potential $\mathcal{G}_\lambda$ is guaranteed by Boltzmann-Gibbs ensemble theory. For simplicity we will consider here the canonical ensemble where the volume V, the number of particles N and the temperature T are fixed. Needless to say that the following results can be generalized to arbitrary ensembles. In the canonical case $G_\lambda(\mathcal{C})$ is equal to $E_\lambda(\mathcal{C})/T$ where $E_\lambda(\mathcal{C})$ is the total energy function (that includes the kinetic plus the potential energy terms). $\mathcal{G}_\lambda$ is equal to $F_\lambda(V, T, N)/T$ where F_λ stands for the Helmholtz free energy.

With these definitions the entropy production (22) is given by,

$$S_p(\Gamma) = \sum_{k=0}^{M-1} \left(G_{\lambda_k}(\mathcal{C}_k) - G_{\lambda_k}(\mathcal{C}_{k+1}) \right) = \frac{1}{T} \sum_{k=0}^{M-1} \left(E_{\lambda_k}(\mathcal{C}_k) - E_{\lambda_k}(\mathcal{C}_{k+1}) \right) \quad . \tag{30}$$

For the boundary term (24) let us take $b(\mathcal{C}) = P_{\lambda_M}^{\text{eq}}(\mathcal{C})$,

$$\begin{aligned} B(\Gamma) &= \log(P_{\lambda_0}^{\text{eq}}(\mathcal{C}_0)) - \log(P_{\lambda_M}^{\text{eq}}(\mathcal{C}_M)) = \\ &= G_{\lambda_M}(\mathcal{C}_M) - G_{\lambda_0}(\mathcal{C}_0) - \mathcal{G}_{\lambda_M} + \mathcal{G}_{\lambda_0} = \\ &= \frac{1}{T}(E_{\lambda_M}(\mathcal{C}_M) - E_{\lambda_0}(\mathcal{C}_0) - F_{\lambda_M} + F_{\lambda_0}) \end{aligned} \tag{31}$$

The total dissipation (25) is then equal to,

$$\mathcal{S}(\Gamma) = S_p(\Gamma) + \frac{1}{T}(E_{\lambda_M}(\mathcal{C}_M) - E_{\lambda_0}(\mathcal{C}_0) - F_{\lambda_M} + F_{\lambda_0}) \tag{32}$$

which can be rewritten as a balance equation for the variation of the energy $E_\lambda(\mathcal{C})$ along a given path,

$$\Delta E(\Gamma) = E_{\lambda_M}(\mathcal{C}_M) - E_{\lambda_0}(\mathcal{C}_0) = T\mathcal{S}(\Gamma) + \Delta F - TS_p(\Gamma) \quad . \tag{33}$$

where $\Delta F = F_{\lambda_M} - F_{\lambda_0}$. This is the first law of thermodynamics where we have identified the term in the lhs with the total variation of the internal energy $\Delta E(\Gamma)$. Whereas $T\mathcal{S}(\Gamma) + \Delta F$ and $TS_p(\Gamma)$ are identified with the mechanical work exerted on the system and the heat delivered to the bath respectively,

$$\Delta E(\Gamma) = W(\Gamma) - Q(\Gamma) \tag{34}$$
$$W(\Gamma) = T\mathcal{S}(\Gamma) + \Delta F \tag{35}$$
$$Q(\Gamma) = TS_p(\Gamma) \quad . \tag{36}$$

By using (30) we obtain the following expressions for work and heat,

$$W(\Gamma) = \sum_{k=0}^{M-1} \left(E_{\lambda_{k+1}}(\mathcal{C}_{k+1}) - E_{\lambda_k}(\mathcal{C}_{k+1}) \right) \tag{37}$$

$$Q(\Gamma) = \sum_{k=0}^{M-1} \left(E_{\lambda_k}(\mathcal{C}_k) - E_{\lambda_k}(\mathcal{C}_{k+1}) \right) \quad . \tag{38}$$

17

The physical meaning of both entropies is now clear. Whereas S_p stands for the heat transferred by the system to the sources (36), the total dissipation term $T\mathcal{S}$ (35) is just the difference between the total mechanical work exerted upon the system, $W(\Gamma)$, and the reversible work, $W_{\text{rev}} = \Delta F$. It is customary to define this quantity as the dissipated work, W_{diss},

$$W_{\text{diss}}(\Gamma) = T\mathcal{S}(\Gamma) = W(\Gamma) - \Delta F = W(\Gamma) - W_{\text{rev}} \quad . \tag{39}$$

The nonequilibrium equality (16) becomes the nonequilibrium work relation originally derived by Jarzynski using Hamiltonian dynamics [31],

$$\langle \exp\left(-\frac{W_{\text{diss}}}{T}\right) \rangle = 1 \quad \text{or} \quad \langle \exp\left(-\frac{W}{T}\right) \rangle = \exp\left(-\frac{\Delta F}{T}\right) \quad . \tag{40}$$

This relation is called the Jarzynski equality (hereafter referred as JE) and can be used to recover free energies from nonequilibrium simulations or experiments (see Sec. 4.2.2). The FT (27) becomes the Crooks fluctuation theorem (hereafter referred as CFT) [44, 45],

$$\frac{P_F(W_{\text{diss}})}{P_R(-W_{\text{diss}})} = \exp\left(\frac{W_{\text{diss}}}{T}\right) \quad \text{or} \quad \frac{P_F(W)}{P_R(-W)} = \exp\left(\frac{W - \Delta F}{T}\right) \quad . \tag{41}$$

The second law of thermodynamics $\overline{W} \geq \Delta F$ also follows naturally as a particular case of (18) by using (39,40). Note that for the heat Q a general relation equivalent to (41) does not exist. We mention three aspects of the JE and the CFT.

- **The fluctuation-dissipation parameter R.** In the limit of small dissipation $W_{\text{diss}} \rightarrow 0$ the linear response result (28) holds. It is then possible to introduce a parameter ,R, that measures deviations from the linear response behavior[1]. It is defined as,

$$R = \frac{\sigma_W^2}{2TW_{\text{diss}}} \tag{42}$$

where $\sigma_W^2 = <W^2> - <W>^2$ is the variance of the work distribution. In the limit $W_{\text{diss}} \rightarrow 0$, a second order cumulant expansion in (40) shows that R is equal to 1 and (28) holds. Deviations from $R = 1$ are interpreted as deviations of the work distribution from a Gaussian. When the work distribution is non-Gaussian the system is far from the linear response regime and (28) is not satisfied anymore.

- **The Kirkwood formula.** A particular case of the JE (40) is the Kirkwood formula [46, 47]. It corresponds to the case where the control parameter only takes two values λ_0 and λ_1. The system is initially in equilibrium at the value λ_0 and, at an arbitrary later time t, the value of λ instantaneously switches to λ_1. In this case (37) reads,

$$W(\Gamma) = \Delta E_\lambda(\mathcal{C}) = E_{\lambda_1}(\mathcal{C}) - E_{\lambda_0}(\mathcal{C}) \quad . \tag{43}$$

In this case a path corresponds to a single configuration, $\Gamma \equiv \mathcal{C}$, and (40) becomes,

$$\overline{\exp\left(-\frac{\Delta E_\lambda(\mathcal{C})}{T}\right)} = \exp\left(-\frac{\Delta F}{T}\right) \tag{44}$$

the average $\overline{(..)}$ is taken over all configurations $\mathcal{C}$ sampled according to the equilibrium distribution taken at λ_0, $P_{\lambda_0}^{\text{eq}}(\mathcal{C})$.

---

[1]Sometimes R is called fluctuation-dissipation ratio, not to be confused with the identically called but different quantity introduced in glassy systems, see Sec.6.2, that quantifies deviations from the fluctuation-dissipation theorem that is valid in equilibrium.

- **Heat exchange between two bodies.** Suppose that we take two bodies initially at equilibrium at temperatures T_H, T_C where T_H, T_C stand for a hot and a cold temperature. At time $t = 0$ we put them in contact and ask about the probability distribution of heat flow between them. In this case, no work is done between the two bodies and the heat transferred is equal to the energy variation of each of the bodies. Let Q be equal to the heat transferred from the hot to the cold body in one experiment. It can be shown [48] that in this case the total dissipation $\mathcal{S}$ is given by,

$$\mathcal{S} = Q(\frac{1}{T_c} - \frac{1}{T_H}) \tag{45}$$

and the equality (40) reads,

$$\langle \exp\left(-Q(\frac{1}{T_c} - \frac{1}{T_H})\right) = 1 \rangle \tag{46}$$

showing that, in average, net heat is always transferred from the hot to the cold body. Yet, sometimes, we also expect some heat to flow from the cold to the hot body. Again, the probability of such events will be exponentially small with the size of the system.

3.3.2 Nonequilibrium steady states (NESS)

Most investigations in nonequilibrium systems were initially carried out in NESS. It is widely believed that NESS are among the best candidate nonequilibrium systems to possibly extend Boltzmann-Gibbs ensemble theory beyond equilibrium [49, 50].

We can distinguish two types of NESS: Time-dependent conservative (C) systems and non-conservative (NC) systems. In the C case the system is acted by a time-dependent force that derives from an external potential. In the NC case the system is driven by (time dependent or not) non-conservative forces. In C systems the control parameter λ has the usual meaning: it specifies the set of external parameters that, once fixed, determine an equilibrium state. Examples are: a magnetic dipole in an oscillating field (λ is the value of the time-dependent magnetic field); a bead confined in an moving optical trap and dragged through water (λ is the position of the center of the moving trap); a fluid sheared between two plates (λ is the time-dependent relative position of the upper and lower plates). In C systems we assume local detailed balance so (8) still holds.

In contrast to the C case, in NC systems the local detailed balance property, in the form of (8), does not hold because the system does not reach thermal equilibrium but a stationary or steady state. It is then customary to characterize the NESS by the parameter λ and the stationary distribution by $P^{\mathrm{ss}}_\lambda(\mathcal{C})$. NESS systems in the linear regime (i.e. not driven arbitrarily far from equilibrium) satisfy the Onsager reciprocity relations where the fluxes are proportional to the forces. NESS can be maintained, either by keeping constant the forces or the fluxes. Examples of NC systems are: the flow of a current in an electric circuit (e.g. $\lambda = I, \Delta V$ is either the constant current flowing through the circuit or the constant voltage difference); a Poiseuille fluid flow inside a cylinder (λ could be either the constant fluid flux, Φ, or the pressure difference, ΔP); heat flowing between two sources kept at two different temperatures (λ could be either the heat flux, J_Q, or the temperature difference, ΔT); the particle exclusion process ($\lambda = \mu^{+,-}$ are the rates of inserting and removing particles at both

ends of the chain). In NESS of NC type the local detailed balance property (8) holds but replacing $P_\lambda^{\text{eq}}(\mathcal{C})$ by the corresponding stationary distribution, $P_\lambda^{\text{ss}}(\mathcal{C})$,

$$\frac{\mathcal{W}_\lambda(\mathcal{C} \to \mathcal{C}')}{\mathcal{W}_\lambda(\mathcal{C}' \to \mathcal{C})} = \frac{P_\lambda^{\text{ss}}(\mathcal{C}')}{P_\lambda^{\text{ss}}(\mathcal{C})} \quad . \tag{47}$$

In a steady state in a NC system λ is maintained constant. Because the local form of detailed balance (47) holds the main results of Sec. 3 follow. In particular, the nonequilibrium equality (16) and the FT (27) are still true. However there is an important difference. In steady states the reverse process is identical to the forward process $P_F(\mathcal{S}) = P_R(\mathcal{S})$ because λ is maintained constant. Therefore (16) and the FT (27) become,

$$\langle \exp(-\mathcal{S}) \rangle = 1 \tag{48}$$

$$\frac{P(\mathcal{S})}{P(-\mathcal{S})} = \exp(\mathcal{S}) \quad . \tag{49}$$

We can now extract a general FT for the entropy production S_p in NESS. Let us assume that, in average, S_p grows linearly with time, i.e. $S_p \gg B$ for large t. Because $\mathcal{S} = S_p + B$ (23), in the large t limit fluctuations in $\mathcal{S}$ are asymptotically dominated by fluctuations in S_p. In average, fluctuations in S_p grow like $\sqrt{t}$ whereas fluctuations in the boundary term are finite. Therefore, (23) should be asymptotically valid in the large t limit. By taking the logarithm in the right expression we obtain,

$$S = \log(P(S)) - \log(P(-S)) \to S_p + B = \log(P(S_p + B)) - \log(P(S_p - B)) \quad . \tag{50}$$

In NESS the entropy produced, $S_p(\Gamma)$, along paths of duration t is a fluctuating quantity. Expanding (50) around S_p we get,

$$S_p = \log\Big(\frac{P(S_p)}{P(-S_p)}\Big) + B\Big(\frac{P'(S_p)}{P(S_p)} - \frac{P'(-S_p)}{P(-S_p)} - 1\Big) \tag{51}$$

The average entropy production $\langle S_p \rangle$ is defined by averaging S_p along an infinite number of paths. Dividing (51) by $\langle S_p \rangle$ we get,

$$\frac{S_p}{\langle S_p \rangle} = \frac{1}{\langle S_p \rangle} \log\Big(\frac{P(S_p)}{P(-S_p)}\Big) + \frac{B}{\langle S_p \rangle}\Big(\frac{P'(S_p)}{P(S_p)} - \frac{P'(-S_p)}{P(-S_p)} - 1\Big) \tag{52}$$

We introduce a quantity a that is equal to the ratio between the entropy production and its average value, $a = \frac{S_p}{\langle S_p \rangle}$. We can define the function,

$$f_t(a) = \frac{1}{\langle S_p \rangle} \log\Big(\frac{P(a)}{P(-a)}\Big) \quad . \tag{53}$$

Equation (52) can be rewritten as,

$$f_t(a) = a - \frac{B}{\langle S_p \rangle}\Big(\frac{P'(S_p)}{P(S_p)} - \frac{P'(-S_p)}{P(-S_p)} - 1\Big) \tag{54}$$

In the large time limit, assuming that $\log(P(S_p)) \sim t$, and because B is finite, the second term vanishes relative to the first and $f_t(a) = a + \mathcal{O}(1/t)$. Substituting this result into (53) we

find that an FT holds in the large t limit. However, this is not necessarily always true. Even for very large t there can be strong deviations in the initial and final state that can make the boundary term B large enough to be comparable to $\langle S_p \rangle$. In other words, for certain initial and/or final conditions, the second term in the rhs of (54) can be on the same order and comparable to the first term, a. The boundary term can be neglected only if we restrict the size of such large deviations, i.e. if we require $|a| \leq a^*$ where a^* is a maximum given value. With this proviso, the FT in NESS reads,

$$\lim_{t \to \infty} \frac{1}{\langle S_p \rangle} \log \Big(\frac{P(a)}{P(-a)} \Big) = a \qquad ; \qquad |a| \leq a^* \tag{55}$$

In general it can be very difficult to determine the nature of the boundary terms. A specific result in an exactly solvable case is discussed below in Sec. 4.1.2. Eq.(55) is the Gallavotti-Cohen FT derived in the context of deterministic Anosov systems [28]. In that case S_p stands for the so called phase space compression factor. It has been experimentally tested by Ciliberto and coworkers in Rayleigh-Bernard convection [51] and turbulent flows [52]. Similar relations have been also tested in athermal systems, e.g. in fluidized granular media [53] or the case of two-level systems in fluorescent diamond defects excited by light [54].

The FT (27) also describes fluctuations in the total dissipation for transitions between steady states where λ varies according to a given protocol. In that case, the system starts at time 0 in a given steady state, $P_{\lambda_0}^{\mathrm{ss}}(\mathcal{C})$, and evolves away from that steady state at subsequent times. The boundary term for steady state transitions is then given by,

$$B(\Gamma) = \log(P_{\lambda_0}^{\mathrm{ss}}(\mathcal{C}_0)) - \log(P_{\lambda_M}^{\mathrm{ss}}(\mathcal{C}_M)) \tag{56}$$

where we have chosen the boundary function $b(\mathcal{C}) = P_{\lambda_M}^{\mathrm{ss}}(\mathcal{C})$. In that case the total dissipation is antisymmetric under the time-reversal operation and (27) holds. Only in cases where the reverse process is equivalent to the forward process (49) is an exact result. Transitions between nonequilibrium steady states and definitions of the function $\mathcal{S}$ have been considered by Hatano and Sasa in the context of Langevin systems [55].

4   Examples and applications

In this section we analyze in detail two cases where analytical calculations can be carried out and FTs have been experimentally tested. We have chosen two examples: one extracted from physics, the other from biology. We first analyze the bead in a trap to later consider single molecule pulling experiments. These examples show that there are lots of interesting observations that can be made by comparing theory and nonequilibrium experiments in simple systems.

4.1   A physical system: a bead in an optical trap

It is very instructive to work out in detail the fluctuations of a bead trapped in a moving potential. This case is of great interest for at least two reasons. First, it provides a simple example of both a NETS and a NESS that can be analytically solved in detail. Second, it can be experimentally realized by trapping micron-sized beads using optical tweezers. The first experiments studying nonequilibrium fluctuations in a bead in a trap were carried out by

Evans and collaborators [56] and later on extended in a series of works [57, 58]. Mazonka and Jarzynski [59] and later Van Zon and Cohen [60, 61, 62] have carried out detailed theoretical calculations of heat and work fluctuations. Recent experiments have also analyzed the case of a particle in a non-harmonic optical potential [63]. These results have greatly contributed to clarify the general validity of the FT and the role of the boundary terms appearing in the total dissipation $\mathcal{S}$.

The case of a bead in a trap is also equivalent to the power fluctuations in a resistance in an RC electrical circuit [64] (see Figure 4). The experimental setup is shown in Figure 5. A micron-sized bead is immersed in water and trapped in an optical well. In the simplest case the trapping potential is harmonic. Here we will assume that the potential well can have an arbitrary shape and carry out specific analytical computations for the harmonic case.

Let x be the position of the bead in the laboratory frame and $U(x - x^*)$ the trapping potential of a laser focus that is centered at a reference position x^*. For harmonic potentials we will take $U(x) = (1/2)\kappa x^2$. By changing the value of x^* the trap is shifted along the x coordinate. A nonequilibrium state can be generated by changing the value of x^* according to a protocol $x^*(t)$. In the notation of the previous sections, $\lambda \equiv x^*$ is the control parameter and $\mathcal{C} \equiv x$ is the configuration. A path Γ starts at $x(0)$ at time 0 and ends at $x(t)$ at time t, $\Gamma \equiv \{x(s); 0 \le s \le t\}$.

At low Reynolds number the motion of the bead can be described by a one-dimensional Langevin equation that contains only the overdamping term,

$$\gamma \dot{x} = f_{x^*}(x) + \eta \qquad ; \qquad \langle \eta(t)\eta(s) \rangle = 2T\gamma\delta(t - s) \tag{57}$$

where x is the position of the bead in the laboratory frame, γ is the friction coefficient, $f_{x^*}(x)$ is a conservative force deriving from the trap potential $U(x - x^*)$,

$$f_{x^*}(x) = -(U(x - x^*))' = -\left(\frac{\partial U(x - x^*)}{\partial x}\right) \tag{58}$$

and η is a stochastic white noise.

In equilibrium $x^*(t) = x^*$ is constant in time. In this case, the stationary solution of the master equation is the equilibrium solution

$$P_{x^*}^{\mathrm{eq}}(x) = \frac{\exp(-\frac{U(x-x^*)}{T})}{\int dx \exp(-U(x - x^*)/T)} = \frac{\exp(-\frac{U(x-x^*)}{T})}{\mathcal{Z}} \tag{59}$$

where $\mathcal{Z} = \int dx \exp(-U(x)/T)$ is the partition function that is independent of the reference position x^*. Because the free energy $F = -T\log(\mathcal{Z})$ does not depend on the control parameter x^*, the free energy change is always zero for arbitrary translations of the trap.

Let us now consider a NESS where the trap is moved at constant velocity, $x^*(t) = vt$. It is not possible to solve the Fokker-Planck equation to find the probability distribution in the steady state for arbitrary potentials. Only for harmonic potentials, $U(x) = \kappa x^2/2$, the Fokker-Planck equation can be solved exactly. The result is,

$$P_{x^*}^{\mathrm{ss}}(x) = \left(\frac{2\pi T}{\kappa}\right)^{-\frac{1}{2}} \exp\left(-\frac{\kappa(x - x^*(t) + \frac{\gamma v}{\kappa})^2}{2T}\right) \tag{60}$$

Note that the steady-state solution (60) depends explicitly on time through $x^*(t)$. To obtain a time-independent solution we must change variables $x \to x - x^*(t)$ and describe the motion of the bead in the reference frame that is solidary and moves with the trap. We will come back to this problem later in Sec. 4.1.3.

4.1.1 Microscopic reversibility

In this section we show that the Langevin dynamics (57) satisfies the microscopic reversibility assumption or local detailed balance (8). We recall that x is the position of the bead in the laboratory frame. The transition rates $\mathcal{W}_{x^*}(x \to x')$ for the configuration x at time t to change to x' at a later time $t + \Delta t$ can be computed from (57). We discretize the Langevin equation [65] by writing,

$$x' = x + \frac{f(x - x^*)}{\gamma}\Delta t + \sqrt{\frac{2T\Delta t}{\gamma}}r + \mathcal{O}\big((\Delta t)^2\big) \tag{61}$$

where r is a random Gaussian number of zero mean and unit variance. For a given value of x, the distribution of values x' is also a Gaussian with average and variance given by,

$$\overline{x'} = x + \frac{f(x - x^*(t))}{\gamma}\Delta t + \mathcal{O}\big((\Delta t)^2\big) \tag{62}$$

$$\sigma_{x'}^2 = \overline{(x')^2} - (\overline{(x')})^2 = \frac{2T\Delta t}{\gamma} + \mathcal{O}\big((\Delta t)^2\big) \tag{63}$$

and therefore,

$$\mathcal{W}_{x^*}(x \to x') = (2\pi\sigma_{x'}^2)^{-\frac{1}{2}}\exp\Big(-\frac{(x' - x + \frac{f(x-x^*)\Delta t}{\gamma})^2}{2\sigma_{x'}^2}\Big) \quad . \tag{64}$$

From (64) we compute the ratio between the transition probabilities to first order in Δt,

$$\frac{\mathcal{W}_{x^*}(x \to x')}{\mathcal{W}_{x^*}(x' \to x)} = \exp\Big(-\frac{(x' - x)(f(x - x^*) + f(x' - x^*))}{2T}\Big) \quad . \tag{65}$$

We can now use the Taylor expansions,

$$U(x' - x^*) = U(x - x^*) - f(x - x^*)(x' - x) + \mathcal{O}((x' - x)^2) \tag{66}$$

$$U(x - x^*) = U(x' - x^*) - f(x' - x^*)(x - x') + \mathcal{O}((x' - x)^2) \tag{67}$$

and subtract both equations to finally obtain,

$$(x' - x)(f(x - x^*) + f(x' - x^*)) = 2(U(x' - x^*) - U(x - x^*)) \tag{68}$$

which yields,

$$\frac{\mathcal{W}_{x^*}(x \to x')}{\mathcal{W}_{x^*}(x' \to x)} = \exp\Big(-\frac{U(x' - x^*) - U(x - x^*)}{T}\Big) = \frac{P_{x^*}^{\mathrm{eq}}(x')}{P_{x^*}^{\mathrm{eq}}(x)} \tag{69}$$

which is the local detailed balance assumption (8).

4.1.2 Entropy production, work and total dissipation

Let us consider an arbitrary nonequilibrium protocol $x^*(t)$ where $v(t) = \dot{x}^*(t)$ is the velocity of the moving trap. The entropy production for a given path, $\Gamma \equiv \{x(s); 0 \le s \le t\}$ can be computed using (22),

$$S_p(\Gamma) = \int_0^t ds\,\dot{x}(s)\Big(\frac{\partial \log P_{x^*(s)}^{\mathrm{eq}}(x)}{\partial x}\Big)_{x=x(s)} \quad . \tag{70}$$

23

We now define the variable $y(t) = x(t) - x^*(t)$. From (59) we get [2],

$$S_p(\Gamma) = \frac{1}{T} \int_0^t ds \dot{x}(s) f(x(s) - x^*(s)) = \frac{1}{T} \int_0^t ds(\dot{y}(s) + v(s)) f(y(s)) = \tag{71}$$

$$\frac{1}{T}\left(\int_{y(0)}^{y(t)} dy f(y) + \int_0^t ds v(s) f(s)\right) = \frac{-\Delta U + W(\Gamma)}{T} \tag{72}$$

with

$$\Delta U = U(x(t) - x^*(t)) - U(x(0) - x^*(0)) \quad ; \quad W(\Gamma) = \int_0^t ds v(s) f(s) \quad . \tag{73}$$

where we used (58) in the last equality of (72). ΔU is the variation of internal energy between the initial and final positions of the bead and $W(\Gamma)$ is the mechanical work done on the bead by the moving trap. Using the first law $\Delta U = W - Q$ we get,

$$S_p(\Gamma) = \frac{Q(\Gamma)}{T} \tag{74}$$

and the entropy production is just the heat transferred from the bead to the bath divided by the temperature of the bath.

The total dissipation $\mathcal{S}$ (23) can be evaluated by adding the boundary term (24) to the entropy production. For the boundary term we have some freedom as to which function b we use in the rhs of (24),

$$B(\Gamma) = \log\left(P_{x^*(0)}(x(0))\right) - \log\left(b(x(t))\right) \quad . \tag{75}$$

Because we want $\mathcal{S}$ to be antisymmetric against time-reversal there are two possible choices for the function b depending on the initial state,

- **Nonequilibrium transient state (NETS).** Initially the bead is in equilibrium and the trap is at rest in a given position $x^*(0)$. Suddenly the trap is set in motion. In this case $b(x) = P_{x^*(t)}^{\text{eq}}(x)$ and the boundary term (24) reads,

$$B(\Gamma) = \log\left(P_{x^*(0)}^{\text{eq}}(x(0))\right) - \log\left(P_{x^*(t)}^{\text{eq}}(x(t))\right) \quad . \tag{76}$$

By inserting (59) we obtain,

$$B(\Gamma) = \frac{1}{T}(U(x(t) - x^*(t)) - U(x(0) - x^*(0))) = \frac{\Delta U}{T} \tag{77}$$

and $\mathcal{S} = S_p + B = (Q + \Delta U)/T = W/T$ so the work satisfies the nonequilibrium equality (16) and the FT (27),

$$\frac{P_F(W)}{P_R(-W)} = \exp\left(\frac{W}{T}\right) \tag{78}$$

Note that in the reverse process the bead starts in equilibrium at the final position $x^*(t)$ and the motion of the trap is reversed $(x^*)^R(s) = x^*(t - s)$. The result (78) is valid for

---

[2]Note that $\dot{x}$, the velocity of the bead, is not well defined in (70,72). However, $ds\dot{x}(s) = dx$ it is. Yet we prefer to use the notation in terms of velocities just to make clear the identification between the time integrals in (70,72) and the discrete time-step sum in (22).

arbitrary potentials $U(x)$. In general, the reverse work distribution $P_R(W)$ will differ from the forward distribution $P_F(W)$. Only for symmetric potentials $U(x) = U(-x)$ both work distributions are identical [66]. Under this additional assumption (78) reads,

$$\frac{P(W)}{P(-W)} = \exp(\frac{W}{T}) \tag{79}$$

Note that this is a particular case of the CFT (41) with $\Delta F = 0$.

- **Nonequilibrium steady state (NESS).** If the initial state is a steady state, $P_{\lambda_0}(\mathcal{C}_0) \equiv P^{ss}_{x^*(0)}(x)$, then we choose $b(x) = P^{ss}_{x^*(t)}(x)$. The boundary term reads,

$$B(\Gamma) = \log\left(P^{ss}_{x^*(0)}(x(0))\right) - \log\left(P^{ss}_{x^*(t)}(x(t))\right) \tag{80}$$

Only for harmonic potentials we exactly know the steady state solution (60) so we can write down an explicit expression for B,

$$B(\Gamma) = \frac{\Delta U}{T} - \frac{v\gamma\Delta f}{\kappa T} \tag{81}$$

where ΔU is defined in (73) and $\Delta f = f_{x^*(t)}(x(t)) - f_{x^*(0)}(x(0))$. The total dissipation is given by,

$$S = S_p + B = \frac{Q + \Delta U}{T} - \frac{v\gamma\Delta f}{\kappa T} = \frac{W}{T} - \frac{v\gamma\Delta f}{\kappa T} \quad . \tag{82}$$

It is important to stress that (82) does not satisfy (48,49) because the last boundary term in the rhs of (82) ($v\gamma\Delta f/\kappa T$) is not antisymmetric against time reversal. Van Zon and Cohen [60, 61, 62] have analyzed in much detail work and heat fluctuations in the NESS. They find that work fluctuations satisfy the exact relation,

$$\frac{P(W)}{P(-W)} = \exp\left(\frac{W}{T}\frac{1}{1 + \frac{\tau}{t}(\exp(-\frac{t}{\tau}) - 1)}\right) \tag{83}$$

where t is the time window over which work is measured and τ is the relaxation time of the bead in the trap, $\tau = \gamma/\kappa$. Note that the FT (79) is satisfied in the limit $\tau/t \to 0$. Corrections to the FT are on the order of τ/t as expected (see discussion in the last part of Sec. 3.3.2). Computations can be also carried out for heat fluctuations. The results are expressed in terms of the relative fluctuations of the heat, $a = \frac{S_p}{\langle S_p \rangle}$. The large deviation function $f_t(a)$ (53) is given by,

$$\lim_{t\to\infty} f_t(a) = a \quad (0 \le a \le 1);$$
$$\lim_{t\to\infty} f_t(a) = a - (a-1)^2/4 \quad (1 \le a < 3);$$
$$\lim_{t\to\infty} f_t(a) = 2 \quad (3 \le a); \tag{84}$$

and $f_t(-a) = -f_t(a)$. Very accurate experiments to test (83,84) have been carried out by Garnier and Ciliberto who measured the Nyquist noise in an electric resistance [67]. Their results are in very good agreement with the theoretical predictions which include corrections in the convergence of (84) on the order of $1/t$ as expected. A few results are shown in Figure 4.
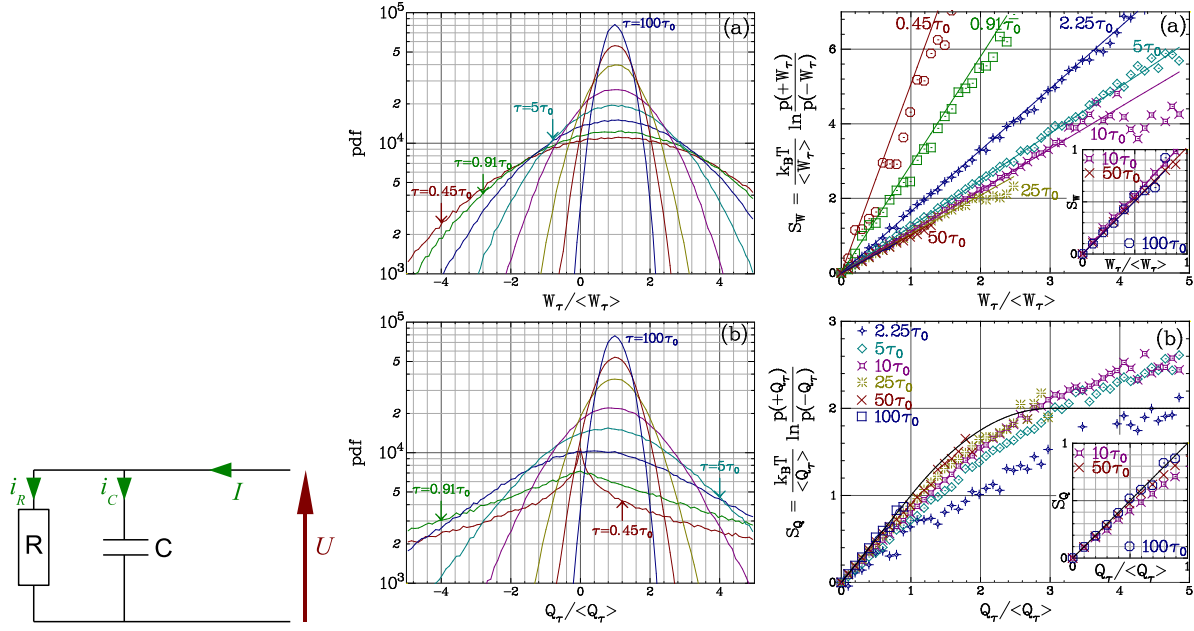
Figure 4: *Heat and work fluctuations in an electrical circuit (left). PDF distributions (center) and verification of the FTs (83,84) (right). Figure taken from [67].*

4.1.3 Transitions between steady states

Hatano and Sasa [55] have derived an interesting result for nonequilibrium transitions between steady states. Despite of the generality of Hatano and Sasa's approach, explicit computations can be worked out only for harmonic traps. In the present example the system starts in a steady state described by the stationary distribution (60) and is driven away from that steady state by varying the speed of the trap, v. The stationary distribution can be written in the frame system that moves solidary with the trap. If we define $y(t) = x - x^*(t)$ then (60) becomes,

$$P_v^{\mathrm{ss}}(y) = (2\pi T/\kappa)^{-\frac{1}{2}} \exp\left(-\frac{\kappa(y + \frac{\gamma v}{\kappa})^2}{2T}\right) \quad . \tag{85}$$

Note that, when expressed in terms of the reference moving frame, the distribution in the steady state becomes stationary or time independent. The transition rates (64) can also be expressed in the reference system of the trap,

$$\mathcal{W}_v(y \to y') = \left(\frac{4\pi T \Delta t}{\gamma}\right)^{-\frac{1}{2}} \exp\left(-\frac{\gamma(y' - y + (v + \frac{\kappa}{\gamma}y)\Delta t)^2}{4T\Delta t}\right) \tag{86}$$

where we have used $f(x - x^*) = f(y) = -\kappa y$. The transition rates $\mathcal{W}_v(y \to y')$ now depend on the velocity of the trap. This shows that, for transitions between steady states, $\lambda \equiv v$ plays the role of the control parameter, rather than the value of x^*. A path is then defined by the evolution $\Gamma \equiv \{y(s); 0 \le s \le t\}$ whereas the perturbation protocol is specified by the time evolution of the speed of the trap $\{v(s); 0 \le s \le t\}$.

The rates $\mathcal{W}_v(y \to y')$ satisfy the local detailed balance property (47). From (86) and (85)

26

we get (in the limit $\Delta t \to 0$),

$$\frac{\mathcal{W}_v(y \to y')}{\mathcal{W}_v(y' \to y)} = \frac{P_v^{\mathrm{ss}}(y')}{P_v^{\mathrm{ss}}(y)} = \tag{87}$$

$$= \exp\Big(-\frac{\kappa}{2T}(y'^2 - y^2) - \frac{\gamma v}{T}(y' - y)\Big) = \exp\Big(-\big(\frac{\Delta U}{T} - \frac{v \gamma \Delta f}{\kappa T}\big)\Big) \tag{88}$$

Note that the exponent in the rhs of (88) is equal to the boundary term (81). In the reference system of the trap we can then compute the entropy production S_p and the total dissipation S. From either (22) or (88) and using (85) we get,

$$S_p(\Gamma) = \int_0^t ds \dot{y}(s) \Big(\frac{\log(P_v^{\mathrm{ss}}(y))}{\partial y}\Big)_{y=y(s)} = -\frac{\Delta U}{T} + \frac{\gamma}{\kappa T} \int_0^t ds v(s) \dot{F}(s) = \tag{89}$$

$$= -\frac{1}{T}\Big(\Delta U - \frac{\gamma}{\kappa}(\Delta(vF)) + \frac{\gamma}{\kappa}\int_0^t ds \dot{v}(s) F(s)\Big) \tag{90}$$

where we integrated by parts in the last step of the derivation. For the boundary term (56) we get,

$$B(\Gamma) = \log\Big(P_{v(0)}^{\mathrm{ss}}(y(0))\Big) - \log\Big(P_{v(t)}^{\mathrm{ss}}(y(t))\Big) = \tag{91}$$

$$\frac{1}{T}\Big(\Delta U - \frac{\gamma}{\kappa}(\Delta(vF)) + \frac{\gamma^2 \Delta(v^2)}{2\kappa}\Big) \tag{92}$$

where we used (85). By adding (90) and (92) we obtain the total dissipation,

$$S = S_p + B = \frac{1}{T}\Big(\Delta(\frac{\gamma^2 v^2}{2\kappa}) - \frac{\gamma}{\kappa}\int_0^t ds \dot{v}(s) F(s)\Big) = \tag{93}$$

$$= -\frac{\gamma}{\kappa}\int_0^t ds \dot{v}(s)(F(s) - \gamma v(s)) \tag{94}$$

The quantity S (called Y by Hatano and Sasa) satisfies the nonequilibrium equality (16) and the FT (27). Only for time reversal invariant protocols, $v^R(s) = v(t - s)$, we have $P_F(S) = P_R(S)$, and the FT (49) is also valid. We emphasize two aspects of (94),

- **Generalized second law for steady state transitions.** From the inequality (18) and (94) we obtain,

$$\frac{\gamma}{\kappa}\int_0^t ds \dot{v}(s) F(s) \leq \Delta(\frac{\gamma^2 v^2}{2\kappa}) \tag{95}$$

  which is reminiscent of the Clausius inequality $Q \geq -T\Delta S$ where the average dissipation rate $\overline{P}_{\mathrm{diss}} = \gamma v^2$ plays the role of a state function similar to the equilibrium entropy. In contrast to the Clausius inequality the transition now occurs between steady states rather than equilibrium states [68].

- **Non-invariance of entropy production under Galilean transformations.** In steady states where $\dot{v} = 0$, S_p (90) becomes a boundary term and $S = 0$ (94). We saw in (74) that S_p is equal to the heat delivered to the environment (and therefore proportional to the time elapsed t) whereas now S_p is a boundary term that does not grow with t. This important difference arises from the fact that the entropy production
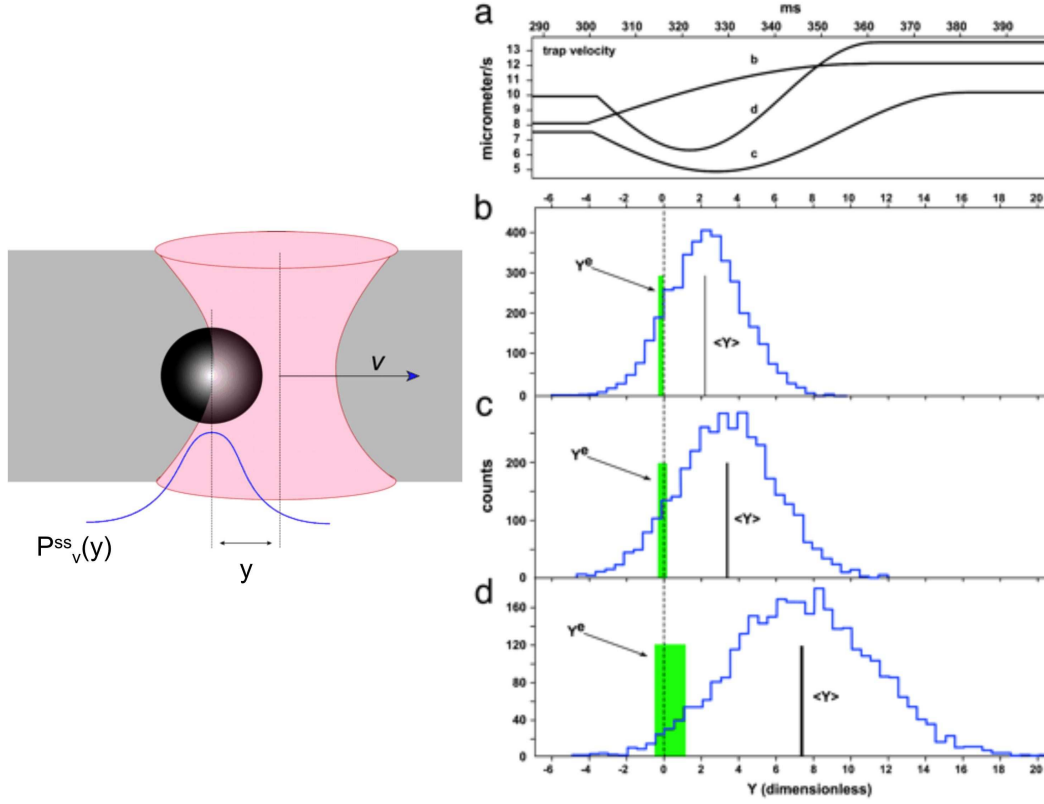
Figure 5: *(Left) Bead confined in a moving optical trap. (Right) Total entropy $\mathcal{S}$ distributions (b,c,d) for the velocity protocols shown in (a). Figure taken from [68].*

is not invariant under Galilean transformations. In the reference of the moving trap the bath is moving at a given speed which impedes to define the heat in a proper way. To evaluate the entropy production for transitions between steady states one has to resort to the description where x^* is the control parameter and $x^*(t) = \int_0^t ds\, v(s)$ is the perturbation protocol. In such description the results (73) and (74) are still valid.

These results have been experimentally tested for trapped beads accelerated with different velocity protocols [68]. Some results are shown in Figure 5.

4.2 A biological system: pulling biomolecules

The development of accurate instruments capable of measuring forces in the piconewton range and extensions on the order of the nanometer gives access to a wide range of phenomena in molecular biology and biochemistry where nonequilibrium processes that involve small energies on the order of a few $k_B T$ are measurable (see Sec. 2). From this perspective the study of biomolecules is an excellent playground to explore nonequilibrium fluctuations. The most successful investigations in this area have been achieved in single molecule experiments using optical tweezers [69]. In these experiments biomolecules can be manipulated one at a time by applying mechanical force at their ends. This allows us to measure small energies under varied conditions opening new perspectives in the understanding of fundamental problems in
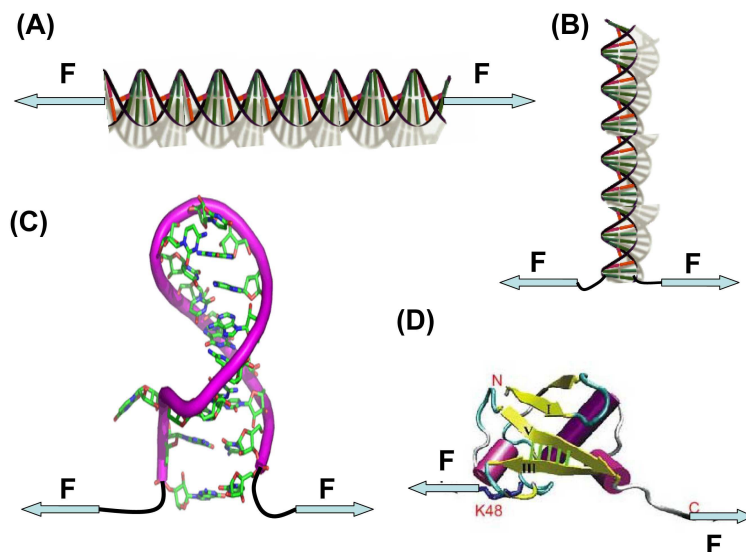
Figure 6: *Pulling single molecules. (A) Stretching DNA; (B) Unzipping DNA; (C) Mechanical unfolding of RNA and (D) Mechanical unfolding of proteins.*

biophysics, e.g. the folding of biomolecules [70, 71, 72]. The field of single molecule research is steadily growing with new molecular systems being explored that show nonequilibrium behavior characteristic of small systems. The reader interested in a broader view of the area of single molecules research is suggested to have a look at reference [73].

4.2.1 Single molecule force experiments

In single molecule force experiments it is possible to apply force on individual molecules by grabbing their ends and pulling them apart [74, 75, 76, 77]. Examples of different ways in which mechanical force is applied to single molecules are shown in Figure 6. In what follows we will consider single molecule force experiments using optical tweezers, although everything we will say extends to other force techniques (AFM, magnetic tweezers or biomembrane force probe, see [73]) In these experiments, the ends of the molecule (for example DNA [78]) are labeled with chemical groups (e.g. biotin or digoxigenin) that can bind specifically to their complementary molecular partners (e.g. streptavidin or anti-digoxigenin respectively). Beads are then coated with the complementary molecules and mixed with the DNA in such a way that a tether connection can be made between the two beads through specific attachments. One bead is in the optical trap and used as a force sensor. The other bead is immobilized on the tip of a micropipette that can be moved by using a piezo-controlled stage to which the pipette is attached. The experiment consists in measuring force-extension curves (FECs) by moving the micropipette respect to the trap position [79]. In this way it is possible to investigate the mechanical and elastic properties of the DNA molecule [80, 81].

Many experiments have been carried out by using this setup: the stretching of single DNA molecules, the unfolding of RNA molecules or proteins and the translocation of molecular motors (Figure 2). Here we focus our attention in force experiments where mechanical work can be exerted on the molecule and nonequilibrium fluctuations measured. The most successful

studies along this line of research are the stretching of small domain molecules such as RNA [82] or protein motifs[83]. Small RNA domains consist of a few tens of nucleotides folded into a secondary structure that is further stabilized by tertiary interactions. Because an RNA molecule is too small to be manipulated with micron-sized beads, it has to be inserted between molecular handles. These act as polymer spacers that avoid non-specific interactions between the bead and the molecule as well as the contact between the two beads.

The basic experimental setting is shown in Figure 7. We also show a typical FEC for an RNA hairpin and a protein. Initially the FEC shows an elastic response due to the stretching of the molecular handles. Then, at a given value of the force, the molecule under study unfolds and a rip is observed in both force and extension. The rip corresponds to the unfolding of the small RNA/protein molecule. The molecule is then repeatedly stretched and relaxed starting from the equilibrated native/extended state in the pulling/relaxing process. In the pulling experiment the molecule is driven out of equilibrium to a NETS by the action of a time dependent force. The unfolding/refolding reaction is stochastic, the dissociation/formation of the molecular bonds that maintain the native structure of the molecule is being determined by the Brownian motion of the surrounding water molecules [84]. Each time the molecule is pulled different unfolding and refolding values of the force are observed (inset of Figure 7B). The average value of the force at which the molecule unfolds during the pulling process increases with the loading rate (roughly proportional to the pulling speed) in a logarithmic way as expected for a two-state process (see discussion at the end of Sec. 5.2.1 and equation (143)).

Single molecule pulling experiments can be described with the formalism developed in Sec. 3.3.1. In the simplest setting the configurational variable $\mathcal{C}$ corresponds to the molecular extension of the complex (handles plus inserted molecule) and the control parameter λ is either the force f measured in the bead or the molecular extension of the system, x. For small enough systems the thermodynamic equation of state is dependent on what is the variable that is externally controlled [86]. In the actual experiments, the assumption that either the force or the extension are controlled is just an approximation. Neither the molecular extension or the force can be really controlled in optical tweezers [87]. For example, in order to control the force a feedback mechanism must operate at all times. This feedback mechanism has a time delay response so the force is never really constant [88, 89]. By assuming the case where the force is constant we are neglecting some corrections in the analysis[3]. Under some conditions these corrections are shown to be unimportant (see below). Let us now consider that the force acting on the inserted molecule is controlled (the so called isotensional ensemble). For a molecule that is repeatedly pulled from a minimum force value, $f_{\min}$, up to a maximum force, $f_{\max}$, the work (37) along a given path is given by,

$$W_f(\Gamma) = \int_{f_{\min}}^{f_{\max}} df \frac{\partial E(x,f)}{\partial f} = -\int_{f_{\min}}^{f_{\max}} x(f) df \qquad (96)$$

where the energy function is given by $E(x,f) = E(x,0) - fx$, $E(x,0)$ being the energy function of the molecule at zero force. The subindex f in W_f is written to underline the fact that we are considering the isotensional case where f is the control parameter. The Jarzynski equality (40) and the FT (41) hold with ΔF equal to the free energy difference between the initial

---

[3]By using two traps, it is possible to maintain a constant force [90]. This is also possible with magnetic tweezers. However, because of the low stiffness of the magnetic trap, the spatial resolution due to thermal fluctuations is limited to a few tens of nanometers.
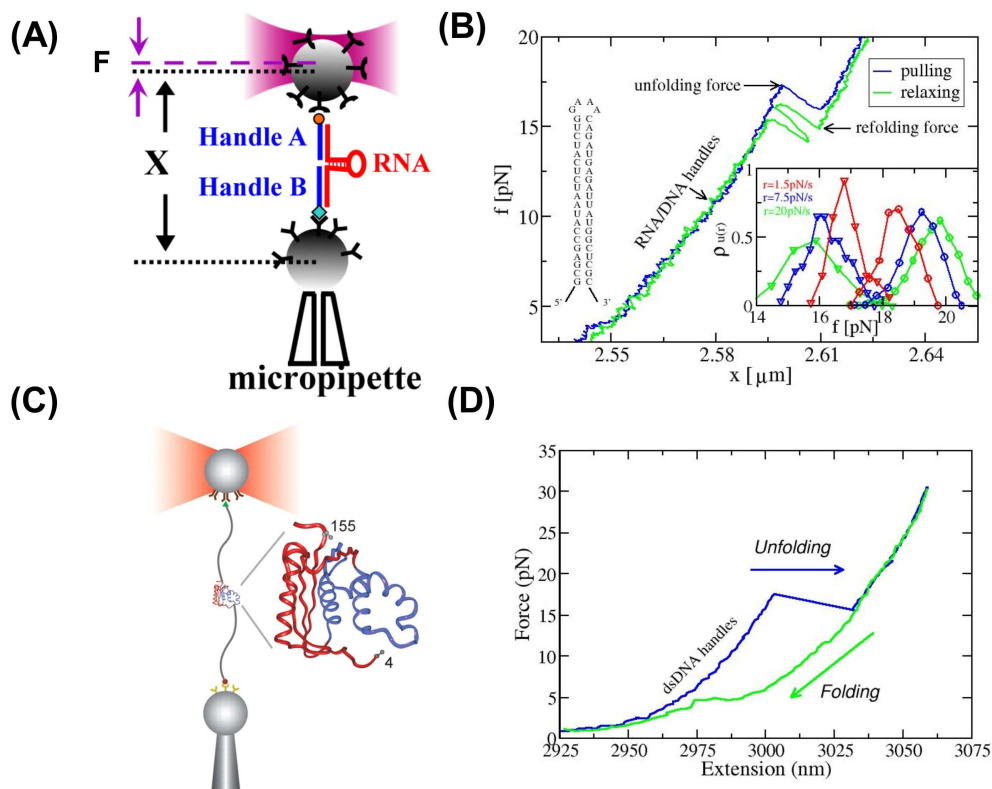
Figure 7: *Mechanical unfolding of RNA molecules (A,B) and proteins (C,D) using optical tweezers. (A) Experimental setup in RNA pulling experiments. (B) Pulling cycles in the homologous hairpin and force rip distributions during the unfolding and refolding at three pulling speeds. (C) Equivalent setup in proteins. (D) Force extension curve when pulling the protein RNAseH. Figure (B) taken from [85]. Figures (A,D) are a courtesy from C. Cecconi [83].*

and final equilibrium states. We assume that the molecule is immersed in water at constant temperature T, pressure p and acted by a force f. The thermodynamic free energy $F(T, p, f)$ in this description is the Legendre transform of the Gibbs free energy at zero force, ambient temperature T and pressure p, $G(T, p)$ [91, 92],

$$F(T, p, f) = G(T, p) - fx(T, p, f) \rightarrow x(T, P, f) = -\frac{\partial F(T, p, f)}{\partial f} \quad . \tag{97}$$

We are interested in knowing the Gibbs free energy difference at zero force, ΔG, rather than the free energy difference ΔF between the folded state at $f_{\min}$ and the unfolded-extended state at $f_{\max}$. We can express (40,41) in terms of G (rather than F) and define the corrected work $W_f^c(\Gamma)$ along a path,

$$W_f^c(\Gamma) = W_f(\Gamma) + \Delta(xf) = W_f(\Gamma) + (x_{\max} f_{\max} - x_{\min} f_{\min}) \tag{98}$$

where the extensions $x_{\min}, x_{\max}$ are now fluctuating quantities evaluated at the initial and final times along each pulling. The corrected work $W_f^c(\Gamma)$ includes an additional boundary term and therefore does not satisfy neither the JE and the CFT. If we now consider that x is the control parameter then we can define the equivalent of (96) (the so-called isometric ensemble),

$$W_x(\Gamma) = W_f(\Gamma) + \Delta(xf) = \int_{x_{\min}}^{x_{\max}} f(x)dx \tag{99}$$

where now x is controlled and $x_{\min}, x_{\max}$ are fixed by the pulling protocol. Equations (98,99) look identical, however they refer to different experimental protocols. Note that the term $W_f(\Gamma)$ appearing in (99) is now evaluated between the initial and final forces at fixed initial and final times. Both works W_x, W_f satisfy the relations (40,41). For a reversible process where f is controlled we have $W_f^{\text{rev}} = \Delta F$ whereas if x is controlled we have $W_x^{\text{rev}} = \Delta G$. In experiments it is customary to use (99) for the work. First, because that quantity is more easily recognized as the mechanical work. Second, because it gives the free energy difference between the folded and the unfolded states at zero force, a quantity that can be compared with thermal denaturation experiments.

In general neither the force or the molecular extension can be controlled in the experiments so both definitions (96,98,99) result into approximations to the *true* mechanical work that satisfies (40,41). The control parameter in single molecule experiments using optical tweezers is the distance between the center of trap and the immobilized bead [87]. Both the position of the bead in the trap and extension of the handles are fluctuating quantities. It has been observed [93, 94, 95] that in pulling experiments the proper work that satisfies the FT includes some corrections to the expressions (97,99) mainly due to the effect of the trapped bead. There are two considerations to take into account when analyzing experimental data:

- W_x **or** W_f? Let us suppose that f is the control parameter. In this case the JE and CFT (40,41) are valid for the work (96). How large is the error that we make when we apply the JE using W_x instead? This question has been experimentally addressed by Ciliberto and coworkers [96, 97] who measured the work in an oscillator system with high precision (within tenths of $k_B T$). As shown in (99) the difference between both works is mainly a boundary term, $\Delta(xf)$. Fluctuations of this term can be a problem if they are on the same order than fluctuations of W_x itself. For an harmonic oscillator of stiffness constant

equal to κ, the variance of fluctuations in fx are equal to $\kappa\delta(x^2)$, i.e. approximately on the order of $k_B T$ due to the fluctuation-dissipation relation. Therefore, for experimental measurements that do not reach such precision, W_x or W_f are equally good.

- **The effect of the bead or cantilever.** Hummer and Szabo [93] have analyzed the effect of a force sensor attached to the system (i.e. the bead in the optical trap or the cantilever in the AFM) in the work measurements. To this end they consider a simplified model of the experimental setup (Figure 8). In such model the molecular system (that includes the molecule of interest -RNA or protein- and the handles) is connected to a spring (that models the trapped bead or the AFM cantilever) and the whole system is embedded in a thermal bath. The total extension of the molecular system is x but the control parameter is $z = x + x_b$ where x_b is the position of the bead respect to the center of the trap. The total free energy of the system is given by $F(x) + (1/2)\kappa x_b^2$ where $F(x)$ is the free energy of the molecular system alone and κ is the stiffness of the trap. The molecular extension x and the distance x_b are related by the force balance equation,

$$f = \kappa x_b = \frac{\partial F(x)}{\partial x} \tag{100}$$

where we assume that the bead is locally equilibrated at all values of the nonequilibrium molecular extension x (this is a good approximation as the bead relaxes fast enough compared to the typical time for the unfolding/refolding of the molecule). The mechanical work (37) is then given by,

$$W(\Gamma) = \int_{z_{\min}}^{z_{\max}} f dz = W_x(\Gamma) + \Delta\left(\frac{f^2}{2\kappa}\right) \tag{101}$$

where we used $dz = dx_b + dx$ and (100). The difference between the proper work W and W_x is again a boundary term. Because z is the control parameter the JE and the CFT are valid for the work W but not for W_x. Again, the FT will not hold if fluctuations in the boundary term are important. The variance of these fluctuations is given by,

$$\langle\delta\left(\frac{f^2}{2\kappa}\right)\rangle \sim \frac{k_B T \kappa}{\kappa_x + \kappa} \leq k_B T \tag{102}$$

where κ_x is the stiffness of the molecular system [98, 87]. Usually, $\kappa_x \gg \kappa$ so fluctuations in the boundary term are again smaller than $k_B T$. In general, as a rule of thumb, we can say that it does not matter much which mechanical work we measure if we do not seek for free energy estimates with an accuracy less than $k_B T$. This is true unless the bead (cantilever) does not equilibrate within the timescale of the experiments. This may be the case when κ is too low and (100) is not applicable.

4.2.2 Free energy recovery

As we already emphasized the JE (40) and the FT (41) can be used to predict free energy differences. In single molecule experiments it is usually difficult to pull molecules in a reversible way due to drift effects in the instrument. It is therefore convenient to devise nonequilibrium methods (such as the JE or the CFT) to extract equilibrium free energies differences from
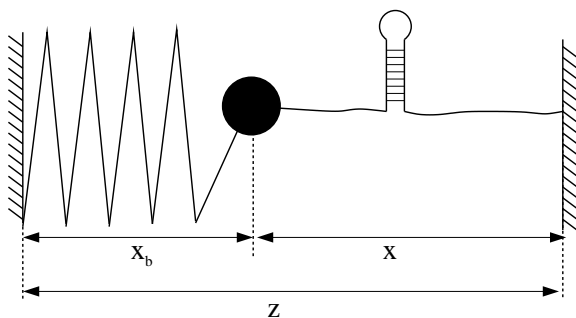
Figure 8: *A molecular system of extension x is connected at its leftmost end to a bead trapped in an optical well (or to the tip of an AFM cantilever) and at its rightmost end to an immobilized surface (or a bead fixed to the tip of micropipette). The position of the bead relative to the center of the trap, x_b, gives a read out of the acting force $f = \kappa x_b$. The control parameter in this setup is $z = x_b + x$ whereas both x_b and x are fluctuating quantities.*

data obtained in irreversible processes. The first experimental test of the JE was carried out by pulling RNA hairpins that are derivatives of the L21 Tetrahymena ribozyme [99]. In these experiments RNA molecules were pulled not too fast, the average dissipated work in such experiments was less $6k_BT$ and the work distributions turned out to be approximately Gaussian. Recent experiments have studied RNA molecules that are driven farther away from equilibrium in the non-linear regime. In such non-linear regime the average dissipated work is non-linear with the pulling speed [100] and the work distribution strongly deviates from a Gaussian [101]. In addition, these experiments have provided the first experimental test of the CFT (41). These measurements have also shown the possibility to recover free energy differences by using the CFT with larger accuracy than that obtained by using the JE alone. There are two main predictions of the CFT (41) that have been scrutinized in these experiments,

- **Forward and reverse work distributions cross at $W = \Delta G$.** In order to obtain ΔG we can measure the forward and reverse work distributions $P_F(W), P_R(-W)$ and look at the work value W^* where they cross, $P_F(W^*) = P_R(-W^*)$. According to (41) both distributions should cross at $W^* = \Delta G$ independently of how far the system is driven out of equilibrium (i.e. independently of the pulling speed). Figure 9 shows experiments on a short canonical RNA hairpin CD4 (i.e. just containing Watson-Crick complementary base pairs) at three different pulling speeds which agree very well with the FT prediction.

- **Verification of the CFT.** The CFT (41) can be tested by plotting $\log(P_F(W)/P_R(-W))$ as a function of W. The resulting points should fall in a straight line of slope 1 (in k_BT units) that intersects the work axis at $W = \Delta G$. Of course, this relation can be tested only in the region of work values along the work axis where both distributions (forward and reverse) overlap. An overlap between the forward and reverse distributions is hardly

34

Figure 9: *(A) Structure of the homologous CD4 hairpin. (B) FECs at a loading rate of 1.7pN/s. (C) Unfolding and refolding work distributions at three loading rates (see inset). The unfolding and refolding work distributions cross at a value ΔG independent of the pulling speed as predicted by the CFT. Data correspond to 100,400 and 700 pulls for the lowest, medium and highest pulling speeds respectively. (D) Test of the CFT at the intermediate loading rate 7.5pN/s for 4 different tethers. The trend of the data is reproducible from tether to tether and consistent with the CFT prediction. Figures taken from [101].*
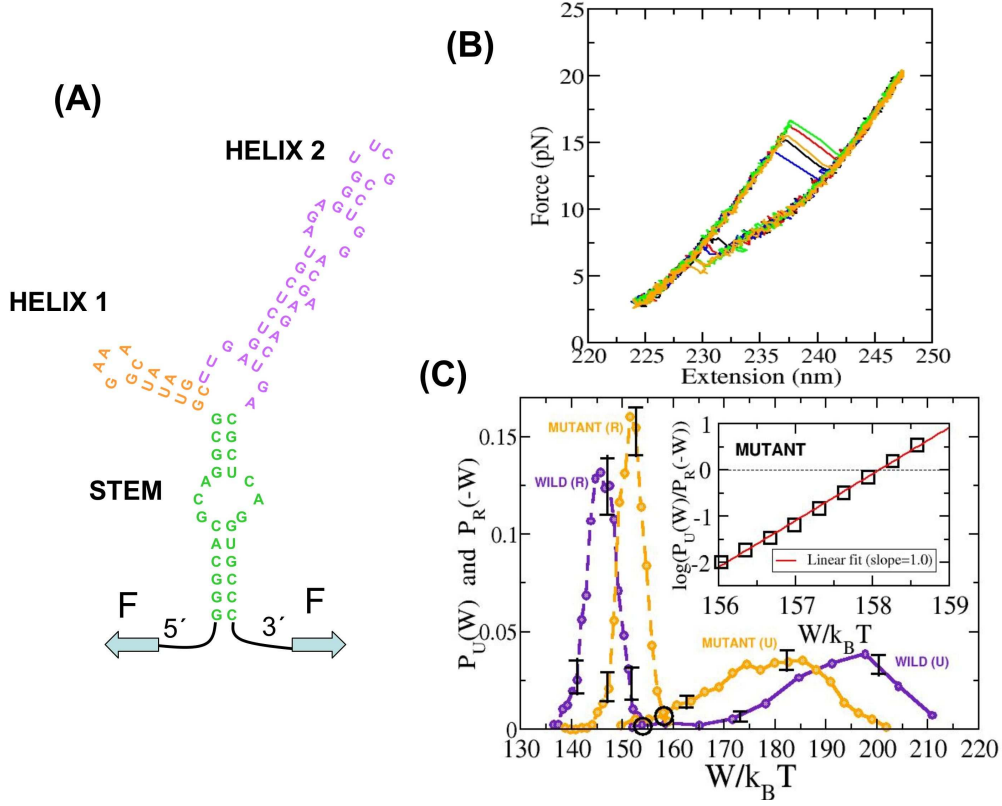
Figure 10: *(A) Secondary structure of the three way junction S15. (B) A few FECs for the wild type. (C) Unfolding/refolding work distributions for the wild type and the mutant. (Inset) Experimental verification of the validity of the CFT for the mutant where unfolding and refolding distributions overlap each other over a limited range of work values. Data correspond to 900 pulls for the wild type and 1200 pulls for the mutant. Figure taken from [101].*

observed if the molecules are pulled too fast or if the number of pulls is too small. In such cases, other statistical methods (Bennet's acceptance ratio or maximum likelihood methods, Sec. 4.2.3) can be applied to get reliable estimates of ΔG. The validity of the CFT has been tested in the case of the RNA hairpin CD4 previously mentioned and the three way junction RNA molecule as well. Figures 9C,D and 10C show results for these two molecules.

In general, both the JE and the CFT are only valid in the limit of an infinite number of pulls. For a finite number of pulls, N, the estimated value for ΔG that is obtained by applying the JE is biased [102]. The free-energy estimate F_k^{JE} for a given set, k, of N work values $W_1^k, W_2^k, ..., W_N^k$ is defined as,

$$F_k^{\mathrm{JE}} = -T \log\Big(\frac{1}{N} \sum_{i=1}^{N} \exp(-\frac{W_i^k}{T})\Big) \quad . \tag{103}$$

The free-energy bias is defined by averaging the estimator F_k^{JE} over an infinite number of sets,

$$B(N) = \lim_{M\to\infty}\Big[\frac{1}{M}\sum_{k=1}^{M} F_k^{\mathrm{JE}}\Big] - \Delta F \qquad (104)$$

where ΔF is the true free energy difference. The bias $B(N)$ converges to 0 for $N \to \infty$. However, it is of practical importance to devise methods to estimate how many pulls are required to obtain the Jarzynski free energy estimate F^{JE} within a reasonable error far from the true value [103, 100]. The bias is a complicated mathematical object because the Jarzynski average catches important contributions from large deviations of the work. As we will see later in Sec. 5.3.2, the bias is a large deviation function that requires specific mathematical methods to analyze its finite N behavior and large N convergence. There we proof that, for large N, the bias decreases as $1/N$, a result that is known as Woods formula [103]. In the intermediate N regime the behavior of the bias is more complicated [104]. Free-energy recovery techniques are also used in numerical simulations to evaluate free-energy differences [105, 106, 107, 108] and reconstruct free-energy profiles or potentials of mean-field force [109, 110].

4.2.3 Efficient strategies and numerical methods

An important question is to understand the optimum nonequilibrium protocol to recover free-energies using the JE given specific constraints in experiments and simulations. There are several considerations to take into account,

- **Faster or slower pulls?.** In single molecule experiments tethers break often so it is not possible to repeatedly pull the same tether an arbitrary number of times. Analogously, in numerical simulations only a finite amount of computer time is available and only a limited number of paths can be simulated. Given these limitations, is it better to perform many fast pulls or a few number of slower pulls to recover the free energy difference using the JE? In experiments, drift effects in the instrument always impose severe limitations to the minimum speed at which molecules can be pulled. To obtain good quality data it is advisable to carry out pulls as fast as possible. In numerical simulations the question about the best strategy for free energy recovery has been considered in several papers [111, 112, 113, 102]. The general conclusion that emerges from these studies is that, in systems that are driven far away from equilibrium, it is preferable to carry out many pulls at high speed than a few number of them at slower speeds. The reason can be intuitively understood. Convergence in the JE is dominated by the so-called outliers, i.e. work values that deviate a lot from the average work and are smaller than ΔF. The outliers contribute a lot to the exponential average (40). For higher pulling speeds we can perform more pulls so there are more chances to catch a large deviation event, i.e. to catch an outlier. At the same time, because at higher speeds the pulling is more irreversible, the average dissipated work becomes larger making the free energy estimate less reliable. However the contribution of the outliers required to recover the right free-energy is more important than the opposite effect due to the increase of the average dissipated work. We should also mention that periodically oscillating pulls have been also considered, however it is unclear whether they lead to improved free energy estimates [114, 115].

- **Forward or reverse process?.** Suppose we want to evaluate the free energy difference between two states, A and B, by using the JE. Is it better to estimate ΔF by carrying out irreversible experiments from A to B, or is it better to do them from B to A? Intuitively it seems natural that the less irreversible process among the two (forward and reverse) which is the one with smaller dissipated work W_{diss}, is also the most convenient in order to extract the free energy difference. However this is not the case. In general, a larger average dissipate work implies a larger work variance (42), i.e. larger fluctuations. The larger are the fluctuations, the larger the probability to catch a large deviation that contributes to the exponential average. It seems reasonable that, if outliers contribute much more to get the right free energy than proper tuning of the average value of the work, then the process that more fluctuates, i.e. the more dissipative one, is the process that must be sampled to efficiently recover ΔF. This result was anticipated in [116] and analyzed in more detail in [117]. For Gaussian work distributions, the minimum number of pulls, N^*, required to efficiently recover free energy differences within $1k_BT$ by using the JE grows exponentially with the dissipated work along the nonequilibrium process [100]. However, for general work distributions, the value of $N^*_{F(R)}$ along the forward (reversed) process depends on the average dissipated work along the reverse (forward) process [117]. This implies that,

$$N^*_{F(R)} \sim \exp\left(\frac{W^{R(F)}_{\text{diss}}}{T}\right) \tag{105}$$

and the process that dissipates most between the forward and the reverse is the best one to efficiently recover ΔF.

Until now we discussed strategies to recover free energy differences using the JE. We might be interested in free energy recovery by combining the forward and reverse distributions at the same time that we use the CFT. This is important in either experiments [101] or simulations [118, 119] where it is convenient and natural to use data from the forward and reverse process. The best strategy to efficiently recover free energies using the forward and reverse processes was proposed by C. Bennett long time ago in the context of equilibrium sampling [120]. The method has been later extended by Crooks to the nonequilibrium case [45] and is known as Bennett's acceptance ratio method. The basis of the method is as follows. Let us multiply both sides of (41) by the function $g_\mu(W)$,

$$g_\mu(W)\exp\left(-\frac{W}{T}\right)P_F(W) = g_\mu(W)P_R(-W)\exp\left(-\frac{\Delta F}{T}\right) \tag{106}$$

where $g_\mu(W)$ is an arbitrary real function that depends on the parameter μ. Integrating both sides between $W = -\infty$ and $W = \infty$ gives,

$$\langle g_\mu(W)\exp\left(-\frac{W}{T}\right)\rangle_F = \langle g_\mu(W)\rangle_R\exp\left(-\frac{\Delta F}{T}\right) \tag{107}$$

where $\langle...\rangle_{(F,R)}$ denote averages over the forward and reverse process. Taking the logarithm at both sides we have,

$$z_R(\mu) - z_F(\mu) = \frac{\Delta F}{T} \tag{108}$$

where we have defined,

$$z_R(\mu) = \log\Big(\langle g_\mu(W) \rangle_R\Big) \tag{109}$$

$$z_F(\mu) = \langle g_\mu(W) \exp\Big(-\frac{W}{T}\Big) \rangle_F \quad . \tag{110}$$

Equation (108) implies that the difference between both functions z_F, z_R must be a constant over all μ values. The question we would like to answer is the following. Given a finite number of forward and reverse pulls, what is the optimum choice for $g_\mu(W)$ that gives the best estimate (108) for ΔF? For a finite number of experiments N_F, N_R along the forward and reverse process we can write,

$$\langle A(W) \rangle_{F(R)} = \frac{1}{N_{F(R)}} \sum_{i=1}^{N_{F(R)}} A(W_i) \tag{111}$$

for any observable A. Equation (107) yields an estimate for ΔF,

$$(\Delta F)^{\text{est}} = T\Big(\log\Big(\langle g_\mu(W) \rangle_R\Big) - \log\Big(\langle g_\mu(W) \exp\Big(-\frac{W}{T}\Big) \rangle_F\Big)\Big) \quad . \tag{112}$$

Minimization of the variance,

$$\sigma^2_{\Delta F} = \langle\Big((\Delta F)^{\text{est}} - \Delta F\Big)^2\rangle \tag{113}$$

($\langle .. \rangle$ denotes the average over the distributions P_F, P_R) respect all possible functions $g_\mu(W)$ shows [120, 45] that the optimal solution is given by,

$$g_\mu(W) = \frac{1}{1 + \frac{N_F}{N_R} \exp\Big(\frac{W-\mu}{T}\Big)} \tag{114}$$

and $\mu = \Delta F$. The same result has been obtained by Pande and coworkers by using maximum likelihood methods [121]. In this case, one starts from a whole set of work data encompassing N_F forward and N_R reversed values. One then defines the likelihood function of distributing all work values between the forward and reverse sets. Maximization of the likelihood leads to Bennett's acceptance ratio formula. To extract ΔF is then customary to plot the difference in the lhs of (108), $z_R(\mu) - z_F(\mu)$, as a function of μ by using (109,110). The intersection with the line $z_R(\mu) - z_F(\mu) = \mu$ gives the best estimate for ΔF. An example of this method is shown in Figure 11. Recently, the maximum likelihood method has been generalized to predict free energy differences between more than two states [122].

5   Path thermodynamics

5.1   The general approach

The JE (40) indicates a way to recover free energy differences by measuring the work along all possible paths that start from an equilibrium state. Its mathematical form reminds a lot
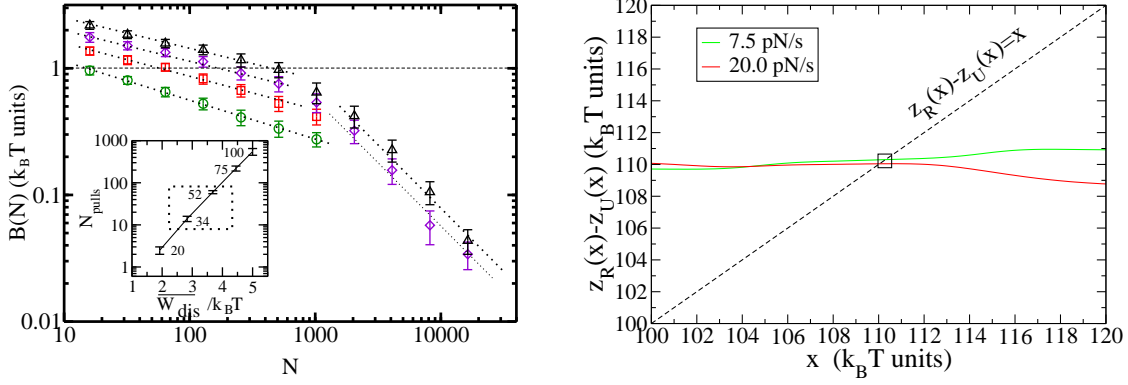
Figure 11: *(Left) Bias as a function of the number of pulls N for a two-states model. The inset shows the number of pulls as a function of the dissipated work required to recover the free-energy with an error within $1k_BT$. (Right) Function $z_R - z_F$ for the data shown in Figure 9C at the two largest pulling speeds. Left figure taken from [100, 3]. Right figure taken from the supplementary material in Ref.[101].*

of the partition function in the canonical ensemble used to compute free energies in statistical mechanics. The formulae for the two cases read,

$$\sum_{\mathcal{C}} \exp(-\frac{E(\mathcal{C})}{T}) = \exp(-\frac{F}{T}) \quad \text{(partition function)} \tag{115}$$

$$\sum_{\Gamma} \exp(-\frac{W(\Gamma)}{T}) = \exp(-\frac{\Delta F}{T}) \quad \text{(Jarzynski equality)} \tag{116}$$

where F is the equilibrium free energy of the system at temperature T. Throughout this section we take $k_B = 1$. In the canonical ensemble the entropy $S(E)$ is equal to the logarithm of the density of states with a given energy E. That density is proportional to the number of configurations with energy equal to E. Therefore (115) becomes,

$$\exp\left(-\frac{F}{T}\right) = \sum_{\mathcal{C}} \exp\left(-\frac{E(\mathcal{C})}{T}\right) = \sum_{E} \exp\left(S(E) - \frac{E}{T}\right) = \sum_{E} \exp\left(-\frac{\Phi(E)}{T}\right) \tag{117}$$

where $\Phi(E) = E - TS$ is the free-energy functional. In the large volume limit the sum in (117) is dominated by the value $E = E^{\text{eq}}$ where $F(E)$ is minimum. The value E^{eq} corresponds to the equilibrium energy of the system and $\Phi(E^{\text{eq}})$ is the equilibrium free energy. The following chain of relations hold,

$$F = \Phi(E^{\text{eq}}) \quad ; \quad \left(\frac{\partial \Phi(E)}{\partial E}\right)_{E=E^{\text{eq}}} = 0 \rightarrow \left(\frac{\partial S(E)}{\partial E}\right)_{E=E^{\text{eq}}} = \frac{1}{T} \tag{118}$$

The equilibrium energy E^{eq} is different from the most probable energy, E^{mp}, defined by $S'(E = E^{\text{mp}}) = 0$. E^{mp} is the average energy we would find if we were to randomly select configurations all with identical *a priori* probability. The equilibrium energy, rather than the most probable energy, is the thermodynamic energy for a system in thermal equilibrium.

40

Proceeding in an similar way for the JE we can define the *path entropy* $S(W)$ as the logarithm of the density of paths with work equal to W, $P(W)$,

$$P(W) = \exp(S(W)) \quad . \tag{119}$$

We can rewrite (116) in the following way,

$$\exp\left(-\frac{\Delta F}{T}\right) = \sum_{\Gamma} \exp\left(-\frac{W(\Gamma)}{T}\right) = \int dW\, P(W) \exp\left(-\frac{W}{T}\right) =$$

$$\int dW \exp\left(S(W) - \frac{W}{T}\right) = \int dW \exp\left(-\frac{\Phi(W)}{T}\right) \tag{120}$$

where $\Phi(W) = W - TS(W)$ is the *path free energy*. In the large volume limit the sum in (120) is dominated by the work value, $W^{\dagger}$, where $\Phi(W)$ is minimum. Note that the value $W^{\dagger}$ plays the role of the equilibrium energy in the canonical case (118). From (120) the path free energy $\Phi(W^{\dagger})$ is equal to the free energy difference ΔF. The following chain of relations hold,

$$\Delta F = \Phi(W^{\dagger}) = W^{\dagger} - TS(W^{\dagger}) \tag{121}$$

$$\left(\frac{\partial \Phi(W)}{\partial W}\right)_{W=W^{\dagger}} = 0 \rightarrow \left(\frac{\partial S(W)}{\partial W}\right)_{W=W^{\dagger}} = \frac{1}{T} \tag{122}$$

At the same time, $W^{\dagger}$ is different from the most probable work, W^{mp}, defined as the work value at which $S(W)$ is maximum,

$$\left(\frac{\partial S(W)}{\partial W}\right)_{W=W^{\mathrm{mp}}} = 0 \rightarrow \left(\frac{\partial \Phi(W)}{\partial W}\right)_{W=W^{\mathrm{mp}}} = 1 \quad . \tag{123}$$

The role of $W^{\mathrm{mp}}, W^{\dagger}$ in the case of the JE (115) and $E^{\mathrm{mp}}, E^{\mathrm{eq}}$ in the partition function case (116) appear exchanged. W^{mp} is the work value typically observed upon repetition of the same experiment a large number of times. In contrast, in the partition function case (115), E^{mp} is not the typical energy, the typical energy being E^{eq}. In addition, $W^{\dagger}$ is not the typical work but the work that must be sampled along paths in order to be able to extract the free energy difference using the JE. As we have already emphasized, as the system size increases, less and less paths can sample the region of work values around $W^{\dagger}$. Therefore, although both formalisms (partition function and JE) are mathematically similar, the physical meaning of the quantities $W^{\dagger}$ and E^{eq} is different. In the large volume limit E^{eq} is almost *always* observed whereas $W^{\dagger}$ is almost *never* observed.

In general, from the path entropy we can also define a *path temperature*, $\hat{T}(W)$,

$$\frac{\partial S(W)}{\partial W} = \lambda(W) = \frac{1}{\hat{T}(W)} \rightarrow \hat{T}(W^{\dagger}) = T \quad . \tag{124}$$

where $\lambda(W)$ is a Lagrange multiplier that transforms the path entropy $S(W)$ into the path free energy $\Phi(W)$, equation (121). The mathematical relations between the new quantities $W^{\dagger}$ and W^{mp} can be graphically represented for a given path entropy $S(W)$. This is shown in Figure 12.

The path thermodynamics formalism allows us to extract some general conclusions on the relation between $W^{\dagger}$ and W^{mp}. Let us consider the CFT (41). In terms of the path entropies for the forward and reverse processes, $S_F(W)$ and $S_R(W)$, (41) can be written as,

$$S_F(W) - S_R(-W) = \frac{W - \Delta F}{T} \rightarrow (S_F)'(W) + (S_R)'(-W) = \frac{1}{T} \tag{125}$$
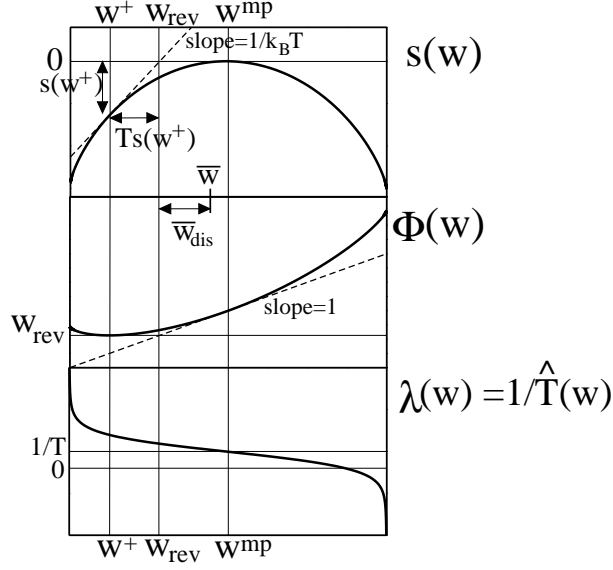
41

Figure 12: *Upper panel: Path entropy $s(w)$. Middle panel: Path free-energy $\Phi(w) = w - Ts(w)$. Lower panel: Lagrange multiplier $\lambda(w)$ equal to the inverse of the path temperature $1/\hat{T}(w)$. w^{mp} is the most probable work value given by $s'(w^{\mathrm{mp}}) = \lambda(w^{\mathrm{mp}}) = 0$ or $\Phi'(w^{\mathrm{mp}}) = 1$; $w^{\dagger}$ is the value of the work that has to be sampled to recover free energies from nonequilibrium work values using the JE. This is given by $s'(w^{\dagger}) = 1/T$ or $\Phi'(w^{\dagger}) = 0$; $w_{\mathrm{rev}}, \overline{w_{\mathrm{dis}}}$ are the reversible and average dissipated work respectively. Figure taken from [116].*

where we used the definition (119) and later derived with respect to W. By inserting $W = W_F^{\dagger}$ and $-W_R^{\dagger}$ in the rhs of (125) and using (122,123) we obtain the following chain of relations,

$$(S_F)'(W_F^{\dagger}) + (S_R)'(-W_F^{\dagger}) = \frac{1}{T} \rightarrow (S_R)'(-W_F^{\dagger}) = 0 \rightarrow W_F^{\dagger} = -W_R^{\mathrm{mp}} \tag{126}$$

$$(S_F)'(-W_R^{\dagger}) + (S_R)'(W_R^{\dagger}) = \frac{1}{T} \rightarrow (S_F)'(-W_R^{\dagger}) = 0 \rightarrow W_R^{\dagger} = -W_F^{\mathrm{mp}} \quad . \tag{127}$$

The rightmost equalities in (126,127) imply that the most probable work along the forward (reverse) process is equal to the work value ($W^{\dagger}$) that must be sampled, in a finite number of experiments, along the reverse (forward) process for the JE to be satisfied. This result has been already discussed in Sec. 4.2.3: the process that dissipates most between the forward and the reverse is the one that samples more efficiently the region of values in the vicinity of $W^{\dagger}$. This conclusion that may look counterintuitive can be rationalized by noting that larger dissipation implies also larger fluctuations and therefore more chances to get rare paths that sample the vicinity of $W^{\dagger}$. The symmetries (126,127) were originally discussed in [116] and analyzed in detail for the case of the gas contained in a piston [117].

We close this section by analyzing the case where the work distribution is Gaussian. The Gaussian case describes the linear response regime usually (but not necessarily) characterized by small deviations from equilibrium. Let us consider the following distribution,

$$P(W) = (2\pi\sigma_W^2)^{-\frac{1}{2}} \exp\left(-\frac{(W - W^{\mathrm{mp}})^2}{2\sigma_W^2}\right) \tag{128}$$

42

where the average value of the work, $\langle W \rangle$, is just equal to the most probable value W^{mp}. The path entropy is given by $S(W) = -(W - W^{\mathrm{mp}})^2/(2\sigma_W^2) + \text{constant}$, so (123) is satisfied. From (124) we get,

$$\hat{T}(W) = -\frac{\sigma_W^2}{W - W^{\mathrm{mp}}} \rightarrow W^\dagger = W^{\mathrm{mp}} - \frac{\sigma_W^2}{T} \quad . \tag{129}$$

From (122) and (129) we get $W^\dagger = \Delta F - (\sigma_W^2/2T)$. Therefore,

$$W^\dagger_{\mathrm{diss}} = W^\dagger - W_{\mathrm{rev}} = W^\dagger - \Delta F = -\frac{\sigma_W^2}{2T} \tag{130}$$

$$W^{\mathrm{mp}}_{\mathrm{diss}} = W^{\mathrm{mp}} - W_{\mathrm{rev}} = W^{\mathrm{mp}} - \Delta F = \frac{\sigma_W^2}{2T} \tag{131}$$

leading to the final result $W^\dagger_{\mathrm{diss}} = -W^{\mathrm{mp}}_{\mathrm{diss}} = -\langle W_{\mathrm{diss}} \rangle$. Therefore, in order to recover the free energy using the JE, paths with negative dissipated work and of magnitude equal to the average dissipated work must be sampled. Sometimes the paths with negative dissipated work are referred as *transient violations of the second law*. This name has raised strong objections among some rows of physicists. Of course the second law remains inviolate. The name just stresses the fact that paths with negative dissipated work must be experimentally accessible to efficiently recover free energy differences. Note that, for the specific Gaussian case, we get $\langle W_{\mathrm{diss}} \rangle = \frac{\sigma_W^2}{2T}$ and therefore the fluctuation-dissipation parameter R (42) is equal to 1 as expected for systems close to equilibrium. The result $R = 1$ has been shown to be equivalent to the validity of the fluctuation-dissipation theorem [95].

5.2 Computation of the work/heat distribution

The JE and the CFT describe relations between work distributions measured in NETS. However, they do not imply a specific form of the work distribution. In small systems fluctuations of the work relative to the average work are large so work distributions can strongly deviate from Gaussian distributions and be highly non trivial. In contrast, as the system size increases, deviations of the work respect to the average value start to become rare and exponentially suppressed with the size of the system. To better characterize the pattern of nonequilibrium fluctuations it seems important to explore analytical methods that allow us to compute, at least approximately, the shape of the energy distributions (e.g. heat or work) along nonequilibrium processes. Of course there is always the possibility to carry out exact calculations in specific solvable cases. In general, however, the exact computation of the work distribution turns out to be a very difficult mathematical problem (solvable examples are [123, 124, 125, 126, 127]) that is related to the evaluation of large deviation functions (Sec 5.3). This problem has traditionally received a lot of attention by mathematicians and we foresee it may become a central area of research in statistical physics in the next years.

5.2.1 An instructive example

To put the problem in proper perspective let us consider an instructive example: an individual magnetic dipole of moment μ subject to a magnetic field H and embedded in a thermal bath. The dipole can switch between the up and down configurations, $\pm\mu$. The transition rates

between the up and down orientations are of the Kramers type [128, 129],

$$k_{-\mu \to \mu}(H) = k_{\text{up}}(H) = k_0 \frac{\exp(\frac{\mu H}{T})}{2\cosh(\frac{\mu H}{T})} \tag{132}$$

$$k_{\mu \to -\mu}(H) = k_{\text{down}}(H) = k_0 \frac{\exp(\frac{-\mu H}{T})}{2\cosh(\frac{\mu H}{T})} \tag{133}$$

with $k_0 = k_{\text{up}}(H) + k_{\text{down}}(H)$ independent of H. The rates (132,133) satisfy detailed balance (8),

$$\frac{k_{\text{down}}(H)}{k_{\text{up}}(H)} = \frac{P^{\text{eq}}(\mu)}{P^{\text{eq}}(-\mu)} = \exp\left(-\frac{2\mu H}{T}\right) \tag{134}$$

with $P^{\text{eq}}(+(-)\mu) = \exp(-(+)\mu H/T)/\mathcal{Z}$ where $\mathcal{Z} = 2\cosh(\mu H/T)$ is the equilibrium partition function. In this system there are just two possible configurations, $\mathcal{C} = -\mu, \mu$. We consider a nonequilibrium protocol where the control parameter H is varied as a function of time, $H(t)$. The dynamics of the dipole is a continuous time Markov process, and a path is specified by the time-sequence $\Gamma \equiv \{\mu(t)\}$.

Let us consider the following protocol: the dipole starts in the down state $-\mu$ at $H = -H_0$. The field is then ramped from $-H_0$ to $+H_0$ at a constant speed $r = \dot{H}$, so $H(t) = rt$ (Figure 13A). The protocol lasts for a time $t_{\max} = 2H_0/r$ and the field stops changing when it has reached the value H_0. The free energy difference between the initial and final state is 0 because the free energy is an even function of H. To ensure that the dipole initially points down and that this is an equilibrium state, we take the limit $H_0 \to \infty$ but we keep the ramping speed r finite. In this way we generate paths that start at $H = -\infty$ at $t = -\infty$ and end up at $H = \infty$ at $t = \infty$. We can now envision all possible paths followed by the dipole. The up configuration is statistically preferred for $H > 0$ whereas the down configuration is preferred for $H < 0$. Therefore, in a typical path the dipole will stay in the down state until the field is reversed. At some point, after the field changes sign, the dipole will switch from the down to the up state and remain in the up state for the rest of the protocol. In average there will be always a time lag between the time at which the field changes sign and the time at which the dipole reverses orientation. In another paths the dipole will reverse orientation before the field changes sign, i.e. when $H < 0$. These sort of paths become more and more rare as the ramping speed increases. Finally, in the most general case, the dipole can reverse orientation more than once. The dipole will always start in the down orientation and end in the up orientation with multiple transitions occurring along the path.

The work along a given path is given by (37),

$$W(\Gamma) = -\int_{-\infty}^{\infty} dt \, \dot{H}(t)\mu(t) = -r \int_{-\infty}^{\infty} dt \, \mu(t) \tag{135}$$

Note that because $E_H(\mu) = E_{-H}(-\mu)$ then $\Delta E = 0$ and $Q(\Gamma) = W(\Gamma)$ so heat and work distributions are identical in this example. Moreover, due to the time reversal symmetry of the ramping protocol, the work distribution $P(W)$ is identical along the forward and reverse process. Therefore we expect that the JE (40) and the CFT (41) are both satisfied with $\Delta F = 0$,

$$\frac{P(W)}{P(-W)} = \exp\left(\frac{W}{T}\right) \quad ; \quad \left\langle \exp\left(-\frac{W}{T}\right)\right\rangle = 1 \tag{136}$$
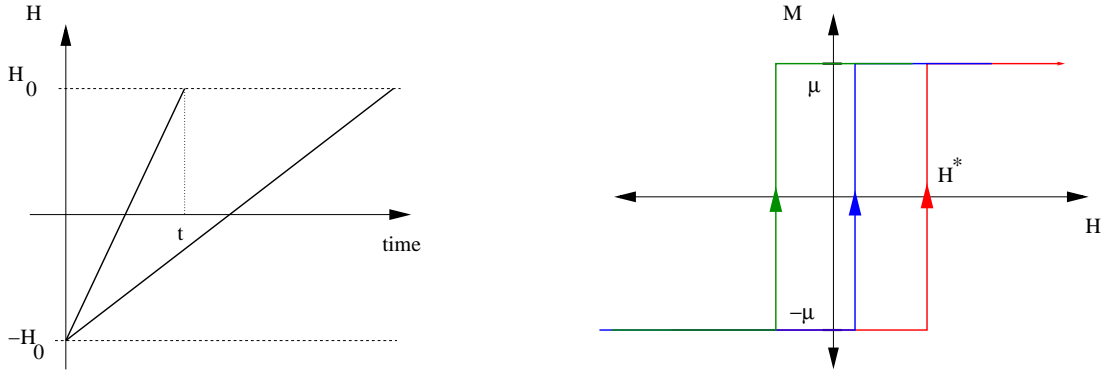
44

Figure 13: *(Left) Ramping protocol. The ramping speed is defined by $r = 2H_0/t$ where t is the duration of the ramp. (Right) Three examples of paths where the down dipole reverses orientation at different values of the field, H^*.*

The exact computation of $P(W)$ in this simple one-dipole model is already a very arduous task that, to my knowledge, has not yet been exactly solved. We can however consider a limiting case and try to elucidate the properties of the work (heat) distribution. Here we consider the limit of large ramping speed r where the dipole executes just one transition from the down to the up orientation. A few of these paths are depicted in Figure 13B. This is also called a first order Markov process because it only includes transitions that occur in just one direction (from down to up). In this reduced and oversimplified description a path is fully specified by the value of the field H^* at which the dipole reverses orientation. The work along one of these paths is given by,

$$W(\Gamma \equiv H^*) = -\lim_{H_0 \to \infty} \int_{-H_0}^{H_0} dH \mu(H) = ((H^* + H_0) - (H_0 - H^*))\mu = 2\mu H^* \qquad (137)$$

According to the second law, $\langle W \rangle = \langle Q \rangle \geq 0$, which implies that the average switching field is positive, $\langle H^* \rangle \geq 0$ (as expected due to the time lag between the reversal of the field and the reversal of the dipole). The work distribution is just given by the switching field distribution $p(H^*)$. This is a quantity easy to compute. The probability that the dipole is in the down state at field H satisfies a master equation that only includes the death process,

$$\frac{\partial p_{\text{down}}(H)}{\partial H} = -k_{\text{up}}(H)p_{\text{down}}(H) \quad . \qquad (138)$$

This equation can be exactly solved,

$$p_{\text{down}}(H) = \exp\left(-\frac{1}{r} \int_{-\infty}^{H} dH k_{\text{up}}(H)\right) \qquad (139)$$

where we have inserted the initial condition $p_{\text{down}}(-\infty) = 1$. The integral in the exponent can be easily evaluated using (132,133). We get,

$$p_{\text{down}}(H) = \left(1 + \exp(\frac{2\mu H}{T})\right)^{-\frac{Tk_0}{2\mu r}} \qquad (140)$$

45

The switching field probability distribution $p(H^*)$ is given by $p(H^*) = -(p_{\text{down}})'(H^*)$. From (137) we get,

$$P(W) = \frac{1}{2T}\left(1 + \exp(\frac{W}{T})\right)^{-\frac{Tk_0}{2\mu r}} \frac{\exp(\frac{W}{T})}{\cosh(\frac{W}{T})} \tag{141}$$

and from this result we obtain the path entropy,

$$S(W) = \log(P(W)) = -\frac{Tk_0}{2\mu r}\log\left(\exp(\frac{W}{T}) + 1\right) + \frac{W}{2T} - \log\left(\cosh(\frac{W}{2T})\right) + \text{constant} \tag{142}$$

It is important to stress that (141) does not satisfy (136) except in the limit $r \to \infty$ where this approximation becomes exact. We now compute $W^{\text{mp}}, W^\dagger$ in the large r limit. We obtain to the leading order,

$$S'(W^{\text{mp}}) = 0 \to W^{\text{mp}} = T\log(\frac{2\mu r}{k_0 T}) + \mathcal{O}(\frac{1}{r}) \tag{143}$$

$$S'(W^\dagger) = \frac{1}{T} \to W^\dagger = -T\log(\frac{2\mu r}{k_0 T}) + \mathcal{O}(\frac{1}{r}) \tag{144}$$

so the symmetry (126) (or (127)) is satisfied to the leading order (yet it can be shown how the $1/r$ corrections appearing in $W^{\text{mp}}, W^\dagger$ (143,144) are different). We can also compute the leading behavior of the fluctuation-dissipation parameter R (42) by observing that the average work $\langle W \rangle$ is asymptotically equal to the most probable work. The variance of the work, σ_W^2, is found by expanding $S(W)$ around W^{mp},

$$S(W) = S(W^{\text{mp}}) + \frac{S''(W^{\text{mp}})}{2}(W - W^{\text{mp}})^2 + (\text{higher order terms}) \tag{145}$$

$$\sigma_W^2 = -\frac{1}{S''(W^{\text{mp}})} \tag{146}$$

A simple computation shows that $\sigma_W^2 = 2T$ and therefore,

$$R = \frac{\sigma_W^2}{2TW_{\text{diss}}} \to \frac{1}{\log(\frac{2\mu r}{k_0 T})} \tag{147}$$

so R decays logarithmically to zero. The logarithmic increase of the average work with the ramping speed (143) is just a consequence of the logarithmic increase of the average value of the switching field $\langle H^* \rangle$ with the ramping speed. This result has been also predicted for the dependence of the average breakage force of molecular bonds in single molecule pulling experiments. This phenomenology, related to the technique commonly knownn as dynamic force spectroscopy, allows to explore free energy landscapes by varying the pulling speed over several orders of magnitude [130, 131].

5.2.2 A mean-field approach

We now focus our attention in describing an analytical method useful to compute work distributions, $P(W)$, in mean-field systems. The method has been introduced in [116] and developed in full generality by A. Imparato and L. Peliti [132, 133]. This section is a bit technical. The reader not interested in the details can just skip this section and go to Sec 5.3.

The idea behind the method is the following. We express the probability distribution $P(W)$ as a sum over all paths that start from a given initial state. This sum results in a path integral that can be approximated by its dominant solution or classical path in the large N limit, N being the number of particles. The present approach exploits the fact that, as soon as N becomes moderately large, the contribution to the path integral is very well approximated by the classical path. In addition, the classical path exactly satisfies the FT. Here we limit ourselves to show in a very sketchy way how the method applies to solve the specific example shown in Sec. 5.2.1. A detailed and more complete derivation of the method can be found in [116, 133]

We come back to the original model (132,133) and include all possible paths where the dipole reverses orientation more than once. The problem now gets too complicated so what we do is to modify the original model by considering an ensemble of non-interacting N identical dipoles. A configuration in the system is specified by the N-component vector $\mathcal{C} \equiv \{\vec{\mu} = (\mu_i)_{1 \leq i \leq N}\}$ with $\mu_i = \pm \mu$ the two possible orientations of each dipole. A path is specified by the time-sequence $\Gamma \equiv \{\vec{\mu}(s); 0 \leq s \leq t\}$. The energy of the system is given by,

$$E(\mathcal{C}) = -hM(\mathcal{C}) = -h \sum_{i=1}^{N} \mu_i \tag{148}$$

where $M = \sum_i \mu_i$ is the total magnetisation. The equilibrium free energy is $F = -N \log(2 \cosh(\mu H/T))$ and the kinetic rules are the same as given in (132,133) and are identical for each dipole. The work along a given path is given by (135),

$$W(\Gamma) = -\int_0^t ds \dot{H}(s) M(s) \tag{149}$$

so the work probability distribution is given by the path integral,

$$P(W) = \sum_{\Gamma} P(\Gamma) \delta(W(\Gamma) - W) = \int \mathcal{D}[\vec{\mu}] \delta \left(W + \int_0^t ds \dot{H}(s) M(s) \right) \tag{150}$$

where we have to integrate over all paths where $\vec{\mu}$ starts at time 0 in a given equilibrium state up to a final time t. To solve (150) we use the integral representation of the delta function,

$$\delta(x) = (1/2\pi) \int_{-\infty}^{\infty} d\lambda \exp(-i\lambda x) \quad . \tag{151}$$

We also insert the following factor,

$$1 = \int \frac{\mathcal{D}[\gamma] \mathcal{D}[m]}{2\pi} \exp \left(\frac{i}{\Delta t} \int \gamma(s)(m(s) - \frac{1}{N} \sum_{i=1}^{N} \mu_i(s)) \right) \tag{152}$$

where Δt is the discretization time-step and we have introduced new scalar fields $\gamma(s), m(s)$. After some manipulations one gets a closed expression for the work distribution $P(w)$ ($w = W/N$ is the work per dipole). We quote the final result [116],

$$P(w) = \mathcal{N} \int d\lambda \mathcal{D}[\gamma] \mathcal{D}[m] \exp \left(Na(w, \lambda, \gamma, m) \right) \tag{153}$$

47

where $\mathcal{N}$ is a normalization constant and a represents an action given by,

$$a(w, \lambda, \gamma, m) = \lambda\left(w + \int_0^t ds \dot{H}(s)M(s)\right) + \quad (154)$$

$$\frac{1}{2}\int_0^t ds\left(m(s)(2\dot{\gamma}(s) + c(s)) + d(s)\right) + \log\left(\exp(\gamma(0))k_{\mathrm{up}}(H_i) + exp(-\gamma(0)k_{\mathrm{down}}(H_i)\right) \quad (155)$$

with,

$$c(s) = k_{\mathrm{down}}(H(s))\left(\exp(-2\gamma(s)) - 1\right) - k_{\mathrm{up}}(H(s))\left(\exp(2\gamma(s)) - 1\right) \quad (156)$$

$$d(s) = k_{\mathrm{down}}(H(s))\left(\exp(-2\gamma(s)) - 1\right) + k_{\mathrm{up}}(H(s))\left(\exp(2\gamma(s)) - 1\right) \quad (157)$$

where the rates $k_{\mathrm{up}}, k_{\mathrm{down}}$ are given in (132,133) and we have assumed an initial equilibrium state at the the initial value of the field, $H(0) = H_i$. Equation (155) has to be solved together with the boundary conditions,

$$\gamma(t) = 0 \quad ; \quad m(0) = \tanh\left(\gamma(0) + \frac{\mu H_i}{T}\right) \quad . \quad (158)$$

Note that these boundary conditions break causality. The function γ has the boundary at the final time t whereas m has the boundary at the initial time 0. Causality is broken because by imposing a fixed value of the work w along the paths we are constraining the time evolution of the system.

To compute $P(w)$ we take the large volume limit $N \to \infty$ in (153). For a given value of w the probability distribution is given by,

$$P(w) \propto \exp(Ns(w)) = \exp\left(Na(w, \lambda(w), \gamma_w(s), m_w(s))\right) \quad (159)$$

where s is the path entropy (119) and the functions $\lambda(w), \gamma_w(s), m_w(s)$ are solutions of the saddle point equations,

$$\frac{\delta a}{\delta \lambda} = w + \mu\int_0^t m_w(s)\dot{H}(s)ds = 0 \quad (160)$$

$$\frac{\delta a}{\delta \gamma(s)} = \dot{m}_w(s) + m_w(s)(k_{\mathrm{up}}(s) + k_{\mathrm{down}}(s)) -$$

$$(k_{\mathrm{up}}(s) - k_{\mathrm{down}}(s)) + m_w(s)d_w(s) + c_w(s) = 0 \quad (161)$$

$$\frac{\delta a}{\delta m(s)} = \dot{\gamma}_w(s) + \lambda(w)\mu\dot{H}(s) + \frac{1}{2}c_w(s) = 0 \quad . \quad (162)$$

These equations must be solved together with the boundary conditions (158). Note that we use the subindex (or the argument) w in all fields (λ, m, γ) to emphasize that there exists a solution of these fields for each value of the work w. From the entropy s in (159) we can evaluate the path free energy, the path temperature and the values $w^{\mathrm{mp}}, w^\dagger$ introduced in Sec. 5.1. We enumerate the different results:

- **The path entropy** $s(w)$. By inserting (162) into (155) we get,

$$s(w) = \lambda(w)w + \frac{1}{2}\int_0^t d_w(s)ds + \log\left(\exp(\gamma(0))k_{\mathrm{up}}(H_i) + \exp(-\gamma(0))k_{\mathrm{down}}(H_i)\right) \quad . \quad (163)$$

From the stationary conditions (160,161,162) the path entropy (159) satisfies,

$$s'(w) = \frac{ds(w)}{dw} = \frac{\partial a(w, \lambda(w), \gamma_w(s), m_w(s))}{\partial w} = \lambda(w) \quad . \tag{164}$$

The most probable work can be determined by finding the extremum of the path entropy $s(w)$,

$$s'(w^{\mathrm{mp}}) = \lambda(w^{\mathrm{mp}}) = 0. \tag{165}$$

where we used (123). The saddle point equations (160,161,162) give $\gamma_{w^{\mathrm{mp}}}(s) = c_{w^{\mathrm{mp}}}(s) = d_{w^{\mathrm{mp}}}(s) = 0$ and,

$$\dot{m}_{w^{\mathrm{mp}}}(s) = -m_{w^{\mathrm{mp}}}(s)(k_{\mathrm{up}}(s) + k_{\mathrm{down}}(s)) + (k_{\mathrm{up}}(s) - k_{\mathrm{down}}(s)) \quad . \tag{166}$$

which is the solution of the master equation for the magnetisation. The stationary solution of this equation gives the equilibrium solution $m^{\mathrm{eq}}(s) = \tanh(\mu H(s)/T)$ corresponding to a quasistationary or reversible process.

- **The path free energy.** The path free energy $f = \Phi/N$ (121) is given by,

$$f^{\dagger} = f(w^{\dagger}) = \frac{\Delta F}{N} = w_{\mathrm{rev}} = w^{\dagger} - Ts(w^{\dagger}) = \frac{T}{2} \int_0^t d_{w^{\dagger}}(s) ds \tag{167}$$

where $w^{\dagger}$ is given by,

$$s'(w^{\dagger}) = \lambda(w^{\dagger}) = \frac{1}{T} \tag{168}$$

and the path temperature (124) satisfies the identity,

$$\hat{T}(w) = \frac{1}{\lambda(w)} \quad ; \quad \hat{T}(w^{\dagger}) = T \tag{169}$$

This set of equations can be numerically solved. Figure 14 shows some of the results.

5.3 Large deviation functions and tails

A large deviation function $\hat{P}(x)$ of a function $P_L(x)$ is defined if the following limit exists,

$$\hat{P}(x) = \lim_{L \to \infty} \frac{1}{L} \log(P_L(\frac{x}{L})) \quad . \tag{170}$$

From this point of view the distribution of the entropy production in NESS, $P(a)$ (55), where $a = \mathcal{S}_p/\langle \mathcal{S}_p \rangle$ and the work distribution, $P(W)$ (159), define large deviation functions. In the first case, $\lim_{t \to \infty} f_t(a)$ is the large deviation function (e.g. (84)), the average entropy production $\langle \mathcal{S}_p \rangle$ being the equivalent of L in (170). In the second case the path entropy $s(w) = S(W)/N$ (119,159) is a large deviation function where L in (170) corresponds to the size N. Large deviation functions are interesting for several reasons,

- **Nonequilibrium theory extensions.** By knowing the large deviation function of an observable in a nonequilibrium system (e.g. the velocity or position density) we can characterize the probability of macroscopic fluctuations. For example, by knowing the function $s(w)$ we can determine the probability of macroscopic work fluctuations $\delta W \propto$
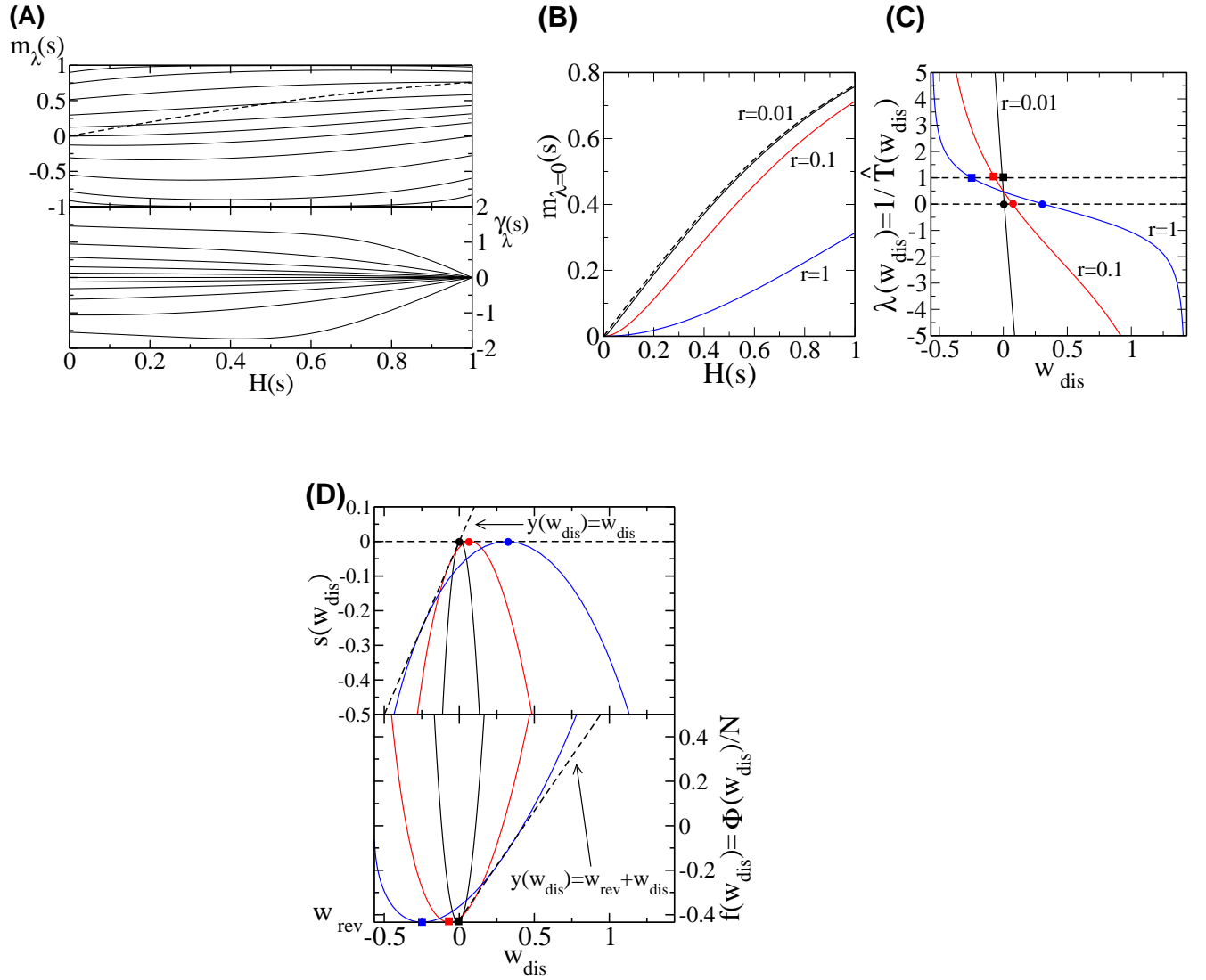
Figure 14: *Various results for the mean-field solution (160,161,162) of a dipole in field that is ramped from $H_i = 0$ to $H_f = 1$. (A) Fields $m_\lambda(s)$ and $\gamma_\lambda(s)$ at the ramping speed $r = 1$. Curves correspond to different values of λ ($\lambda = -5, -2, -1, -0.5, -0.2, 0., 0.2, 0.5, 1, 2, 5$ from top to bottom in the upper and lower panel). The dashed line in $m_\lambda(s)$ is the equilibrium solution $m_{eq}(H) = \tanh(H)$ corresponding to the reversible process $r \to 0$. (B) Magnetization $m_\lambda(s)$ for the most probable path $\lambda = 0$. The dashed line corresponds to the reversible trajectory, $r \to 0$. (C) Lagrange multiplier $\lambda(w_{dis})$ for three ramping speeds. The intersection of the different curves with the dashed line $\lambda = 0$ gives w^{mp} (filled circles) whereas the intersection with $\lambda = -1$ gives $w^\dagger$ (filled squares). The intersection of all three curves around $\lambda = 0.5$ is only accidental (looking at a larger resolution such crossing is not seen). (D) Path entropy and free energy corresponding to the solutions shown in (B,C) (larger speeds correspond to wider distributions). Path entropies are maximum and equal to zero at $w_{dis}^{mp} = w^{mp} - w_{rev}$ (filled circles) whereas path free-energies are minimum and equal to $f^\dagger = w_{rev}$ at $w_{dis}^\dagger$ (filled squares). Figure taken from [116].*

50

N, where N is the size of the system. Large deviations (for example, in work) may depend on the particular details (e.g. the rules) of the nonequilibrium dynamics. In contrast, small deviations (i.e. $\delta W \propto \sqrt{N}$) are usually insensitive to the microscopic details of the dynamics. Nonequilibrium systems are non-universal and often strongly dependent on the microscopic details of the system. In this regard, understanding large or macroscopic deviations may be a first step in establishing a general theory for nonequilibrium systems.

- **Spectrum of large deviations.** There are few examples where large deviations can be analytically solved. Over the past years a large amount of work has been devoted to understand large deviations in some statistical models such as exclusion processes. General results include the additivity principle in spatially extended systems [134, 135, 136] and the existence of exponential tails in the distributions [137]. These general results and the spectrum of large deviations are partially determined by the validity of the FT (27) which imposes a specific relation between the forward and the reverse work /heat distributions. For example, exponential tails in the work distribution $P(W)$ (119) correspond to a path-entropy $S(W)$ that is linear in W. This is the most natural solution of the FT, see (125).

- **Physical interpretation of large deviations.** In small systems, large deviations are common and have to be considered as important as small deviations. This means that, in order to understand the nonequilibrium behavior of small systems, a full treatment of small and large deviations is necessary. The latter are described by the shape of the large deviation function. The physical interpretation of small and large deviations may be different. For example, if we think of the case of molecular motors, small deviations (respect to the average) of the number of mechanochemical cycles may be responsible of the average speed of a molecular motor whereas large deviations may be relevant to understand why molecular motors operate so efficiently along the mechanochemical cycle.

5.3.1 Work and heat tails

Let us consider the case of a NETS that starts initially in equilibrium and is driven out of equilibrium by some external driving forces. As we have seen in (159), $\frac{1}{N}\log(P(w)) = s(w)$ is a large deviation function. At the same time we could also consider the heat distribution $P(Q)$ and evaluate its large deviation function $\frac{1}{N}\log(P(Q)) = s(q)$ where $q = Q/N$. Do we expect $s(q)$ and $s(w)$ to be identical? Heat and work differ by a boundary term, the energy difference. Yet the energy difference is extensive with N, therefore boundary terms modify the large deviation function so we expect that $s(q)$ and $s(w)$ are different. An interesting example is the case of the bead in the harmonic trap discussed in Sec. 4.1. Whereas the work distribution measured along arbitrary time intervals is always Gaussian, the heat distribution is characterized by a Gaussian distribution for small fluctuations $\delta Q = Q - <Q> \propto \sqrt{t}$, plus exponential tails for large deviations $\delta Q \propto t$. The difference between the large deviation function for the heat and the work arises from a boundary term, the energy difference. Again, in the large t limit, the boundary term is important for large fluctuations when $a = |Q|/\langle Q \rangle \geq a^* = 1$ (84). Large deviation functions depend always on boundary terms and these can never be neglected.

Let us come back now to the example of Sec. 5.2.1 where we considered work distributions in a system of non-interacting dipoles driven by an externally varying magnetic field. Again we will focus the discussion on the particular case where the initial value of the field is negative and large $H_i = -H_0 \to -\infty$, and the field is ramped at speed r until reaching the final value $H_f = H_0 \to \infty$. In this case $Q = W$ for individual paths so both large deviation functions $s(q), s(w)$ are identical. In what follows we will use heat instead of work for the arguments of all functions. In addition $s_F = s_R$ due to the time-reversal symmetry of the protocol. Exponential tails are indicated by a path-temperature $\hat{T}(q)$ (124) which is constant along a finite interval of heat values.

In Sec. 5.2.1 we have evaluated the path entropy $s(q)$ (163) for an individual dipole ($N = 1$) in the approximation of a first order Markov process. The following result has been obtained (142),

$$s(q) = -\frac{Tk_0}{2\mu r} \log(\exp(\frac{q}{T}) + 1) + \frac{q}{2T} - \log(\cosh(\frac{q}{2T})) + \text{constant} \quad . \tag{171}$$

For $|q| \to \infty$ we get,

$$s(q \to \infty) = -\frac{qk_0}{2\mu r} + \mathcal{O}\left(\exp(-\frac{q}{T})\right) \tag{172}$$

$$s(q \to -\infty) = \frac{q}{T} + \mathcal{O}\left(\exp(\frac{q}{T})\right) \tag{173}$$

The linear dependence of $s(q)$ on q leads to

$$\hat{T}(q \to \infty) = T^- = -\frac{2\mu r}{k_0} \tag{174}$$

$$\hat{T}(q \to -\infty) = T^+ = T \tag{175}$$

$$\tag{176}$$

where we use the notation T^+, T^- to stress the fact that these path temperatures are positive and negative respectively. Both path temperatures are constant and lead to exponential tails for positive and negative work values. Note that equation (125) reads,

$$s(q) - s(-q) = \frac{q}{T} \to (s)'(q) + (s)'(-q) = \frac{1}{T} \to \frac{1}{T^+} + \frac{1}{T^-} = \frac{1}{T} \tag{177}$$

which is satisfied by (174,175) up to $1/r$ corrections.

Another interesting limit is the quasistatic limit $r \to 0$. Based on the numerical solution of the saddle point equations (160,161,162), it was suggested in [116] that $\hat{T}(q)$ converged to a constant value over a finite range of work values. Figure 15A show the results obtained for the heat distributions whereas the path temperature is shown in Figure 15B. A more detailed analysis [133] has shown that a plateau is never fully reached for a finite interval of heat values when $r \to 0$. The presence of a plateau has been interpreted as the occurrence of a first order phase transition in the path entropy $s(q)$ [133].

There is an interesting analogy between the different type of work/heat fluctuations and the emission of light radiation by atoms in a cavity. Atoms can absorb and reemit photons following two different mechanisms. One type of radiative mechanism is called stimulated because it depends on the density of blackbody radiation in the cavity (directly related to the temperature of the cavity). The other radiative mechanism is called spontaneous and is
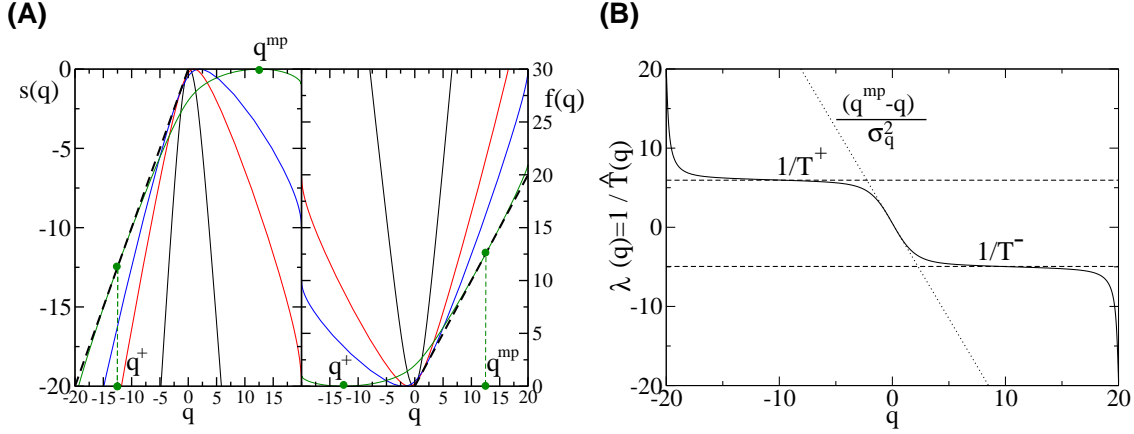
Figure 15: *(A) Heat distributions (path entropy $s(q)$ and path free energy $f(q)$) evaluated at four ramping speeds $r = 0.1, 0.5, 1, 10$ (from the most narrower to the most wider distributions). The dashed line in the left panel is $y(q) = q/T$ (we take $T = 1$) and is tangent to $s(q)$ at $q^\dagger$ (dots are shown for $r = 10$). The dashed line in the right panel corresponds to $y(q) = q$ and is tangent to the function $f(q)$ at the value q^{mp} (dots shown for $r = 10$). (B) $\lambda(q)$ for the lowest speed $r = 0.1$. It shows a linear behavior for small values of q, $\lambda(q) = (1/\sigma_q^2)(q^{\mathrm{mp}} - q)$ and two plateaus for $q \gg 1$ and $q \ll -1$. The former contributes as a Gaussian component in the heat distribution describing the statistics of small deviations respect to the most probable value (stimulated sector). The latter gives rise to two exponential tails for the distribution describing the statistics of rare events (spontaneous sector). Figure adapted from [116].*

independent on the density of radiation in the cavity (i.e. it does not depend on its temperature). The stimulated process contributes to the adsorption and emission of radiation by atoms. The spontaneous process only contributes to the emitted radiation. In general, the path entropy $s(w)$ contains two sectors reminiscent of the stimulated and spontaneous processes in the blackbody radiation,

- **The FDT or stimulated sector.** This sector is described by Gaussian work fluctuations (128) leading to $s(q) = -(q - q^{\mathrm{mp}})^2/(2\sigma_q^2) + \text{constant}$. Therefore we get (129),

$$\lambda(q) = \frac{1}{\hat{T}(q)} = -\frac{q - q^{\mathrm{mp}}}{\sigma_q^2} \tag{178}$$

  which behaves linearly in q for small deviations around q^{mp}. Note that $\hat{T}(q)$ satisfies (177) and therefore

$$\sigma_q^2 = 2Tq^{\mathrm{mp}}, \tag{179}$$

  leading to a fluctuation-dissipation parameter $R = 1$, a result equivalent to the validity of the fluctuation-dissipation theorem (FDT). This sector we call stimulated because work fluctuations (179) depend directly on the temperature of the bath.

- **The large deviation or spontaneous sector.** Under some conditions this sector is well reproduced by exponential tails in the work distribution describing large or macro-

scopic deviations. In this sector,

$$\frac{1}{\hat{T}(q)} - \frac{1}{\hat{T}(-q)} = \frac{1}{T} \rightarrow \frac{1}{T^+} + \frac{1}{T^-} = \frac{1}{T} \quad . \tag{180}$$

The physical interpretation of T^+, T^- is as follows. Because T^- is negative then T^- describes fluctuations where net heat is released to the bath, whereas T^+ is positive and describes fluctuations where net heat is absorbed from the bath. Equation (180) imposes $T^+ < |T^-|$ implying that large deviations also satisfy the second law: the average net amount of heat supplied to the bath ($\propto |T^-|$) is always larger that the average net heat absorbed from the bath ($\propto T^+$). In the previous example (174,175), T^+ converges to the bath temperature whereas T^- diverges to $-\infty$ when $r \rightarrow \infty$. We call this sector spontaneous because the energy fluctuations mainly depend on the nonequilibrium protocol (in the current example, such dependence is contained in the r-dependence of T^-, (174)).

5.3.2 The bias as a large deviation function

The bias defined in (103) is still another example of a large deviation function. Let us define the variable,

$$X = \sum_{i=1}^{N} \exp(-\frac{W_i}{T}) \tag{181}$$

where $W_i \rightarrow W_i - \Delta F$ stands for the dissipated work. The free-energy estimate (103) satisfies the relation,

$$x = \exp(-\frac{F^{\text{JE}} - \Delta F}{T}) \quad ; \quad x = \frac{X}{N} = \frac{1}{N} \sum_{i=1}^{N} \exp(-W_i) \tag{182}$$

where N is the total number of experiments. The N values W_i are extracted from a distribution $P(W)$ that satisfies the relations,

$$\langle 1 \rangle = \int_{-\infty}^{\infty} P(W)dW = 1 \quad ; \quad \langle \exp(-W) \rangle = \int_{-\infty}^{\infty} \exp(-W)P(W)dW = 1 \quad . \tag{183}$$

We follow the same procedure as in Sec. 4.2.2 and extract N different values W_i to obtain a single x using (182). By repeating this procedure a large number of times, M, we generate the probability distribution of x, that we will call $\mathcal{P}_N(x)$, in the limit $M \rightarrow \infty$. The bias (104) is defined by,

$$B(N) = -T\langle \log(x) \rangle = -T \int_{-\infty}^{\infty} \log(x)\mathcal{P}_N(x)dx \quad . \tag{184}$$

In the following we show that $\mathcal{P}_N(x)$ defines a large deviation function in the limit $N \rightarrow \infty$. We write,

$$\mathcal{P}_N(x) = \int \prod_{i=1}^{N} dW_i P(W_i)\delta\Big(x - \frac{1}{N} \sum_{i=1}^{N} \exp(-W_i)\Big) =$$

$$= \frac{1}{2\pi i} \int_{-i\infty}^{i\infty} d\mu \exp\Big(\mu x - \frac{\mu}{N} \sum_{i=1}^{N} \exp(-W_i)\Big) \prod_{i=1}^{N} P(W_i)dW_i =$$

$$= \frac{N}{2\pi i} \int_{-i\infty}^{i\infty} d\hat{\mu} \exp\Big(N\hat{\mu}x + N\log(\int dW P(W) \exp(-\hat{\mu}\exp(-W)))\Big) =$$

$$= \frac{N}{2\pi i} \int_{-i\infty}^{i\infty} d\hat{\mu} \exp\Big(N g(\hat{\mu}, x)\Big) \sim_{N\to\infty} \exp\Big(N g(\hat{\mu}^*, x)\Big) \tag{185}$$

where in the second line we used the integral representation of the delta function (151); in the third line we separate the integrals and independently integrate the contribution of each variable W_i; in the last line we apply the saddle point integration method to the function $g(\hat{\mu}, x)$ defined as,

$$g(\hat{\mu}, x) = \hat{\mu}x + \log\Big(\int_{-\infty}^{\infty} \exp(-\hat{\mu}\exp(-W))\Big) \tag{186}$$

where $\hat{\mu}^*$ is equal to the absolute maximum of $g(\hat{\mu}, x)$,

$$\Big(\frac{\partial g(\hat{\mu}, x)}{\partial \hat{\mu}}\Big)_{\hat{\mu}=\hat{\mu}^*} = 0 \to x = << \exp(-W) >>_{\hat{\mu}^*} \tag{187}$$

with,

$$<< .. >>_{\hat{\mu}} = \frac{\int_{-\infty}^{\infty} \exp(-W) \exp\Big(-\hat{\mu}\exp(-W)\Big) P(W) dW}{\int_{-\infty}^{\infty} \exp\Big(-\hat{\mu}\exp(-W)\Big) P(W) dW} \quad . \tag{188}$$

The function $g(\hat{\mu}, x)$ evaluated at $\hat{\mu} = \hat{\mu}^*$ defines a large deviation function (170),

$$g^*(x) = g(\hat{\mu}^*(x), x) = \lim_{N\to\infty} \frac{1}{N} \log\Big(\mathcal{P}_N(\frac{X}{N})\Big) = \lim_{N\to\infty} \frac{1}{N} \log\Big(\mathcal{P}_N(x)\Big) \quad . \tag{189}$$

Using (189) we can write for the bias (184) in the large N limit,

$$B(N) = -T \frac{\int dx \log(x) \exp\Big(N g^*(x)\Big)}{\int dx \exp\Big(N g^*(x)\Big)} \quad . \tag{190}$$

The integrals in the numerator and denominator can be estimated by using the saddle point method again. By expanding $g^*(x)$ around the maximum contribution at $x^{\max}$ we get, up to second order,

$$g^*(x) = g^*(x^{\max}) + \frac{1}{2}(g^*)''(x^{\max})(x - x^{\max})^2 \quad . \tag{191}$$

To determine $x^{\max}$ we compute first,

$$(g^*)'(x) = \Big(\frac{\partial g(\hat{\mu}, x)}{\partial \hat{\mu}}\Big)_{\hat{\mu}=\hat{\mu}^*(x)} \Big(\frac{d\hat{\mu}^*(x)}{dx}\Big) + \Big(\frac{\partial g(\hat{\mu}^*, x)}{\partial x}\Big) =$$

$$= \Big(\frac{\partial g(\hat{\mu}^*, x)}{\partial x}\Big) = \hat{\mu}^*(x) \tag{192}$$

where we have used (186,187). The value $x^{\max}$ satisfies,

$$(g^*)'(x^{\max}) = \hat{\mu}^*(x^{\max}) = 0 \quad . \tag{193}$$

Inspection of (187,188) shows that $x^{\max} = 1$. The second term in the rhs of (191) is then given by,

$$(g^*)''(x = 1) = (\hat{\mu}^*)'(x = 1) = \frac{1}{1 - \langle \exp(-2W) \rangle} \tag{194}$$

55

where $\langle ... \rangle$ denotes the average over the distribution $P(W)$ (183). Using (194) and inserting (191) into (190) we finally obtain,

$$B(N) = T\frac{\langle \exp(-2W) \rangle - 1}{2N} + \mathcal{O}\Big(\frac{1}{N^2}\Big) \tag{195}$$

For a Gaussian distribution we get, $B(N) = T\exp(\sigma_W^2 - 1)/(2N)$. Equation (195) was derived in [103]. For intermediate values of N (i.e. for values of N where $B(N) > 1$) other approaches are necessary.

6 Glassy dynamics

Understanding glassy systems (see Sec. 2.1) is a major goal in modern condensed matter physics [138, 139, 140, 141]. Glasses represent an intermediate state of matter sharing some properties of solids and liquids. Glasses are produced by fast cooling of a liquid when the crystallization transition is avoided and the liquid enters the metastable supercooled region. The relaxation of the glass to the supercooled state proceeds by reorganization of molecular clusters inside the liquid, a process that is thermally activated and strongly dependent on the temperature. The relaxation of the supercooled liquid is a nonequilibrium process that can be extremely slow leading to aging. The glass analogy is very fruitful to describe the nonequilibrium behavior of a large variety of systems in condensed matter physics, all them showing a related phenomenology.

The nonequilibrium aging state (NEAS, see Sec.3.1) is a non-stationary state characterized by slow relaxation and a very low rate of energy dissipation to the surroundings. Aging systems fail to reach equilibrium unless one waits an exceedingly large amount of time. For this reason, the NEAS is very different from either the nonequilibrium transient state (NETS) or the nonequilibrium steady state (NESS).

What do aging systems have in common with the nonequilibrium behavior of small systems? Relaxation in aging systems is driven by fluctuations of a small number of molecules that relax by releasing a small amount of stress energy to the surroundings. These molecules are grouped into clusters often called cooperatively rearranging regions (CRRs). A few observations support this interpretation,

- **Experimental facts.** Traditionally, the glass transition has been studied with bulk methods such as calorimetry or light scattering. These measurements perform an average over all mesoscopic regions in the sample, but are not suitable to follow the motion of individual clusters of a few nanometers in extension. The few direct evidences we have on aging as driven by the rearrangement of small regions comes from AFM measurements on glass surfaces, confocal microscopy of colloids and the direct observation of molecular motion (NMR resonance and photobleaching tests) [8]. More indirect evidence is obtained from the heterogeneous character of the dynamics, i.e. the presence of different regions in the system that show a great disparity of relaxation times [142]. The observation of strong intermittent signals [143] in Nyquist noise measurements while the system ages has been interpreted as the result of CRRs, i.e. events corresponding to the rearrangement of molecular clusters. Finally, the direct measure of a correlation length in colloidal glasses hints at the existence of CRRs [144]. Future developments in this

area are expected to come from developments in micromanipulation and nanotechnology applied to direct experimental observation of molecular clusters.

- **Numerical facts.** Numerical simulations are a very useful approach to examine our understanding of the NEAS [145]. Numerical simulations allow to measure correlation functions and other observables which are hardly accessible in experiments. Susceptibilities in glasses are usually defined in terms of four-point correlation functions (two-point in space and two-point in time) which give information about how spatially separated regions are correlated in time [146]. A characteristic quantity is the typical length of such regions. Numerical simulations of glasses show that the maximum length of spatially correlated regions is small, just a few nanometers in molecular glasses or a few radii in colloidal systems. Its growth in time is also exceedingly slow (logarithmic in time) suggesting that the correlation length is small for the experimentally accessible timescales.

- **Theoretical facts.** There are several aspects that suggest that glassy dynamics must be understood as a result of the relaxation of CRRs. Important advances in the understanding of glass phenomena come from spin glass theory [147, 148]. Historically, this theory was proposed to study disordered magnetic alloys which show nonequilibrium phenomena (e.g. aging) below the spin-glass transition temperature. However, it has been shown later how spin glass theory provides a consistent picture of the NEAS in structural glass models that do not explicitly contain quenched disorder in the Hamiltonian [149, 150, 151, 152]. Most of the progress in this area comes from the study of mean-field models, i.e. systems with long-range interactions. The success of mean-field theory to qualitatively reproduce most of the observed phenomenology in glasses suggests that NEAS are determined by the relaxation of mean-field like regions, maybe the largest CRRs in the system. Based on this analogy several mean-field based phenomenological approaches have been proposed [153, 154, 155, 156, 157].

In the next sections I briefly discuss some of the theoretical concepts important to understand the glass state and the nonequilibrium aging dynamics.

6.1 A phenomenological model

To better understand why CRRs are predominantly small we introduce here a simple phenomenological aging model inspired by mean-field theory [154]. The model consists of a set of regions or domains of different sizes s. A region of size s is just a molecular cluster (colloidal cluster), containing s molecules (or s colloidal particles). The system is prepared in an initial high energy configuration where spatially localized regions in the system contain some stress energy. That energy can be irreversibly released to the environment if a cooperative rearrangement of that region takes place. The release occurs when some correlated structures are built inside the region by a cooperative or anchorage mechanism. Anchorage occurs when all s molecules in that region move to collectively find a transition state that gives access to the *release pathway*, i.e. a path in configurational space that activates the rearrangement process. Because the cooperative process involves s particles, the characteristic time to anchor the transition state is given by,

$$\frac{\tau_s}{\tau_0} \propto \left(\frac{\tau^*}{\tau_0}\right)^s = \exp\left(\frac{Bs}{T}\right) \tag{196}$$

where $\tau^* = \tau_0 \exp(B/T)$ is the activated time required to anchor one molecule, τ_0 is a microscopic time and B is the activation barrier which is equal to the energy of the transition state. How CRRs exchange energy with the environment? Once relaxation starts, regions of all sizes contain some amount of stress energy ready to be released to the environment in the form of heat. The first time a given region rearranges it typically releases an amount of heat $\overline{Q}$ that does not scale with the size of the region. After the first rearrangement has taken place the region immediately equilibrates with its environment. Subsequent rearrangement events in that same region do not release more stress energy to the environment. These regions can either absorb or release heat from/to the environment as if they were thermally equilibrated with the bath, the net average heat exchanged with the environment being equal to 0. The release of the stored stress energy in the system proceeds in a hierarchical fashion. At a given age t (the time elapsed after relaxation starts, also called waiting time) only the CRRs of size s^* have some stress energy $\overline{Q}$ available to be released to the environment. Smaller regions with $s < s^*$ already released their stress energy sometime in the past being now in thermal equilibrium with the environment. Larger regions with $s > s^*$ have not had yet enough time to release their stress energy. Only the CRRs with s in the vicinity of s^* contribute to the overall relaxation of the glass toward the supercooled state. That size s^* depends on the waiting time or time elapsed since the relaxation started.

Let $n_s(t)$ be the number of CRRs of size s at time t. At a given time the system is made out of non-overlapping regions in the system that randomly rearrange according to (196). After a rearrangement occurs CRRs destabilize probably breaking up into smaller regions. In the simplest description we can assume that regions can just gain or loose one particle from the environment with respective (gain,loose) rates k_s^g, k_s^l with $k_s^g + k_s^l = k_s$. k_s, the rate of rearrangement, is proportional to $1/\tau_s$ where τ_s is given in (196). To further simplify the description we just take $k_s^g = gk_s, k_s^l = lk_s$ with $g + l = 1$. Consequently, the balance equations involve the following steps:

$$\mathcal{D}_s \rightarrow \mathcal{D}_{s-1} + p \quad ; \quad \mathcal{D}_s + p \rightarrow \mathcal{D}_{s+1} \tag{197}$$

with rates k_s^l, k_s^g, where $\mathcal{D}_s$ denotes a region of size s and p a particle (an individual molecule or a colloidal particle) in the system. The balance equations for the occupation probabilities read ($s \geq 2$),

$$\frac{\partial n_s(t)}{\partial t} = k_{s+1}^l n_{s+1}(t) + k_{s-1}^g n_{s-1}(t) - k_s n_s(t) \quad . \tag{198}$$

This set of equations must be solved together with mass conservation $\sum_{s=1}^{\infty} s n_s(t) = \text{const}$. The equations can be numerically solved for all parameters of the model. Particularly interesting results are found for $g \ll l$. Physically this means that, after rearranging, regions are more prone to loose molecules than to capture them, a reasonable assumption if a cooperative rearrangement leads to a destabilization of the region. A few remarkable results can be inferred from this simple model,

- **Time dependent correlation length.** In Figure 16 (left panel) we show the time evolution for $n_s(t)$. At any time it displays a well defined time-dependent cutoff value $s^*(t)$ above which $n_s(t)$ abruptly drops to zero. The distribution of the sizes of the CRRs scales like $n_s(t) = (1/s^*)\hat{n}(s/s^*)$ where s^* is a waiting time dependent cutoff size (data not shown). The NEAS can be parametrized by either the waiting time or the size of the region $s^*(t)$. Relaxation to equilibrium is driven by the growth of $s^*(t)$ and

its eventual convergence to the stationary solution of (198). The size $s^*(t)$ defines a characteristic growing correlation length, $\xi(t) = (s^*(t))^{\frac{1}{d}}$, where d is the dimensionality of the system. Because $s^*(t)$ grows logarithmically in time (196) sizes as small as $\simeq 10$ already require 10^{33} iteration steps. Small CRRs govern the relaxation of the system even for exceedingly long times.

- **Logarithmic energy decay.** The release of stress energy to the environment occurs when the regions of size s^* rearrange for the first time. The advance of the *front* in $n_s(t)$ located at $s = s^*$ is the leading source of energy dissipation. Cooperative rearrangements of regions of size smaller than s^* have already occurred several times in the past and do not yield a net thermal heat flow to the bath whereas regions of size larger than s^* have not yet released their stress energy. The supercooled state is reached when the cutoff size s^* saturates to the stationary solution of (198) and the net energy flow between the glass and the bath vanishes. The rate of energy decay in the system is given by the stress energy $\overline{Q}$ released by regions of size $s^*(t)$ times their number $n_{s^*}(t) = \hat{n}(1)/s^*$, divided by the activated time (196) (equal to the waiting time $t \sim \exp(Bs^*/T)$),

$$\frac{\partial E}{\partial t} \sim \frac{\overline{Q} n_{s^*}(t)}{t} \sim \frac{\overline{Q}}{s^* t} \quad . \tag{199}$$

Because $s^*(t) \sim T \log(t)$ then the energy decays logarithmically with time, $E(t) \sim 1/\log(t)$.

- **Aging.** If we assume independent exponential relaxations for the CRRs we obtain the following expression for the two-times correlation function,

$$C(t, t+t') = \sum_{s \geq 1} s n_s(t) \exp(-t'/\tau_s) \tag{200}$$

where t denotes the waiting time after the initiation of the relaxation and τ_s is given by (196). In the right panel of Figure 16 we show the correlation function (200) for different values of t (empty circles in the figure). Correlations (200) are excellently fitted by a stretched exponential with a t dependent stretching exponent β_s,

$$C(t, t+t') \equiv C_t(t') = \exp\left(-\left(\frac{t'}{\tau_t}\right)^{\beta_s(t)}\right) \quad . \tag{201}$$

In the right panel of Figure 16 we also show the best fits (continuous lines). Correlation functions show simple aging and scale like t'/t with $t = \exp(s^*/T)$ where s^* is the waiting-time dependent cutoff size.

- **Configurational entropy and effective temperature.** An important concept in the glass literature that goes back to Adam and Gibbs in the Fifties [158, 159] is the configurational entropy, also called complexity and denoted by $\mathcal{S}_c$ [145]. It is proportional to the logarithm of the number of cooperative regions with a given free-energy F, $\Omega(F)$

$$\mathcal{S}_c(F) = \log\left(\Omega(F)\right) \quad . \tag{202}$$

At a given time t after relaxation starts, the regions of size s^* contain a characteristic free energy F^*. Fluctuations in these regions lead to rearrangements that release a net

amount of heat to the environment (199). Local detailed balance implies that, after a rearrangement takes place, new regions with free energies around F^* are generated with identical probability. Therefore,

$$\frac{\mathcal{W}(F \to F')}{\mathcal{W}(F' \to F)} = \frac{\Omega(F')}{\Omega(F)} = \exp\Big(\mathcal{S}_c(F') - \mathcal{S}_c(F)\Big) \tag{203}$$

where $\mathcal{W}(F \to F')$ is the rate to create a region of free energy F' after rearranging a region of free energy F. Note the similarity between (203) and (8). If $\Delta F' = F' - F$ is much smaller than $\mathcal{S}_c(F)$ we can expand the difference in the configurational entropy in (203) and write,

$$\frac{\mathcal{W}(\Delta F)}{\mathcal{W}(-\Delta F)} = \exp\Big(\Big(\frac{\partial \mathcal{S}_c(F)}{\partial F}\Big)_{F=F^*} \Delta F\Big) = \exp\Big(\frac{\Delta F}{T_{\text{eff}}(F^*)}\Big) \tag{204}$$

with the shorthand notation $\mathcal{W}(\Delta F) = \mathcal{W}(F \to F')$ and the time-dependent effective temperature $T_{\text{eff}}(F^*)$ defined as,

$$\frac{1}{T_{\text{eff}}(F^*)} = \Big(\frac{\partial \mathcal{S}_c(F)}{\partial F}\Big)_{F=F^*} \quad . \tag{205}$$

In the present phenomenological model only regions that have not yet equilibrated (i.e. of size $s \geq s^*(t)$) can release stress energy in the form of a net amount of heat to the surroundings. This means that only transitions with $\Delta F < 0$ contribute to the overall relaxation toward equilibrium.

Therefore, the rate of energy dissipated by the system can be written as,

$$\frac{\partial E}{\partial t} \propto \frac{1}{t} \frac{\int_{-\infty}^0 dx\, x \mathcal{W}(x)}{\int_{-\infty}^0 dx\, \mathcal{W}(x)} = \frac{2T_{\text{eff}}(F^*)}{t} \quad . \tag{206}$$

where we take

$$\mathcal{W}(\Delta F) \propto \exp\Big(\frac{\Delta F}{2T_{\text{eff}}(F^*)}\Big) \tag{207}$$

as the solution of (204). Identifying (206) and (199) we get,

$$T_{\text{eff}}(F^*) = \frac{\overline{Q}}{2s^*} \quad . \tag{208}$$

The time dependence of s^* derived in (199) shows that the effective temperature decreases logarithmically in time.

6.2   Nonequilibrium temperatures

The concept of a nonequilibrium temperature has stimulated a lot the research in the area of glasses. This concept has been promoted by Cugliandolo and Kurchan in the study of mean-field models of spin glasses [160, 161] that show violations of the fluctuation-dissipation theorem (FDT) in the NEAS. The main result in the theory is that two-time correlations $C(t, t_w)$ and responses $R(t, t_w)$ satisfy a a modified version of the FDT. It is customary to
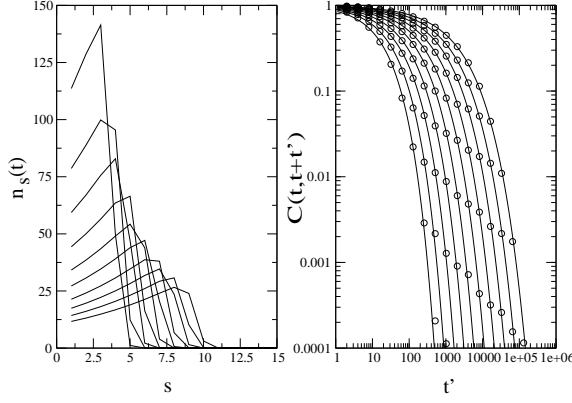
Figure 16: $n_s(t)$ *(left panel) and $C(t, t + t')$ (right panel) for different waiting times $t = 10^{14} - 10^{33}$ for the numerical solution of (198) with $l = 8, g = 1$ and $T = 0.45$. The relaxation time and the stretching exponent are very well fitted by $\tau_t = 2.2t^{0.35}$, $\beta_s(t) = 0.34 + 0.45t^{-0.06}$. Figure taken from [154].*

introduce the effective temperature through the fluctuation-dissipation ratio (FDR) [162] defined as,

$$T_{\text{eff}}(t_w) = \lim_{t_w \to \infty} \frac{\frac{\partial C(t, t_w)}{\partial t_w}}{R(t, t_w)} \tag{209}$$

in the limit where $t - t_w \gg t_w$. In contrast, in the limit $t - t_w \ll t_w$ local equilibrium holds and $T_{\text{eff}}(t_w) = T$. In general $T_{\text{eff}}(t_w) \geq T$, although there are exceptions to this rule and even negative effective temperatures have been found [163]. These predictions have been tested in many exactly solvable models and numerical simulations of glass formers [145]. In what follows we try to emphasize how the concept of the effective temperature $T_{\text{eff}}(t_w)$ contributes to our understanding of nonequilibrium fluctuations in small systems.

Particularly illuminating in this direction is the study of mean-field spin glasses. These models have the advantage that can be analytically solved in the large volume limit. At the same time, numerical simulations allow to investigate finite-size effects in detail. Theoretical calculations in mean-field spin glasses are usually carried out by first taking the infinite-size limit and later the long time limit. Due to the infinite range nature of the interactions this order of limits introduces pathologies in the dynamical solutions and excludes a large spectrum of fluctuations that are relevant in real systems. The infinite-size limit in mean-field models, albeit physically dubious, is mathematically convenient. Because analytical computations for finite-size systems are not available we can resort to numerical simulations in order to understand the role of finite-size effects in the NEAS. A spin glass model that has been extensively studied is the random orthogonal model (ROM) [164], a variant of the Sherrington-Kirkpatrick model [165], known to reproduce the ideal mode coupling theory [166]. The model is defined in terms of the following energy function,

$$\mathcal{H} = -\sum_{(i,j)} J_{ij}\sigma_i\sigma_j \tag{210}$$

where the σ_i are N Ising spin variables ($\sigma = \pm 1$) and J_{ij} is a random $N \times N$ symmetric orthogonal matrix with zero diagonal elements. In the limit $N \to \infty$ this model has the same

thermodynamic properties as the random-energy model of Derrida [167, 168] or the p-spin model [169] in the large p limit [170, 171]. The ROM shows a dynamical transition at a characteristic temperature T_{dyn} (that corresponds to the mode coupling temperature T_{MCT} in mode coupling theories for the glass transition [172]). Below that temperature ergodicity is broken and the phase space splits up into disconnected regions that are separated by infinitely high energy barriers. For finite N the dynamics is different and the dynamical transition is smeared out. The scenario is then much reminiscent of the phenomenological model we discussed in Sec. 6.1. Different sets of spins collectively relax in finite timescales, each one representing a CRR. There are two important and useful concepts in this regard,

- **The free energy landscape.** An interesting approach to identify CRRs in glassy systems is the study of the topological properties of the potential energy landscape [173]. The slow dynamics observed in glassy systems in the NEAS is attributed to the presence of minima, maxima and saddles in the potential energy surface. Pathways connecting minima are often separated by large energy barriers that slow down the relaxation. Stillinger and Weber have proposed to identify phase space regions with the so-called inherent structures (IS) [174, 175]. The inherent structure of a region in phase space is the configuration that can be reached by energy minimization starting from any configuration contained in the region. Inherent structures are used as labels for regions in phase space. Figure 17 (left panel) shows a schematic representation of this concept. Figure 17 (right panel) shows the relaxation of the energy of the inherent structure energy starting from a high energy initial nonequilibrium state [176, 177, 178]. Inherent structures are a useful way to keep track of all cooperative rearrangements that occur during the aging process [179].

- **FD plots.** Numerical tests of the validity of the FDR (209) use fluctuation-dissipation plots (FD plots) to represent the integrated response as a function of the correlation. The integrated version of relation (209) is expressed in terms of the susceptibility,

$$\chi(t, t_w) = \int_{t_w}^{t} dt' R(t, t') \quad . \tag{211}$$

By introducing (211) in (209) we obtain,

$$\chi(t, t_w) = \int_{t_w}^{t} dt' \frac{1}{T_{\mathrm{eff}}(t')} \frac{\partial C(t, t')}{\partial t'} = \frac{1}{T_{\mathrm{eff}}(t_w)} \Big(C(t, t) - C(t, t_w) \Big) \tag{212}$$

where we have approximated $T_{\mathrm{eff}}(t')$ by $T_{\mathrm{eff}}(t_w)$. By measuring the susceptibility and the correlation function for a fixed value of t_w and plotting one respect to the other, the slope of the curve χ respect to C gives the effective temperature. This result follows naturally from (212) if we take $C(t, t)$ time independent (which is the case for spin systems). If not, proper normalization of the susceptibility and correlations by $C(t, t)$ is required and a similar result is obtained [180]. A numerical test of these relations in the ROM and in binary Lennard-Jones mixtures is shown in Figure 18. We stress that these results have been obtained in finite-size systems. As the system becomes larger the timescales required to see rearrangements events become prohibitively longer and the relaxation of the system toward equilibrium drastically slows down.
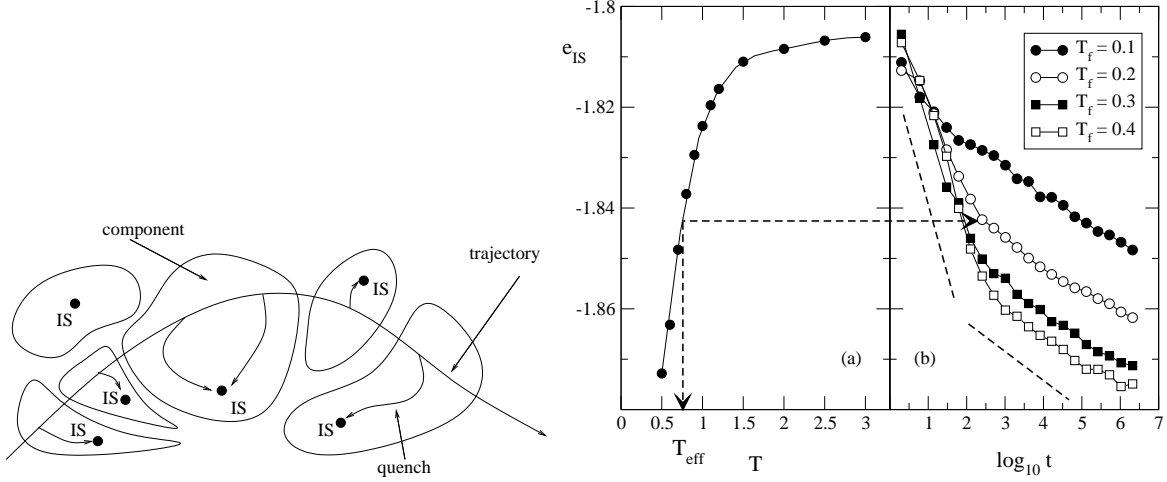
Figure 17: *(Left) Stillinger and Weber decomposition. Schematic picture showing regions or components in phase space that are labeled by a given IS. (Right) Relaxation in the ROM. Panel (a): Equilibrium average $e_{\rm IS}$ a function of temperature. The arrows indicate the construction of the effective temperature $T_{\rm eff}(t_w)$ (209). Panel (b): Average inherent structure energy as function of time for initial equilibrium temperatures $T_{\rm i} = 3.0$ and final quench temperatures $T_{\rm f} = 0.1, 0.2, 0.3$ and 0.4. The average is over 300 initial configurations. The system size is $N = 300$. Left figure taken from [179]. Right figure taken from [177, 178]*

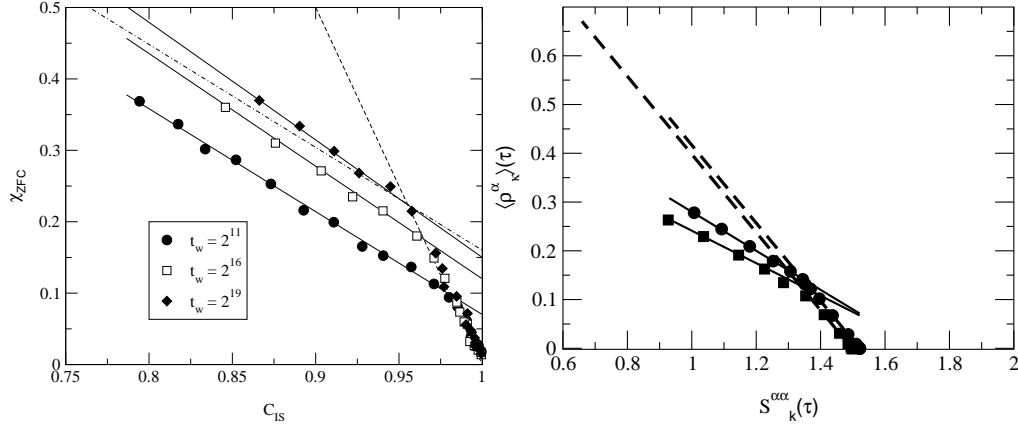
Figure 18: *(Left panel) Integrated response function as a function of IS correlation function, i.e, the correlation between different IS configurations, for the ROM. The dashed line has slope $T_{\rm f}^{-1} = 5.0$, where $T_{\rm f}$ is the final quench temperature, whereas the full lines are the prediction from (205) and $F^* = E_{\rm IS}(t_w)$: $T_{\rm eff}(2^{11}) \simeq 0.694$, $T_{\rm eff}(2^{16}) \simeq 0.634$ and $T_{\rm eff}(2^{19}) \simeq 0.608$. The dot-dashed line is $T_{\rm eff}(t_w)$ for $t_{\rm w} = 2^{11}$ drawn for comparison. Figure taken from [177]. (Right panel) Response versus the dynamical structure factor for the binary mixture Lennard-Jones particles system in a quench from the initial temperature $T_{\rm i} = 0.8$ to a final temperature $T_{\rm f} = 0.25$ and two waiting times $t_w = 1024$ (square) and $t_w = 16384$ (circle). Dashed lines have slope $1/T_{\rm f}$ while thick lines have slope $1/T_{\rm eff}(t_w)$. Figure taken from [181].*

6.3 Intermittency

Indirect evidence of nonequilibrium fluctuations due to CRRs in structural glasses has been obtained in Nyquist noise experiments by Ciliberto and coworkers. In these experiments a polycarbonate glass is placed between the plates of a condenser and quenched at temperatures below the glass transition temperature. Voltage fluctuations are then recorded as a function of time during the relaxation process and the effective temperature is measured,

$$T_{\text{eff}}(\omega, t_w) = \frac{S_Z(\omega, t_w)}{4\mathcal{R}(Z(\omega, t_w))} \tag{213}$$

where $\mathcal{R}(Z(\omega, t_w))$ is the real part of the impedance of the system and $S_Z(\omega, t_w)$ is the noise spectrum of the impedance that can be measured from the voltage noise [143].

Experimental data shows a strong variation of the effective temperature with the waiting time by several orders of magnitude. The voltage signal is also intermittent with strong voltage spikes at random times. The distribution of the times between spikes follows a power law characteristic of trap models. These results point to the fact that the observed voltage spikes correspond to CRRs occurring in the polycarbonate sample. Finally, the probability distribution function (PDF) of the voltage signal strongly depends on the cooling rate in the glass suggesting that relaxational pathways in glasses are very sensitive to temperature changes. A related effect that goes under the name of Kovacs effect has been also observed in calorimetry experiments, numerical simulations and exactly solvable models [182, 183, 184].

A physical interpretation of the intermittency found in aging systems has been put forward based on exactly solvable models of glasses [185, 186, 187]. According to this, energy relaxation in glassy systems follows two different mechanisms (see Sec. 5.3.1): stimulated relaxation and spontaneous relaxation. In the NEAS the system does not do work but exchanges heat with the environment. At difference with previous Sections here we adopt the following convention: $Q > 0$ ($Q < 0$) denotes heat absorbed (released) by the system from (to) the environment. In the NEAS, $\Delta E = Q$, the energy released by the system is dissipated in the form of heat. In the phenomenological model put forward in Sec. 6.1 different CRRs can exchange (adsorb or release) heat to the environment. The regions that cooperatively rearrange for the first time release stress energy to the environment and contribute to the net energy dissipation of the glass. We call this mechanism the *spontaneous relaxation*. Regions that have already rearranged for the first time can absorb or release energy from/to the bath several times but do not contribute to the net heat exchanged between the system and the bath. We call this mechanism the *stimulated relaxation*. There are several aspects worth mentioning,

- **Heat distribution.** The distribution of heat exchanges $Q = E(t_w) - E(t)$ for the stimulated process is a Gaussian distribution with zero mean and finite variance. This process corresponds to the heat exchange distribution of the system in equilibrium at the quenching temperature. In contrast, in the spontaneous process a net amount of heat is released to the bath. *Spontaneous heat* arises from the fact that the system has been prepared in a nonequilibrium high-energy state. Let us consider a glass that has been quenched at a temperature T and has relaxed for an age t_w. During aging, CRRs that release stress energy (in the form of heat $Q < 0$) to the environment satisfy the relation (204),

$$\frac{P^{\text{sp}}(Q)}{P^{\text{sp}}(-Q)} = \exp\Big(\frac{Q}{T_{\text{eff}}(F^*)}\Big) \tag{214}$$

Therefore, as in the phenomenological model (207), we expect,

$$P^{\mathrm{sp}}(Q) \propto \exp\Big(\frac{Q}{2T_{\mathrm{eff}}(F^*)}\Big) \quad \text{for} \quad Q < 0 \quad .\tag{215}$$

Note that $T_{\mathrm{eff}}(F^*)$ depends on the age of the system through the value of the typical free-energy of the CRRs that release their stress energy at t_w, $F^*(t_w)$. This relation has been numerically tested in the ROM (210) by carrying out aging simulations at different temperatures and small sizes N [185] (see next item).

- **Numerical tests.** How to measure the heat distribution (215) in numerical simulations of NEAS? A powerful procedure that uses the concept of inherent structures goes as follows. The heat exchanged during the time interval $[t_w, t]$ $(t > t_w)$ has to be averaged over many aging paths (ideally an infinite number of paths). Along each aging path many rearrangement events occur between t_w and t. Most of them are stimulated, a few of them are spontaneous. In fact, because the spontaneous process gets contribution only from those cooperative regions that rearrange for the first time, its PDF signal gets masked by the much larger one coming from the stimulated component where rearrangements events from a single region contribute more than once. To better disentangle both processes we measure, for a given aging path, the heat exchange corresponding to the first rearrangement event observed after t_w. To identify a rearrangement event we keep track of the IS corresponding to the run time configuration. Following the IS is an indirect way of catching rearranging events due to CRRs. Only when the system changes IS we know that a cooperative rearrangement event has taken place. Rearrangement events take place at different times t after t_w, therefore the heat distribution $P^{\mathrm{sp}}(Q)$ is measured along an heterogeneous set of time intervals. The results for the heat distributions at various ages t_w are shown in Figure 19. We notice the presence of two well defined contributions to the heat PDFs: A Gaussian central component plus additional exponential tails at large and negative values of Q. The Gaussian component corresponds to the stimulated process, however its mean is different from zero. The reason of this apparent discrepancy lies in the numerical procedure used to measure the heat PDF: the average *stimulated heat* is not equal to the net exchanged heat (which should be equal to 0) because different aging paths contribute to the heat exchange along different time intervals. The Gaussian component should be equal to the heat PDF for the system in thermal equilibrium at the same temperature and therefore independent of t_w. Indeed the variance of the Gaussian distribution is found to be independent of t_w [185].

- **Spontaneous events release stress energy.** One striking aspect of the spontaneous process is that, according to (214), the probability of heat absorption $(Q > 0)$ should be much larger than the probability of heat release $(Q < 0)$. However, this is not observed in the numerical results of Figure 19 where the exponential tail is restricted to the region $Q < 0$. Why spontaneous events are not observed for $Q > 0$? The reason is that spontaneous events can only release and not absorb energy from the environment, see (215). This is in the line of the argumentation put forward in Sec. 6.1 where the first time that cooperative regions release the stress energy, it gets irreversibly lost as heat in the environment. As the number of stressed regions monotonically decreases as a function
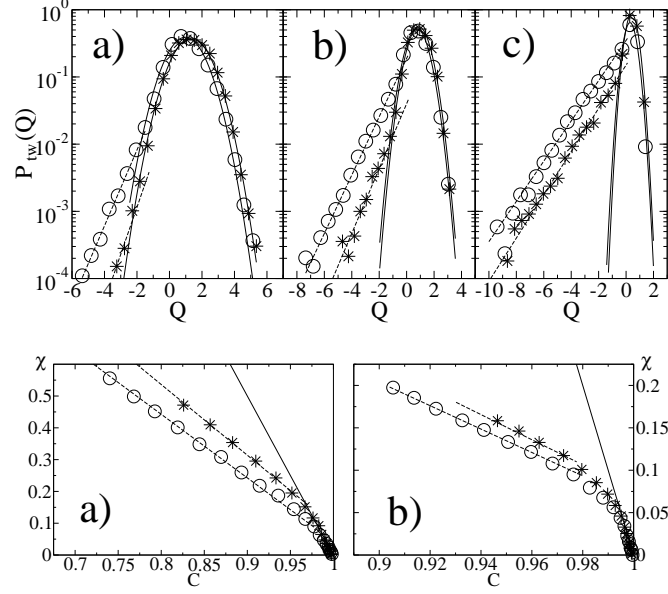
Figure 19: *Heat exchange PDFs for $T = 0.3$ (a), $T = 0.2$ (b), $T = 0.1$ (c). Circles are for $t_w = 2^{10}$ and asterisks for $t_w = 2^{15}$. The continuous lines are Gaussian fits to the stimulated sector, the dashed lines are the exponential fits to the spontaneous sector. Figure taken from [185].*

of time the weight of the heat exponential tails decreases with the age of the system as observed in Figure 19. The idea that only energy decreasing events contribute to the effective temperature (215) makes it possible to define a time-dependent configurational entropy [188].

- **Zero-temperature relaxation.** This interpretation rationalizes the aging behavior found in exactly solvable entropy barrier models that relax to the ground state and show aging at zero temperature [189, 190]. At $T = 0$, the stimulated process is suppressed (microscopic reversibility (8) does not hold), and (204) holds by replacing the free energy of a CRR by its energy, $F = E$. In these models a region corresponds to just a configuration in phase space and relaxation occurs through spontaneous rearrangements where configurations are visited only once. In entropic barrier models the effective temperature (205) still governs aging at $T = 0$. Because the energy is a monotonically decreasing quantity for all aging paths, (204) does not strictly hold as $\mathcal{W}(\Delta E > 0) = 0$. Yet, the effective temperature obtained from (204) has been shown to coincide with that derived from the FDR (209) [186, 187].

7   Conclusions and outlook

We have presented a general overview of several topics related to the nonequilibrium behavior of small systems: from fluctuations in mesoscopic systems such as small beads in optical traps up to molecular machines and biomolecules. The main common theme being that,

under appropriate conditions, physical systems exchange small amounts of energy with the environment leading to large fluctuations and strong deviations from the average behavior. We call such systems *small* because of their properties and behavior are markedly different from macroscopic systems. We started our tour by stressing the similarities between colloidal systems and molecular machines: intermittency and nonequilibrium behavior are common aspects there. We have then discussed fluctuation theorems (FTs) in detail, and focused our discussion in two well studied systems: the bead in a trap and single molecule force experiments. Experimental results in such systems show the presence of large tails in heat and work distributions in marked contrast to Gaussian distributions, characteristic of macroscopic systems. Such behavior can be rationalized by introducing a path formalism that quantifies work/heat distributions. Finally, we revised some of the main concepts in glassy dynamics where small energy fluctuations appear an essential underlying ingredient of the observed slow relaxation. Yet, we still lack a clear understanding of the right theory that unifies all phenomena and a clear and direct observation of the postulated small and cooperatively rearranging regions remains an experimental challenge. We envision three future lines of research,

- **Developments in FTs.** FTs are simple results that provide a new view to better understand issues related to irreversibility and the second law of thermodynamics. The main assumption of FTs is microscopic reversibility or local equilibrium, an assumption that has received some criticism [191, 192, 193]. Establishing limitations to the validity of FTs is the next task for the future. At present no experimental result contradicts any of the FTs, mainly because the underlying assumptions are respected in the experiments or because current techniques are not accurate enough to detect systematic discrepancies. Under some experimental conditions, we might discover that microscopic reversibility breaks down and a more refined and fundamental description of the relevant degrees of freedom in the system becomes necessary. Validation of FTs under different and far from equilibrium conditions will be useful to test the main assumptions.

- **Large deviation functions.** The presence of large tails can be investigated in statistical mechanics theories by exact analytical solutions of simple models, by introducing simplified theoretical approaches or even by designing smart and efficient algorithms. In all cases, we expect to obtain a good theoretical understanding of the relation between large deviations and nonequilibrium processes. Ultimately, this understanding can be very important in biological systems where nonequilibrium fluctuations and biological function may have gone hand by hand during biological evolution on earth over the past 4.5 billion years. A very promising line of research in this area will be the study of molecular motors where the large efficiency observed at the level of a single mechanochemical cycle might be due to a very specific adaptation of the molecular structure of the enzyme to its environment. This fact may have important implications at the level of single molecules and cellular structures.

- **Glassy systems.** We still need to have direct and clear experimental evidence of the existence of the cooperatively rearranging regions, responsible for most of the observed nonequilibrium relaxational properties in glasses. However, the direct observation of these regions will not be enough. It will be also necessary to have a clear idea of how to identify them in order to extract useful statistical information that can be interpreted

in the framework of a predictive theory. Numerical simulations will be very helpful in this regard. If the concept of nonequilibrium temperature has to survive the time then it will be necessary also to provide accurate experimental measurements at the level of what we can now get from numerical simulations.

Since the discovery of Brownian motion in 1827 by the biologist Robert Brown and the later development of the theory for the Brownian motion in 1905, science is witnessing an unprecedented convergence of physics toward biology. This was anticipated several decades ago by Erwin Schrödinger who, in his famous monography published in 1944 and entitled *What is life?* [194], wrote when talking about the motion of a clock: "The true physical picture includes the possibility that even a regularly going clock should all at once invert its motion and, working backward, rewind its own spring -at the expense of the heat of the environment. The event is just 'still a little less likely' than a 'Brownian fit' of a clock without driving mechanism". Biological systems seem to have exploited thermal fluctuations to built new molecular designs and structures that efficiently operate out of equilibrium at the molecular and cellular level [195, 196, 197, 198]. The synergy between structure and function is most strong in living systems where nonequilibrium fluctuations are at the root of their amazing and rich behavior.

8   List of abbreviations

CFT   Crooks fluctuation theorem
JE   Jarzynski equality
FDT   fluctuation-dissipation theorem
FEC   Force-extension curve
FT   Fluctuation theorem
IS   inherent structure
PDF   probability distribution function

References

[1] T. L. Hill. *Thermodynamics of small systems*. Dover Publications, New York, 1994.

[2] D. H. E. Gross. *Microcanonical thermodynamics, phase transitions in "Small systems"*. World Scientific Lecture Notes in Physics. World scientific, Singapore, 2001.

[3] F. Ritort. Work fluctuations, transient violations of the second law and free-energy recovery methods. In B. Duplantier J. Dalibard and V. Rivasseau, editors, *Bose-Einstein*

Condensation and Entropy, volume 2, pages 193–226. Birkhäuser Verlag, Basel (Available also at http://www.ffn.ub.es/ritort/publications.html), 2004.

[4] C. Bustamante, J. Liphardt and F. Ritort. The nonequilibrium thermodynamics of small systems. *Physics Today*, 58:43–48, 2005.

[5] E. Frey and K. Kroy. Brownian motion: a paradigm of soft matter and biological physics. *Annalen der Physik (Leipzig)*, 14:20–50, 2005.

[6] D. Reguera, J. M. Rubí and J. M. G. Vilar. The mesoscopic dynamics of thermodynamic systems. *Journal of Physical Chemistry*, 109:21502–21515, 2005.

[7] H. Qian. Cycle kinetics, steady state thermodynamics and motors -a paradigm for living matter physics. *Journal of Physics (Condensed Matter)*, 17:S3783–3794, 2005.

[8] L. Cipelletti and L. Ramos. Slow dynamics in glassy soft matter. *Journal of Physics (Condensed Matter)*, 17:R253–R285, 2005.

[9] P. N. Pusey and W. Van Megen. Phase behavior of concentrated suspensions of nearly hard colloidal sphres. *Nature*, 320:340–342, 1986.

[10] E. R. Weeks, J. C. Crocker, A. C. Levitt, A. Schofield and D. A. Weitz. Three-dimensional direct imaging of structural relaxation near the colloidal glass transition. *Science*, 287:627–631, 2000.

[11] R. E. Courtland and E. R. Weeks. Direct visualization of ageing in colloidal glasses. *Journal of Physics (Condensed Matter)*, 15:S359–S365, 2003.

[12] B. Alberts, D. Bray, A. Johnson, J. Lewis, M. Raff, K. Roberts and P. Walter. *Essential Cell Biology*. Garland Publishing, Inc. New York & London, 1998.

[13] J. D. Watson, T. A. Baker, S. P. Bell, A. Gann, M. Levine and R. Losick. *Molecular Biology of the Gene*. Benjamin Cummings, 2004.

[14] E. Eisenberg and T. L. Hill. Muscle contraction and free energy transduction in biological systems. *Science*, 277:999–1006, 1985.

[15] N. J. Córdova, B. Ermentrout and G. F. Oster. Dynamics of single-motor molecules: The thermal ratchet model. *Proceedings of the National Academy of Sciences*, 89:339–343, 1992.

[16] F. Jülicher, A. Adjari and J. Prost. Modeling molecular motors. *Review of Modern Physics*, 69:1269–1281, 1998.

[17] M. E. Fisher and A. B. Kolomeisky. The force exerted by a molecular motor. *Proceedings of the National Academy of Sciences*, 96:6597–6602, 1999.

[18] J. Gelles and R. Landick. Rna polymerase as a molecular motor. *Cell*, 93:13–16, 1998.

[19] A. Klug. A marvelous machine for making messages. *Science*, 292:1844–1846, 2001.

[20] G. Orphanides and D. Reinberg. A unified theory of gene expression. *Cell*, 108:439–451, 2002.

[21] M. D. Wang, M. J. Schnitzer, H. Yin, R. Landick, J. Gelles and S. M. Block. Force and velocity measured for single molecules of rna polymerase. *Science*, 282:902–907, 1998.

[22] R. J. Davenport, G. J. Wuite, R. Landick and C. Bustamante. Single-molecule study of transcriptional pausing and arrest by e. coli rna polymerase. *Science*, 287:2497–2500, 2000.

[23] J. W. Shaevitz, E. A. Abbondanzieri, R. Landick and S. M. Block. Backtracking by single rna polymerase molecules observed at near-base-pair resolution. *Nature*, 426:684–687, 2003.

[24] E. A. Abbondanzieri, W. J. Greenleaf, J. W. Shaevitz, R. Landick and S. M. Block. Direct observation of base-pair stepping by rna polymerase. *Nature*, 438:460–465, 2005.

[25] N. R. Forde, D. Izhaky, G. R. Woodcock, G. J. L. Wuite and C. Bustamante. Using mechanical force to probe the mechanism of pausing and arrest during continuous elongation by escherichia coli rna polymerase. *Proceedings of the National Academy of Sciences*, 99:11682–11687, 2002.

[26] E. G. D. Cohen D. J. Evans and G. P. Morriss. Probability of second law violations in shearing steady states. *Physical Review Letters*, 71:2401–2404, 1993.

[27] D. J. Evans and D. J. Searles. Equilibrium microstates which generate second law violating steady-states. *Physical Review E*, 50:1645–1648, 1994.

[28] G. Gallavotti and E. G. D. Cohen. Dynamical ensembles in nonequilibrium statistical mechanics. *Physical Review Letters*, 74:2694–2697, 1995.

[29] E. G. D. Cohen. Some recent advances in classical statistical mechanics. In P. Garbaczewski and R. Olkiewicz, editors, *Dynamics of dissipation*, volume 597, page 7. Springer-Verlag, Berlin, 2002.

[30] G. Gallavotti. Nonequilibrium thermodynamics? *Preprint*, arXiv:cond-mat/0301172, 2003.

[31] C. Jarzynski. Nonequilibrium equality for free-energy differences. *Physical Review Letters*, 78:2690–2693, 1997.

[32] J. C. Reid, E. M. Sevick and D. J. Evans. A unified description of two theorems in non-equilibrium statistical mechanics: The fluctuation theorem and the work relation. *Europhysics Letters*, 72:726–730, 2005.

[33] D. J. Evans. A nonequilibrium free energy theorem for deterministic systems. *Molecular Physics*, 101:1551–1554, 2003.

[34] D. J. Evans and D. Searles. The fluctuation theorem. *Advances in Physics*, 51:1529–1585, 2002.

[35] C. Maes. On the origin and use of fluctuation relations on the entropy. In B. Duplantier J. Dalibard and V. Rivasseau, editors, *Bose-Einstein Condensation and Entropy*, volume 2, pages 145–191. Birkhäuser Verlag, Basel, 2004.

[36] C. Jarzynski. What is the microscopic response of a system driven far from equilibrium. In P. Garbaczewski and R. Olkiewicz, editors, *Dynamics of dissipation*, volume 597, pages 63–82. Springer-Verlag, Berlin, 2002.

[37] J. Kurchan. Nonequilibrium work relations. *Preprint*, arXiv:cond-mat/0511073, 2005.

[38] J. Kurchan. Fluctuation theorem for stochastic dynamics. *Journal of Physics A*, 31:3719–3729, 1998.

[39] J. L. Lebowitz and H. Spohn. A gallavotti-cohen type symmetry in the large deviation functional for stochastic dynamics. *Journal of Statistical Physics*, 95:333–365, 1999.

[40] U. Seifert. Entropy production along a stochastic trajectory and an integral fluctuation theorem. *Physical Review Letters*, 95:040602, 2005.

[41] G. N. Bochkov and Y. E. Kuzovlev. Non-linear fluctuation relations and stochastic models in nonequilibrium thermodynamics. i. generalized fluctuation-dissipation theorem. *Physica A*, 106:443–479, 1981.

[42] C. Maes and M. H. van Wieren. Time-symmetric fluctuations in nonequilibrium systems. *Physical Review Letters*, 96:240601, 2006.

[43] G. Gallavotti. Chaotic hypothesis: Onsager reciprocity and fluctuation dissipation theorem. *Journal of Statistical Physics*, 84:899, 1996.

[44] G. E. Crooks. Entropy production fluctuation theorem and the nonequilibrium work relation for free-energy differences. *Physical Review E*, 60:2721–2726, 1999.

[45] G. E. Crooks. Path-ensemble averages in systems driven far from equilibrium. *Physical Review E*, 61:2361–2366, 2000.

[46] J. G. Kirkwood. Statistical mechanics of fluid mixtures. *Journal of Chemical Physics*, 3:300–313, 1935.

[47] R. W. Zwanzig. High-temperature equation of state by a perturbation method. i. non-polar gases. *Journal of Chemical Physics*, 22:1420–1426, 1954.

[48] C. Jarzynski and D. K. Wojcik. Classical and quantum fluctuation theorems for heat exchange. *Physical Review Letters*, 92:230602, 2004.

[49] Y. Oono and M. Paniconi. Steady state thermodynamics. *Progress of Theoretical Physics Supplement*, 130:29–44, 1998.

[50] S. Sasa and H. Tasaki. Steady state thermodynamics. *Preprint*, arXiv:cond-mat/0411052, 2004.

[51] S. Ciliberto and C. Laroche. An experimental test of the gallavotti-cohen fluctuation theorem. *Journal de Physique IV (France)*, 8:215–220, 1998.

[52] S. Ciliberto, N. Garnier, S. Hernandez, C. Lacpatia, J. F. Pinton and G. Ruiz-Chavarria. Experimental test of the gallavotti-cohen fluctuation theorem in turbulent flows. *Physica A*, 340:240–250, 2004.

[53] K. Feitosa and N. Menon. Fluidized granular medium as an instance of the fluctuation theorem. *Physical Review Letters*, 92:164301, 2004.

[54] S. Schuler, T. Speck , C. Tierz, J. Wrachtrup and U. Seifert. Experimental test of the fluctuation theorem for a driven two-level system with time-dependent rates. *Physical Review Letters*, 94:180602, 2005.

[55] T. Hatano and S. Sasa. Steady-state thermodynamics of langevin systems. *Physical Review Letters*, 86:3463–3466, 2001.

[56] G. M. Wang, E. M. Sevick, E. Mittag, D. J. Searles and D. J. Evans. Experimental demonstration of violations of the second law of thermodynamics for small systems and short timescales. *Physical Review Letters*, 89:050601, 2002.

[57] D. M. Carberry, J. C. Reid, G. M. Wang, E. M. Sevick, D. J. Searles and D. J. Evans. Fluctuations and irreversibility: An experimental demonstration of a second-law-like theorem using a colloidal particle held in an optical trap. *Physical Review Letters*, 92:140601, 2004.

[58] J. C. Reid, D. M. Carberry, G. M. Wang, E. M. Sevick, D. J. Searles and D. J. Evans. Reversibility in nonequilibrium trajectories of an optically trapped particle. *Physical Review E*, 70:016111, 2004.

[59] O. Mazonka and C. Jarzynski. Exactly solvable model illustrating far-from-equilibrium predictions. *Preprint*, arXiv:cond-mat/9912121.

[60] R. Van Zon and E. G. D. Cohen. Extension of the fluctuation theorem. *Physical Review Letters*, 91:110601, 2003.

[61] R. Van Zon and E. G. D. Cohen. Stationary and transient work-fluctuation theorems for a dragged brownian particle. *Physical Review E*, 67:046102, 2003.

[62] R. Van Zon and E. G. D. Cohen. Extended heat-fluctuation theorems for a system with deterministic and stochastic forces. *Physical Review E*, 69:056121, 2004.

[63] V. Blickle, T. Speck, L. Helden, U. Seifert and C. Bechinger. Thermodynamics of a colloidal particle in a time-dependent non-harmonic potential. *Physical Review Letters*, 96:070603, 2006.

[64] R. Van Zon, S. Ciliberto and E. G. D. Cohen. Power and heat fluctuations for electric circuits. *Physical Review Letters*, 92:313601, 2004.

[65] J. Zinn-Justin. *Quantum Field Theory and Critical Phenomena*. International Series of Monographs on Physics, n 92. Claredon Press, 1996.

[66] M. Baiesi, T. Jacobs, C. Maes and N. S. Skantzos. Fluctuation symmetries for work and heat. *Physical Review E*, 74:021111, 2006.

[67] N. Garnier and S. Ciliberto. Nonequilibrium fluctuations in a resistor. *Physical Review E*, 71:060101(R), 2005.

[68] E. H. Trepagnier, C. Jarzynski, F. Ritort, G. E. Crooks, C. Bustamante and J. Liphardt. Experimental test of hatano and sasa's nonequilibrium steady state equality. *Proceedings of the National Academy of Sciences*, 101:15038–15041, 2004.

[69] M. J. Lang and S. M. Block. Resource letter: Lbot-1: Laser-based optical tweezers. *American Journal of Physics*, 71:201–215, 2003.

[70] I. Tinoco Jr and C. Bustamante. How rna folds. *Journal of Molecular Biology*, 293:271–281, 1999.

[71] D. Thirumalai and C. Hyeon. Rna and protein folding: Common themes and variations. *Biochemistry*, 44:4957–4970, 2005.

[72] A. V. Finkelstein. Proteins: structural, thermodynamic and kinetic aspects. In J. L. Barrat and J. Kurchan, editors, *Slow relaxations and nonequilibrium dynamics*, pages 650–703. Springer-Verlag, Berlin, 2004.

[73] F. Ritort. Single molecule experiments in biological physics: methods and applications. *Journal of Physics (Condensed Matter)*, 18:R531–R583, 2006.

[74] C. Bustamante, J. C. Macosko and G. J. L. Wuite. Grabbing the cat by the tail: manipulating molecules one by one. *Nature Reviews on Molecular and Cell Biology*, 1:130–136, 2000.

[75] T. Strick, J. F. Allemand, V. Croquette and D. Bensimon. The manipulation of single biomolecules. *Physics Today*, 54:46–51, 2001.

[76] T. R. Strick, M. N. Dessinges, G. Charvin, N. H. Dekker, J. K. Allemand, D. Bensimon and V. Croquette. Stretching of macromolecules and proteins. *Reports on Progress in Physics*, 66:1–45, 2003.

[77] C. Bustamante, Y. R. Chemla, N. R. Forde and D. Izhaky. Mechanical processes in biochemistry. *Annual Reviews of Biochemistry*, 73:705–748, 2004.

[78] C. R. Calladine and H. R. Drew. *Understanding DNA: The Molecule & How It Works*. Academic London, 1997.

[79] S. B. Smith, Y. Cui and C. Bustamante. An optical-trap force transducer that operates by direct measurement of light momentum. *Methods in Enzymology*, 361:134–162, 2003.

[80] C. Bustamante, S. B. Smith, J. Liphardt and D. Smith. Single-molecule studies of dna mechanics. *Curr. Opin. Struct. Biol.*, 10:279–285, 2000.

[81] J. Marko and S. Cocco. The micromechanics of dna. *Physics World*, 16:37–41, 2003.

[82] J. Liphardt, B. Onoa, S. B. Smith, I. Tinoco Jr and C. Bustamante. Reversible unfolding of single rna molecules by mechanical force. *Science*, 292:733–737, 2001.

[83] C. Cecconi, E. A. Shank, C. Bustamante and S. Marqusee. Direct observation of the three-state folding of a single protein molecule. *Science*, 309:2057–2060, 2005.

[84] S. Cocco, J. Marko and R. Monasson. Theoretical models for single-molecule dna and rna experiments: from elasticity to unzipping. *Comptes Rendus Physique*, 3:569–584, 2002.

[85] M. Manosas, D. Collin and F. Ritort. Force dependent fragility in rna hairpins. *Physical Review Letters*, 96:218301, 2006.

[86] D. Keller, D. Swigon and C. Bustamante. Relating single-molecule measurements to thermodynamics. *Biophysical Journal*, 84:733–738, 2003.

[87] M. Manosas and F. Ritort. Thermodynamic and kinetic aspects of rna pulling experiments. *Biophysical Journal*, 88:3224–3242, 2005.

[88] J. D. Wen, M. Manosas,P. T. X. Li , S. B. Smith, C. Bustamante, F. Ritort and I. Tinoco Jr. Mechanical unfolding of single rna hairpins. i. effect of machine setup on kinetics. *To be published in Biophysical Journal*, 2007.

[89] M. Manosas, J. D. Wen, P. T. X. Li , S. B. Smith, C. Bustamante, I. Tinoco Jr. and F. Ritort. Mechanical unfolding of single rna hairpins. ii. modeling hopping experiments. *To be published in Biophysical Journal*, 2007.

[90] J. Greenleaf, T. Woodside, A. Abbondanzieri and S. Block. Passive all-optical clamp for high-resolution laser trapping. *Physical Review Letters*, 95:208102, 2005.

[91] I. Tinoco Jr and C. Bustamante. The effect of force on thermodynamics and kinetics of single molecule reactions. *Biophysical Chemistry*, 102:513–533, 2002.

[92] I. Tinoco Jr. Force as a useful variable in reactions: unfolding rna. *Annual Reviews of Biophysics and Biomolecular Structure*, 33:363–385, 2004.

[93] G. Hummer and A. Szabo. Free-energy reconstruction from nonequilibrium single-molecule experiments. *Proceedings of the National Academy of Sciences*, 98:3658–3661, 2001.

[94] C. Jarzynski. How does a system respond when driven away from thermal equilibrium? *Proceedings of the National Academy of Sciences*, 98:3636–3638, 2001.

[95] J. M. Schurr andd B. S. Fujimoto. Equalities for the nonequilibrium work transferred from an external potential to a molecular system: Analysis of single-molecule extension experiments. *Journal of Physical Chemistry B*, 107:14007–14019, 2003.

[96] F. Douarche, S. Ciliberto and A. Petrosyan. An experimental test of the jarzynski equality in a mechanical experiment. *Europhysics Letters*, 70:593–598, 2005.

[97] F. Douarche, S. Ciliberto and A. Petrosyan. Estimate of the free energy difference in mechanical systems from work fluctuations: experiments and models. *Journal of Statistical Mechanics (Theor. Exp.)*, page P09011, 2005.

[98] U. Gerland, R. Bundschuh and T. Hwa. Force-induced denaturation of rna. *Biophysical Journal*, 81:1324–1332, 2001.

[99] J. Liphardt, S. Dumont, S. B. Smith, I. Tinoco Jr and C. Bustamante. Equilibrium information from nonequilibrium measureme nts in an experimental test of the jarzynski equality. *Science*, 296:1833–1835, 2002.

[100] F. Ritort, C. Bustamante and I. Tinoco Jr. A two-state kinetic model for the unfolding of single molecules by mechanical force. *Proceedings of the National Academy of Sciences*, 99:13544–13548, 2002.

[101] D. Collin, F. Ritort, C. Jarzynski, S. B. Smith, I. Tinoco Jr and C. Bustamante. Verification of the crooks fluctuation theorem and recovery of rna folding free energies. *Nature*, 437:231–234, 2005.

[102] J. Gore, F. Ritort and C. Bustamante. Bias and error in estimates of equilibrium free-energy differences from nonequilibrium measurements. *Proceedings of the National Academy of Sciences*, 100:12564–12569, 2003.

[103] R. H. Wood, W. C. F. Mühlbauer and P. T. Thompson. Systematic errors in free energy perturbation calculations due to a finite sample of configuration space: sample-size hysteresis. *Journal of Physical Chemistry*, 95:6670–6675, 1991.

[104] D. M. Zuckermann and T. B. Woolf. Theory of systematic computational error in free energy differences. *Physical Review Letters*, 89:180602, 2002.

[105] B. Isralewitz, M. Gao and K. Schulten. Steered molecular dynamics and mechanical functions of proteins. *Curr. Opin. Struct. Biol.*, 11:224–230, 2001.

[106] M. O. Jensen, S. Park, E. Tajkhorshid and K. Schulten. Energetics of glycerol conduction through aquaglyceroporin glpf. *Proceedings of the National Academy of Sciences*, 99:6731–6736, 2002.

[107] S. Park, F. Khalili-Araghi, E. Tajkhorshid and K. Schulten. Free-energy calculation from steered molecular dynamics simulations using jarzynski's equality. *Journal of Physical Chemistry B*, 119:3559–3566, 2003.

[108] I. Andriocioaei, A. R. Dinner and M. Karplus. Self-guided enhanced sampling methods for thermodynamic averages. *Journal of Chemical Physics*, 118:1074–1084, 2003.

[109] S. Park and K. Schulten. Calculating potentials of mean force from steered molecular dynamics simulation. *Journal of Chemical Physics*, 13:5946–5961, 2004.

[110] G. Hummer and A. Szabo. Free-energy surfaces from single-molecule force spectroscopy. *Accounts of Chemical Research*, 38:504–513, 2005.

[111] G. Hummer. Fast-growth thermodynamic integration: Error and efficiency analysis. *Journal of Chemical Physics*, 114:7330–7337, 2001.

[112] D. A. Hendrix and C. Jarzynski. A "fast growth" method of computing free-energy differences. *Journal of Chemical Physics*, 114:5974–5981, 2001.

[113] D. M. Zuckermann and T. B. Woolf. Overcoming finite-sampling errors in fast-switching free-energy estimates: extrapolative analysis of a molecular system. *Chemical Physics Letters*, 351:445–453, 2002.

[114] O. Braun, A. Hanke and U. Seifert. Probing molecular free energy landscapes by periodic loading. *Physical Review Letters*, 93:158105, 2004.

[115] A. Imparato and L. Peliti. Evaluation of free energy landscapes from manipulation experiments. *Journal of Statistical Mechanics (Theor. Exp.)*, page P03005, 2006.

[116] F. Ritort. Work and heat fluctuations in two-state systems: a trajectory thermodynamics formalism. *Journal of Statistical Mechanics (Theor. Exp.)*, page P10016, 2004.

[117] C. Jarzynski. Rare events and the convergence of exponentially averaged work values. *Physical Review E*, 73:046105, 2006.

[118] I. Kosztin, B. Barz and L. Janosi. Calculating potentials of mean force and diffusion co-efficients from nonequilibrium processes without jarzynski equality. *Journal of Chemical Physics*, 124:064106, 2006.

[119] R. Delgado-Buscaiolini, G. De Fabritiis and P. V. Coveney. Determination of the chemical potential using energy-biased sampling. *Journal of Chemical Physics*, 123:054105, 2005.

[120] C. H. Bennett. Efficient estimation of free-energy differences from monte carlo data. *Journal of Computational Physics*, 22:245–268, 1976.

[121] M. R. Shirts, E. Bair, G. Hooker and V. S. Pande. Equilibrium free energies from nonequilibrium measurements using maximum-likelihood methods. *Physical Review Letters*, 91:140601, 2003.

[122] P. Maragakis, M. Spithchy and M. Karplus. Optimal estimates of free energy estimates from multi-state nonequilibrium work data. *Physical Review Letters*, 96:100602, 2006.

[123] R. C. Lhua and A. Y. Grossberg. Practical applicability of the jarzynski relation in statistical mechanics: a pedagogical example. *Journal of Physical Chemistry B*, 109:6805–6811, 2005.

[124] I. Bena, C. Van den Broeck and R. Kawai. Jarzynski equality for the jepsen gas. *Europhysics Letters*, 71:879–885, 2005.

[125] T. Speck and U. Seifert. Dissipated work in driven harmonic diffusive systems: general solution and application to stretching rouse polymers. *European Physical Journal B*, 43:521–527, 2005.

[126] G. E. Crooks and C. Jarzynski. On the work distribution for the adiabatic compression of a dilute classical gas. *Preprint*, arXiv:cond-mat/0603116, 2006.

[127] B. Cleuren, C. Van den Broeck and R. Kawai. Fluctuation and dissipation of work in a joule experiment. *Physical Review Letters*, 96:050601, 2006.

[128] P. Hanggi, P. Talkner and M. Borkovec. Reaction-rate theory: fifty years after kramers. *Review of Modern Physics*, 62:251–341, 1990.

[129] V. I. Melnikov. The kramers problem: Fifty years of development. *Physics Reports*, 209:1–71, 1991.

[130] E. Evans. Probing the relationship between force -lifetime- and chemistry in single molecular bonds. *Annual Reviews of Biophysics and Biomolecular Structure*, 30:105–128, 2001.

[131] E. Evans and P. Williams. Dynamic force spectroscopy. In H. Flyvbjerg, F. Jüulicher, P. Ormos and F. David, editors, *Physics of Bomolecules and Cells*, volume LXXV, pages 145–204. Springer-Verlag, Berlin, 2002.

[132] A. Imparato and L. Peliti. Work distribution and path integrals in mean-field systems. *Europhysics Letters*, 70:740–746, 2005.

[133] A. Imparato and L. Peliti. Work probability distribution in systems driven out of equilibrium. *Physical Review E*, 72:046114, 2005.

[134] B. Derrida, J. L. Lebowitz and E. R. Speer. Free energy functional for nonequilibrium systems:an exactly solvable case. *Physical Review Letters*, 87:150601, 2001.

[135] B. Derrida, J. L. Lebowitz and E. R. Speer. Large deviation of the density profile in the symmetric simple exclusion process. *Journal of Statistical Physics*, 107:599–634, 2002.

[136] B. Derrida, J. L. Lebowitz and E. R. Speer. Exact large deviation functional of a stationary open driven diffusive system: the asymmetric exclusion process. *Journal of Statistical Physics*, 110:775–810, 2003.

[137] C. Giardina, J. Kurchan and L. Peliti. Direct evaluation of large-deviation functions. *Physical Review Letters*, 96:120603, 2006.

[138] J. Jackle. Models of the glass transition. *Reports on Progress in Physics*, 49:171–231, 1986.

[139] C. A. Angell. Formation of glasses from liquids and biopolymers. *Science*, 267:1924–1935, 1995.

[140] M. D. Ediger, C. A. Angell and S. R. Nagel. Supercooled liquids and glasses. *Journal of Physical Chemistry*, 100:13200 –13212, 1996.

[141] Proceedings of the trieste workshop unifying concepts in glassy physiscs. *Journal of Physics (Condensed Matter)*, 12, 1999.

[142] M. D. Ediger. Spatially heterogeneous dynamics in supercooled liquids. *Annu. Rev. Phys. Chem.*, 51:99–128, 2000.

[143] L. Buisson, L. Bellon and S. Ciliberto. Intermittency in aging. *Journal of Physics (Condensed Matter)*, 15:S1163, 2003.

[144] L. Berthier, G. Biroli, J. P. Bouchaud, L. Cipelletti, D. El Masri, D. L'Hote, F. Ladieu, and M. Pierno. Direct experimental evidence of a growing length scale accompanying the glass transition. *Science*, 310:1797–1800, 2005.

[145] A. Crisanti and F. Ritort. Violations of the fluctuation dissipation in glassy systems: Basic notions and the numerical evidence. *Journal of Physics A*, 36:R181–R290, 2003.

[146] G. Biroli and J. P. Bouchaud. Diverging length scale and upper critical dimension in the mode coupling theory of the glass transition. *Europhysics Letters*, 67:21, 2004.

[147] M. Mezard, G. Parisi and M. A. Virasoro. *Spin-Glass Theory and Beyond*. World Scientific (Singapore), 1987.

[148] A. P. Young (Ed). *Spin Glasses and Random Fields*. World Scientific, Singapore, 1998.

[149] J. P. Bouchaud and M. Mezard. Self induced quenched disorder: a model for the glass transition. *Journal de Physique I (France)*, 4:1109–1114, 1994.

[150] E. Marinari, G. Parisi and F. Ritort. Replica field theory for deterministic models. i. binary sequences with low autocorrelation. *Journal of Physics A*, 27:7615–7646, 1994.

[151] L. F. Cugliandolo, J. Kurchan, G. Parisi and F. Ritort. Matrix models as solvable glass models. *Physical Review Letters*, 74:1012–1015, 1995.

[152] S. Franz and J. Hertz. Glassy transition and aging in a model without disorder. *Physical Review Letters*, 74:2114–2117, 1995.

[153] X. Xia and P. G. Wolynes. Fragilities of liquids predicted from the random first order transition theory of glasses. *Proceedings of the National Academy of Sciences*, 97:2990–2994, 2000.

[154] A. Crisanti and F. Ritort. A glass transition scenario based on heterogeneities and entropy barriers. *Philosophical Magazine B*, 82:143–149, 2002.

[155] J. P. Garrahan and D. Chandler. Coarse-grained microscopic models of glass formers. *Proceedings of the National Academy of Sciences*, 100:9710–9714, 2003.

[156] G. Biroli and J. P. Bouchaud. On the adam-gibbs-kirkpatrick-thirumalai-wolynes scenario for the viscosity increase in glasses. *Journal of Chemical Physics*, 121:7347–7354, 2004.

[157] A. Garriga and F. Ritort. Mode dependent nonequilibrium temperatures in aging systems. *Physical Review E*, 72:031505, 2005.

[158] J. H. Gibbs and E. A. DiMarzio. Nature of the glass transition and the glassy state. *Journal of Chemical Physics*, 28:373–383, 1958.

[159] G. Adam and J. H. Gibbs. On the temperature dependence of cooperative relaxation properties in glass-forming liquids. *Journal of Chemical Physics*, 43:139–146, 1965.

[160] L. F. Cugliandolo and J. Kurchan. Analytical solution of the off-equilibrium dynamics of a long-range spin-glass model. *Physical Review Letters*, 71:173–6, 1993.

[161] L. F. Cugliandolo and J. Kurchan. Weak ergodicity breaking in mean-field spin-glass models. *Philosophical Magazine B*, 71:501–14, 1995.

[162] L. F. Cugliandolo, J. Kurchan and L. Peliti. Energy flow, partial equilibration, and effective temperatures in systems with slow dynamics. *Physical Review E*, 55:3898–914, 1997.

[163] P. Mayer, S. Leonard, L. Berthier, J. P. Garrahan and P. Sollich. Activated aging dynamics and negative fluctuation-dissipation ratios. *Physical Review Letters*, 96:030602, 2006.

[164] E. Marinari, G. Parisi and F. Ritort. Replica field theory for deterministic models. ii. a non-random spin glass with glassy behaviour. *Journal of Physics A*, 27:7647–7668, 1994.

[165] D. Sherrington and A. Kirkpatrick. Solvable model of a spin-glass. *Physical Review Letters*, 35:1792–1796, 1975.

[166] W. Gotze and L. Sjogren. Relaxation processes in supercooled liquids. *Reports on Progress in Physics*, 55:241–376, 1992.

[167] B. Derrida. Random-energy model: Limit of a family of disordered models. *Physical Review Letters*, 45:79–82, 1980.

[168] B. Derrida. Random-energy model: An exactly solvable model of disordered systems. *Physical Review B*, 24:2613–2626, 1981.

[169] E. Gardner. Spin glasses with p-spin interactions. *Nuclear Physics B*, pages 747–65, 1985.

[170] M. Campellone. Some non-perturbative calculations on spin glasses. *Journal of Physics A*, 28:2149–2158, 1995.

[171] E. De Santis, G. Parisi and F. Ritort. On the static and dynamical transition in the mean-field potts glass. *Journal of Physics A*, 28:3025–3041, 1995.

[172] J.-P. Bouchaud, L. F. Cugliandolo, J. Kurchan and M. Mezard. Mode-coupling approximations, glass theory and disordered systems. *Physica A*, 226:243–73, 1996.

[173] M. Goldstein. Viscous liquids and the glass transition: a potential energy barrier picture. *Journal of Physical Chemistry*, 51:3728–3739, 1969.

[174] F. H. Stillinger and T. A. Weber. Hidden structure in liquids. *Physical Review A*, 25:978–989, 1982.

[175] F. H. Stillinger. Statistical-mechanics of metastable matter - superheated and stretched liquids. *Physical Review E*, 52:4685–4690, 1995.

[176] A. Crisanti and F. Ritort. Potential energy landscape of finite-size mean-field models for glasses. *Europhysics Letters*, 51:147, 2000.

[177] A. Crisanti and F. Ritort. Activated processes and inherent structure dynamics of finite-size mean-field models for glasses. *Europhysics Letters*, 52:640, 2000.

[178] A. Crisanti and F. Ritort. Equilibrium and ageing dynamics of simple models for glasses. *Journal of Physics (Condensed Matter)*, 12:6413–6422, 2000.

[179] A. Crisanti and F. Ritort. Inherent structures, configurational entropy and slow glassy dynamics. *Journal of Physics (Condensed Matter)*, 14:1381–1395, 2002.

[180] S. M. Fielding and P. Sollich. Observable dependence of fluctuation-dissipation relations and effective temperatures. *Physical Review Letters*, 88:050603, 2002.

[181] F. Sciortino and P. Tartaglia. Extension of the fluctuation-dissipation theorem to the physical aging of a model glass-formingliquid. *Physical Review Letters*, 86:107–110, 2001.

[182] S. Mossa and F. Sciortino. Crossover (or kovacs) effect in ana ging molecular liquid. *Physical Review Letters*, 92:045504, 2004.

[183] E. La Nave, S. Mossa and F. Sciortino. Potential energy landscape equation of state. *Physical Review Letters*, 88:225701, 2002.

[184] E. M. Bertin, J.-P. Bouchaud, J.-M. Drouffe abd C. Godreche. The kovacs effect in model glasses. *Journal of Physics A*, 36:10701–10719, 2003.

[185] A. Crisanti and F. Ritort. Intermittency of glassy relaxation and the emergence of a nonequilibrium spontanoeus measure in the aging regime. *Europhysics Letters*, 66:253, 2004.

[186] F. Ritort. Stimulated and spontaneous relaxation in glassy systems. In A. Fierro A. Coniglio and H. Hermann, editors, *Unifying concepts in granular media and glassy systems*. Springer-Verlag, 2004.

[187] F. Ritort. Spontaneous relaxation in generalized oscillator models for glassy dynamics. *Journal of Physical Chemistry B*, 108:6893–6900, 2004.

[188] G. Biroli and J. Kurchan. Metastable states in glassy systems. *Physical Review E*, 64:016101, 2001.

[189] F. Ritort. Glassiness in a model without energy barriers. *Physical Review Letters*, 75:1190–1193, 1995.

[190] L. L. Bonilla, F. G. Padilla and F. Ritort. Aging in the linear harmonic oscillator. *Physica A*, 250:315–326, 1998.

[191] E. G. D. Cohen and D. Mauzerall. A note on the jarzynski equality. *Journal of Statistical Mechanics (Theor. Exp.)*, page P07006, 2004.

[192] C. Jarzynski. Nonequilibrium work theorem for a system strongly coupled to a thermal environment. *Journal of Statistical Mechanics (Theor. Exp.)*, page P09005, 2004.

[193] R. D. Astumian. The unreasonable effectiveness of equilibrium-like theory for interpreting nonequilibrium experiments. *American Journal of Physics*, 74:683, 2006.

[194] E. Schrödinger. *What is life.* Cambridge University Press, 1967.

[195] C. De Duve. *Vital Dust: The Origin and Evolution of life on earth.* Perseus Books Group, 1995.

[196] W. R. Loewenstein. *The touchstone of life.* Oxford University Press, 1999.

[197] F. M. Harold. *The way of the cell.* Oxford University Press, 2001.

[198] In H. Flyvbjerg, F. Jülicher, P. Ormos and F. David, editors, *Physics of biomolecules and cells*, volume Session LXXV. Springer (Berlin), 2002.